Spring 5-9-2020

Dynamic Oscillatory Interactions Between Neural Attention and Sensorimotor Systems

Alex Wiesman
University of Nebraska Medical Center

DYNAMIC OSCILLATORY INTERACTIONS BETWEEN NEURAL ATTENTION AND SENSORIMOTOR SYSTEMS

By

Alex I. Wiesman

A DISSERTATION

Presented to the Faculty of

The Graduate College at the University of Nebraska

In Partial Fulfillment of Requirements

For the Degree of Doctor of Philosophy

Interdisciplinary Graduate Program in Biomedical Sciences
(Neuroscience)

Under the Supervision of Dr. Tony W. Wilson

University of Nebraska Medical Center
Omaha, Nebraska
March, 2020

Supervisory Committee:

Max J. Kurz, Ph.D.
Daniel L. Murman, M.D.
David E. Warren, Ph.D.
Daniel T. Monaghan, Ph.D.

ACKNOWLEDGEMENTS

First and foremost, I would like to express my overwhelming gratitude to my mentor and friend, Dr. Tony Wilson, for his guidance and support over the past five years. My success as a student can largely be attributed to his selflessness and undying scientific curiosity, and his positive demeanor made the all-too-common disappointments of academic research much less discouraging. Dr. Wilson has also worked diligently to facilitate a laboratory environment that is welcoming, collaborative, and extremely intellectually engaging. I would like to thank my fellow trainees who sustained this environment for their friendship and support, including graduate students Christine Embury, Brandon Lew, Rachel Spooner, Yasra Arif, Abraham Killanin, and Chloe Meehan, and postdoctoral fellow Dr. Brittany Taylor. Additionally, the scientific advances in this lab are truly a team effort, and I need to acknowledge the massive amount of help given to me by research staff members Rebecca Losh, Mikki Schantell, Jacob Eastman, Michael Rezich, Marie McCusker, Maddie Fung, Chloe Casagrande, Hallie Johnson, Madelyn Willett, Lisa Houseman, Nichole Knott, Sam Koshy, Abril Rangel-Pacheco, Mackenzie Mills, Nathan Coolidge, and Joslynn Hoburg.

I owe special thanks to Drs. Elizabeth Heinrichs-Graham and Amy Proskovec, who were an essential part of my training as a scientist, and somehow put up with my constant shenanigans and bad jokes. I want to thank Tim McDermott for stimulating discussions regarding movies and the origins of consciousness, Boman Groff for always stirring the pot, and Nick Christopher-Hayes for trying, unsuccessfully, to convince me that jelly goes well with Oreos. Further, I am greatly indebted to my scientific collaborators, including Drs. Max Kurz, Daniel Murman, Howard Fox, Susan Swindells, and Pamela May, as well as to my supervisory committee members Drs. Tony Wilson, Max Kurz, Daniel Murman, David Warren, and Daniel Monaghan; all of whom have guided my development towards

becoming a well-rounded academic. My early experiences in research with Drs. Rosemary Strasser and Wallace Thoreson led me towards a career in research, and so I owe my unreserved thanks to them as well. The administrative and support staff at the University of Nebraska Medical Center and the Department of Neurological were also invaluable to me on a daily basis.

Most importantly, I would like to thank my wife, Melanie Bejarano, for knowing, loving, and supporting me like no-one else; my parents, Mark Wiesman and Brenda Everson-Wiesman, for raising me to work hard for the things that I am passionate about and fostering my inquisitive nature; my siblings, Aaron, Drew, and Rachel, who keep me grounded; and my Zeze Ben for seeing potential in me, even when I didn't. Finally, the dedication of our participants, and in particular our participants afflicted with neurological disorders, is inspiring to me, and this work would not have been possible without them.

This work was financially supported by grants to my advisor, Tony W. Wilson, from the National Institutes of Health (R01-MH103220; R01-MH116782; R01-MH118013), the National Science Foundation (1539067), and the Fremont Area Alzheimer's Collaboration. Additionally, my training was supported by a Ruth L. Kirschstein Predoctoral Fellowship from the National Institute on Aging (F31-AG055332), and supplemented by research awards from the NASA Nebraska Space Grant and the Office of Graduate Studies at the University of Nebraska Medical Center. Travel awards from the International Conference on Biomagnetism, Cognitive Neuroscience Society, and Society for Neuroscience were also instrumental in the dissemination of these findings at international venues.

ABSTRACT

The adaptive and flexible ability of the human brain to preference the processing of salient environmental features in the visual space is essential to normative cognitive function, and various neurologically afflicted patient groups report negative impacts on visual attention. While the brain-bases of human attentional processing have begun to be unraveled, very little is known regarding the interactions between attention systems and systems supporting sensory and motor processing. This is essential, as these interactions are dynamic; evolving rapidly in time and across a wide range of functionally defined rhythmic frequencies. Using magnetoencephalography (MEG) and a range of novel cognitive paradigms and analytical techniques, this work attempts to fill critical gaps in this knowledge. Specifically, we unravel the role of dynamic oscillatory interactions between attention and three sensorimotor systems. First, we establish the importance of sub-second occipital alpha (8 – 14 Hz) oscillatory responses in visual distractor suppression during selective attention (Chapter 1) and their essential role in fronto-parietal attention networks during visual orienting (Chapter 2). Next, we examine the divergent effects of directed attention on multi-frequency primary somatosensory neural oscillations in the theta (4 – 8 Hz), alpha, and beta (18 – 26 Hz) bands (Chapter 3). Finally, we extend these findings to the motor system (Chapter 4), and find that the frontal and parietal beta-frequency oscillations known to support motor planning and execution are modulated equivalently by differing subtypes of attentional interference, whereas frontal gamma (64 – 84 Hz) oscillations specifically index the superadditive effect of this interference. These findings provide new insight into the dynamic nature of attention-sensorimotor interactions in the human brain, and will be the foundation for groundbreaking new studies of attentional deficits in patients with common neurological disorders (e.g., Alzheimer's disease, HIV-associated neurocognitive disorders, Parkinson's disease). With an

enhanced knowledge of the temporal and spectral definitions of these impairments, new therapeutic interventions utilizing frequency-targeted neural stimulation can be developed.

TABLE OF CONTENTS

LIST OF FIGURES AND TABLES

LIST OF ABBREVIATIONS

AD	*Alzheimer's disease*
ADL	*Activity of daily living*
ANOVA	*Analysis of variance*
BESA	*Brain electrical source analysis*
BF	*Bayes factor*
CI	*Confidence interval*
CNS	*Central nervous system*
DICS	*Dynamic imaging of coherent sources*
DLPFC	*Dorsolateral prefrontal cortex*
EEG	*Electroencephalography*
ERD	*Event-related desychronization*
FFT	*Fast Fourier transform*
FIR	*Finite impulse response*
fMRI	*Functional magnetic resonance imaging*
fT	*Femto-Tesla*
FWHM	*Full-width half maximum*
HAND	*HIV-associated neurocognitive disorders*
HIV	*Human immunodeficiency virus*
IMI	*Inter-modality interval*
IPI	*Inter-pair interval*
ISI	*Inter-stimulus interval*
JASP	*Jeffrey's amazing statistics program*
M1	*Primary motor cortex*
MCC	*Mid-cingulate cortex*
MEG	*Magnetoencephalography*
MRGS	*Movement-related gamma synchronization*
MRI	*Magnetic resonance imaging*
MSIT	*Multi-source interference task*
PD	*Parkinson's disease*
RM	*Repeated measures*
RT	*Reaction time*
S1/S2	*Stimulation 1/Stimulation 2*
SD	*Standard deviation*
SEM	*Standard error of the mean*
SG	*Sensory gating*
SII	*Secondary somatosensory cortex*
sLORETA	*Standardized low resolution brain electromagnetic tomography*
SPC	*Superior parietal cortex*
SSP	*Signal space projection*
SSVEP	*Steady state visually-evoked potential*
tACS	*Transcranial alternating current stimulation*
TF	*Time-frequency*
tSSS	*Temporal signal-space separation*

INTRODUCTION

Attention in the Human Nervous System:

Current models of the central nervous system (CNS) posit that the brain functions as the center of *predictive inference*. In other words, by actively gathering sensory cues to form a model of the external environment, comparing these measurements to internally generated predictive models, and updating internal weightings based on the discrepancies between the two, the brain allows us to proactively predict and modify our environment to our benefit, by means of our peripheral motor actions. The ability to selectively and flexibly direct sensory systems, such as vision and somatosensation, towards salient environmental stimuli is essential to the formation of a high-fidelity environmental model. This cognitive process, generally termed *attention*, helps our brains to divine signal in a world full of noise, and thus, when dysfunctional, can be debilitating. Importantly, although attention is often discussed as a unitary construct, it is difficult to operationalize in this way, and currently exists as more of a cognitive “umbrella term” rather than a single process. Essential among the cognitive attention sub-systems are *directed enhancement* of salient environmental stimuli, along with concurrent *selective inhibition* of interfering or distracting ones. Despite a great deal of research establishing the neuroanatomically defined brain networks supporting these attentional sub-systems, substantial gaps in knowledge remain regarding how they actually interact with the sensorimotor systems that they modulate.

Neural Oscillations:

Modern invasive and non-invasive recordings of population-level neuronal activity have indicated that the mammalian nervous system samples its environment and

organizes internal information transfer through rhythmic coordination spread across multiple, spectrally-defined rhythms (measured in cycles per second; Hz). As they provide a mechanism for temporally discrete sensory sampling and inter-system information modulation in the human brain, it is perhaps unsurprising that these *neural oscillations* are essential to attention function, however, knowledge of the neural oscillatory dynamics serving attention in healthy adult humans is incomplete. In particular, the rapidly-evolving oscillatory interactions between neural attentional sub-systems and sensorimotor systems have not been well-studied, which poses a major barrier in the way of understanding processing in the complex functional circuitry of the human brain, as well as for the development of non-invasive neurostimulation (e.g., transcranial magnetic and electric stimulation) and behavioral therapies for patient populations affected by attentional impairments. This dearth of research can be partially attributed to limitations in non-invasive neuroimaging technologies: non-invasive methods with the sufficient spatial and temporal precision needed to study these topics are rare, and invasive studies of the healthy human brain are generally ethically dubious.

Neuroimaging with Magnetoencephalography:

MEG is a passive and noninvasive method for quantifying neural activity in the human brain, and represents the ideal methodology by which to study the dynamic attention sensorimotor interactions in question. MEG data are acquired by measuring the miniscule magnetic fields that naturally emanate from population-level neural activity using a whole-head array of sensors that are sensitive at the femto-Tesla (10^{-15} T) level. MEG provides a unique combination of spatial (~ 5 mm) and temporal (< 1 ms) precision that is not achievable with any other method (e.g., fMRI and EEG). The high temporal resolution of MEG recordings also allows for the direct measurement and quantification of neural oscillations, which are now known to provide extremely useful information regarding the

function of spatially defined neural populations. In addition, this enhanced precision allows for measurement of very fast (i.e., millisecond-scale) interactions between distinct neural systems (e.g., attention and somato-motor) that are otherwise invisible.

Goals of the Current Studies:

The current studies aim to address knowledge gaps in the extant literature regarding: (A) the spatial and spectral patterns of rhythmic interactions between oscillatory neural responses in selective attention sub-systems and visual systems (Chapters 1 and 2), (B) the corollary interactions between attention and somatosensory systems (Chapter 3), and (C) the influence of these attention sub-systems on neural motor systems (Chapter 4). With the findings from these studies, we can expect to reach two primary goals. First, we can enhance our developing understanding of the functional role of spectrally limited neural activity in the human brain, across a number of neural systems and behaviorally relevant contexts. For example, although more established in vision, the distinct roles of temporally overlapping multi-spectral neural responses in somatosensation and motor plan execution are uncertain, and a better understanding of the functional implications of these rhythms will provide new insight into the mechanisms by which the human brain processes information and coordinates motor output. Second, and more importantly, these studies will lay the groundwork for upcoming studies of attention-sensorimotor interactions in a number of patient populations who present with deficits in attention. Patients with Alzheimer's disease (AD), HIV-associated neurocognitive disorders (HAND), and Parkinson's disease (PD), among others, all commonly report attentional issues, however the role that these impairments play in clinical outcomes and activities of daily living (ADLs) remains vastly understudied.

CHAPTER 1: OCCIPITAL ALPHA OSCILLATIONS IN SELECTIVE DISTRACTOR SUPPRESSION

The material presented in this chapter was previously published in Wiesman and Wilson, 2019, Alpha frequency entrainment reduces the effect of visual distractors, Journal of Cognitive Neuroscience, 31(9):1392-1403.

Introduction:

A substantial amount of research has connected parieto-occipital alpha oscillations to the active inhibition of visual cortical function (*1, 2*), particularly when these rhythms are measured prior to the onset of a salient visual stimulus or during the maintenance phase of visual working memory tasks (*3-9*). However, the conceptualization of occipital alpha as a suppression mechanism in visual cortex has recently come into question (*10*). Thus, studies aimed at experimentally manipulating occipital alpha in visual cortices and measuring the resulting effects on behavior and associated neural responses are extremely relevant.

In an attempt to manipulate occipital alpha experimentally, many laboratories have turned to frequency-specific entrainment with flickering visual stimuli (*11*). Although it remains unclear whether entrainment responses to stimuli flickering in the alpha-range represent a power-modulation of ongoing rhythmic patterns of neural activity, or more simply a “frequency-following response” (*12*), it is nonetheless established that visual perception appears to be negatively modulated by these stimuli (*13-17*). An enhanced understanding of this phenomenon is crucial, as flickering visual stimuli have been used for decades to “tag” stimuli in vision and cognitive neuroscience research in a supposedly neutral, physiologically-inert fashion (*18*).

Importantly, the impact of task-salience on the negative effects of alpha enhancement through visual entrainment remains unclear, as does the nature of these impairing effects on visual perception (i.e., pre- or post- attentive). Such knowledge is essential to understanding the interaction between attention and the effects of alpha entrainment on

visual perception, which is a rapidly growing area of neuroscience (*19*). As discussed above, previous research has found a detrimental effect of alpha entrainment on visual perception, but virtually all of these studies entrained the visual field corresponding to target stimuli (*13, 14, 16, 17*). Thus, whether similar effects would be observed when the entrained visual field corresponds to non-imperative, or even distracting, stimuli remains to be investigated. Essentially, if such alpha entrainment is associated with similarly detrimental effects on the perception of distracting stimuli, then the expected net effect would be enhanced task performance, which would provide strong support for the conceptualization that alpha entrainment has an “early” inhibitory effect in visual cortex that modulates visual perception.

In this study, we utilized an arrow-based, entrainment version of the classic Eriksen flanker selective attention paradigm and MEG to investigate the dynamic interactions between alpha-targeted entrainment in the visual cortex and behavioral performance. We hypothesized that local entrainment of visual cortex at 10 Hz would result in a reduced interference effect of visual stimuli in that portion of the visual field. Specifically, by entraining visual cortices at two distinct frequencies (i.e., 10 Hz alpha and 30 Hz control) in the specific locations where the interfering arrows would subsequently appear (and not over the target arrow), we hypothesized that pre-stimulus alpha entrainment would selectively decrease the behavioral interference effect of the incongruent flanking arrows. Further, we hypothesized that the strength of pre-stimulus neural entrainment in the alpha range would predict the decreased behavioral interference effect of the distracting flanker stimuli.

Methods:

Participants

Twenty-three healthy young adults were recruited for the study (M_{age} = 26.09; age range: 20-33 years; 16 males; 21 right-handed). Exclusion criteria included any medical illness affecting CNS function, any neurological or psychiatric disorder, history of head trauma, current substance abuse, and any non-removable metal implants that would adversely affect MEG data acquisition. Participants were compensated $50 for their time and travel for taking part in the study. All participants had normal or corrected-to-normal vision. Three participants were excluded early during analysis of the neural data: one due to technical difficulties with data acquisition and two more due to artifactual neural data (i.e., physiologically-implausible amplitude of responses), leaving a remaining twenty total participants for further analysis (M_{age} = 26.00; 15 males; 18 right-handed). The Institutional Review Board at the University of Nebraska Medical Center reviewed and approved this investigation. Written informed consent was obtained from each participant following detailed description of the study. All participants completed the same experimental protocol.

MEG Experimental Design and Behavioral Data Analysis

We used a modified arrow-based version of the classic Eriksen “flanker” paradigm to engage alpha-frequency networks related to selective attention processing (Figure 1). Each trial began with a fixation that was presented for a randomly-varied inter-stimulus interval of 2100-2300 ms. After this, two entrainment stimuli were flickered at a frequency of either 10 or 30 Hz on each side of this central fixation for 1500 ms. A row of 5 arrows was then presented in the same spatial locations as the five previously-presented stimuli (i.e., the central fixation and four surrounding entrainment stimuli) for 1000 ms. Importantly, the presentation of these arrows coincided with what would be the effective “peak” of the ongoing entrained rhythm. Prior to starting the experiment, participants were instructed to respond as quickly and accurately as possible as to whether the middle arrow

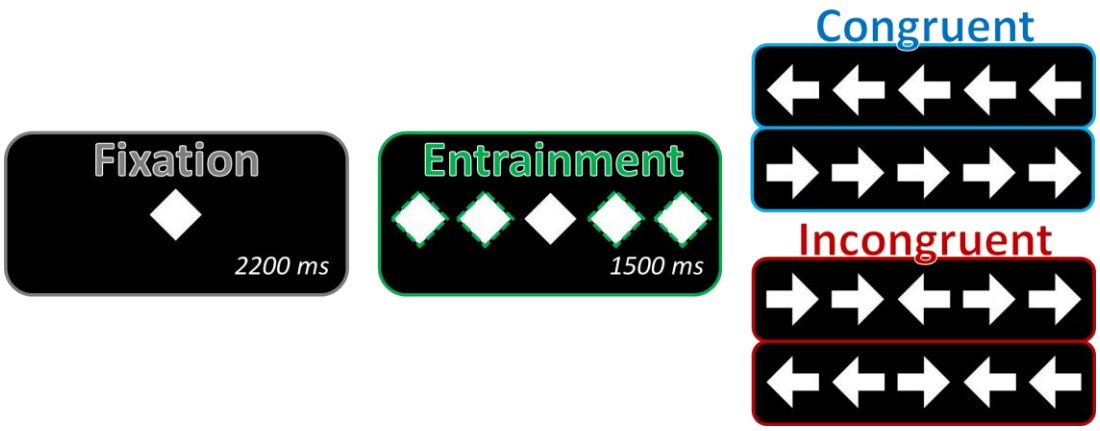

Figure 1. Visual entrainment flanker task paradigm.

The task began with 2200 ms of fixation, followed by 1500 ms of bilateral peripheral visual entrainment (green dotted lines) driven at either 10 or 30 Hz. Upon cessation of the entraining stimuli, one of the four arrow arrays was presented, comprising either a congruent or incongruent visual stimulus. Participants were instructed to indicate (by button press) the direction of the central arrow, while ignoring the interfering information provided by the flanking distractor arrows. Diamonds were chosen for fixation and entrainment stimuli, so as to completely encompass the visual field of the to-be-presented arrow stimuli, while also providing no information regarding the direction of the subsequently-presented arrow stimuli. It is important to note that the five positions of the fixation and entrainment stimuli perfectly overlapped in visual space with the positions of the subsequently-presented arrow stimuli.

was pointing to the left (index finger) or right (middle finger), using their right hand on a non-magnetic button pad. All stimuli prior to the presentation of the flanker arrows (i.e., the fixation and entrainment stimuli) were diamonds of equal height and width as the arrows, so to completely encompass and systematically modulate the visual field of the subsequently presented flanker stimuli. The 300 total trials were pseudo-randomized and equally split between each of the two entrainment (10 Hz and 30 Hz) and flanker congruency (congruent and incongruent) conditions. Correct responses were also pseudo-randomized, such that the direction of the central target arrow was never repeated more than twice in a row. Custom visual stimuli were programmed in Matlab (Mathworks, Inc., Massachusetts, USA) using Psychophysics Toolbox Version 3 (*20*) and back-projected onto a semi-translucent non-ferromagnetic screen at an approximate distance of 42 inches, using a Panasonic PT-D7700U-K model DLP projector with a refresh rate of 60 Hz and a contrast ratio of 4000:1. Flickering stimuli were presented as a square-wave

function with a frequency of either 10 Hz (3 frames on/3 frames off; ~16.67 ms per frame) or 30 Hz (1 frame on/1 frame off), with a luminance contrast of 100% (white stimuli on a black background). The arrow and entrainment stimuli were centered on five locations evenly distributed horizontally across the screen, and each subtended an approximate visual angle of 1.0° horizontally by 1.0° vertically. Including spaces between the arrows, the entire visual array (i.e., all five arrows/entrainment stimuli) subtended an approximate visual angle of 6.3° horizontally by 1.0° vertically. Total MEG recording time was about 24 minutes.

For each participant, reaction time (RT) data were extracted for each individual trial, incorrect and no-response trials were removed, and outliers were then excluded based on a standard threshold of ± 2.5 standard deviations from the mean. The remaining RT data were then averaged within each participant, and these mean RT values were subjected to a 2 (flanker congruency) x 2 (entrainment frequency) repeated measures ANOVA. These participant-level RT means were also used in subsequent statistical analyses, however it is important to note that, when computing the "congruency effect" for these analyses (commonly computed as the Incongruent RT – Congruent RT), we opted to divide the values instead, as this helped minimize the bias resulting from variability in overall response time (i.e., participants with higher overall reaction time could have a higher congruency effect, despite having a similar RT ratio between the two conditions). Importantly, side-by-side comparison of the different methods to compute congruency effects (i.e., subtraction, division, [active-baseline]/[active+baseline]) revealed that this choice made no meaningful difference in our primary finding (i.e., the significant time-varying relationship between 10 Hz entrainment and behavior). Accuracy data were also computed, but were not analyzed for conditional differences due to possible ceiling effects (mean accuracy = 94%) that would obscure meaningful interpretation.

MEG Data Acquisition

All recordings were conducted in a one-layer magnetically-shielded room with active shielding engaged for environmental noise compensation. Neuromagnetic responses were sampled continuously at 1 kHz with an acquisition bandwidth of 0.1– 330 Hz using a 306-sensor Elekta MEG system (Helsinki, Finland) equipped with 204 planar gradiometers and 102 magnetometers. Participants were monitored during data acquisition via real-time audio–video feeds from inside the shielded room. Each MEG dataset was individually corrected for head motion and subjected to noise reduction using the signal space separation method with a temporal extension (*21*).

Structural MRI Processing and MEG Coregistration

Preceding MEG measurement, four coils were attached to the participant's head and localized, together with the three fiducial points and scalp surface, using a 3-D digitizer (Fastrak 3SF0002, Polhemus Navigator Sciences, Colchester, VT, USA). Once the participant was positioned for MEG recording, an electric current with a unique frequency label (e.g., 322 Hz) was fed to each of the coils. This induced a measurable magnetic field and allowed each coil to be localized in reference to the sensors throughout the recording session. Since coil locations were also known in head coordinates, all MEG measurements could be transformed into a common coordinate system. With this coordinate system, each participant's MEG data were co-registered with structural T1-weighted MRI data in BESA MRI (Version 2.0) prior to source-space analysis. Structural MRI data were aligned parallel to the anterior and posterior commissures and transformed into standardized space. Following source analysis (i.e., beamforming; see *MEG Source Imaging and Statistics*), each participant's 4.0 x 4.0 x 4.0 mm functional images were also transformed into standardized space using the transform that was previously applied to the structural MRI volume and spatially resampled.

MEG Preprocessing, Time-Frequency Transformation, and Sensor-Level Statistics

Cardiac artifacts were removed from the data using signal-space projection (SSP), which was subsequently accounted for during source reconstruction (*22*). The continuous magnetic time series was then divided into 3200 ms epochs (-2200 to 1000 ms relative to the onset of the arrow stimuli; -700 to 2500 ms relative to the onset of the entraining stimuli), with the baseline extending from -2000 to -1600 ms prior to the onset of the arrow stimuli (and -500 to -100 ms prior to the onset of the entrainment stimuli). Recall that the entrainment stimuli appeared 1500 ms prior to the arrow stimuli and extended until their onset. Epochs containing artifacts were rejected using a fixed threshold method, supplemented with visual inspection. An average of 255.10 (SD = 13.57) trials per participant (out of 300 total) were used for further analysis, and the mean number of accepted trials per condition did not differ by entrainment frequency, flanker congruency, nor by an interaction between the two terms (2 x 2 repeated measures ANOVA; all p's > .20).

The artifact-free epochs were next transformed into the time-frequency domain using complex demodulation (*23*), and the resulting spectral power estimations per sensor were averaged over trials to generate time-frequency plots of mean spectral density. For visualization, these sensor-level data were normalized by each respective bin's baseline power, which was calculated as the mean power during the -2000 to -1600 ms time period. The time-frequency windows used for subsequent source imaging of the entrainment response were determined *a priori*, based on the duration and frequency of the entrained stimuli. For each of these responses, the spectral window was the frequency of entrainment (i.e., 10 or 30 Hz) ± 0.25 Hz, and the time windows were defined in two successive bins stretching from -1500 to -500 ms prior to arrow stimuli presentation. To facilitate comparison between the baseline and entrainment periods, the duration of the

baseline was extended in time (-2100 to -1600 ms) to match the length (500 ms) of the entrainment bins for source imaging. Since there were no strong *a priori* predictions about the spectral and temporal extent of the alpha-frequency neural responses to the arrow stimuli (i.e., after entrainment), the time-frequency windows used for source imaging of these responses were determined by statistical analysis of the sensor-level spectrograms across the entire array of gradiometers. Each data point in the spectrogram was initially evaluated using a mass univariate approach based on the general linear model. To reduce the risk of false positive results while maintaining reasonable sensitivity, a two stage procedure was followed to control for Type 1 error. In the first stage, paired-sample t-tests against baseline were conducted on each data point and the output spectrogram of t-values was thresholded to define time-frequency bins containing potentially significant oscillatory deviations across all participants. In stage two, time-frequency bins that survived the threshold were clustered with temporally and/or spectrally neighboring bins that were also above the threshold, and a cluster value was derived by summing all of the t-values of all data points in the cluster. Nonparametric permutation testing was then used to derive a distribution of cluster-values and the significance level of the observed clusters (from stage one) were tested directly using this distribution (*24, 25*). For each comparison, 10,000 permutations were computed to build a distribution of cluster values. Based on these analyses, the alpha time-frequency window that contained significant ($p < .05$) oscillatory events across all participants were subjected to a beamforming analysis. Subsequent MEG analyses were performed only on significant oscillatory events that began in the time window preceding the mean RT across all participants, so as to focus on responses underlying visuospatial attention and discrimination, rather than other processes inherent to the later portions of the task (i.e., motor initiation, response/error-checking, etc.).

MEG Source Imaging and Statistics

Cortical networks were imaged through an extension of the linearly constrained minimum variance vector beamformer (dynamic imaging of coherent sources; DICS; *26*), which applies spatial filters to time-frequency sensor data in order to calculate voxel-wise source power for the entire brain volume. The single images are derived from the cross spectral densities of all combinations of MEG gradiometers averaged over the time-frequency range of interest, and the solution of the forward problem for each location on a grid specified by input voxel space. Following convention, we computed noise-normalized, source power per voxel in each participant using active (i.e., task) and passive (i.e., baseline) periods of equal duration and bandwidth. Such images are typically referred to as pseudo-t maps, with units (pseudo-t) that reflect noise-normalized power differences (i.e., active vs. passive) per voxel. For the entrainment maps, the baseline was defined as -2100 to -1600 ms prior to arrow stimulus onset, while the baseline for the arrow stimulus response was defined as -400 to 0 ms prior to the onset of these stimuli. The baseline was shifted for the arrow stimulus response to account for the differential modulation of absolute alpha activity between the two entrainment conditions, as well as to account for individual variability in the strength of this entrainment response. The time-frequency window used to compute source images for the arrow-stimulus response extended temporally from 200 to 550 ms after the onset of the arrows, and spectrally from 8 to 14 Hz. To generate participant-level maps for the entrainment responses, we averaged the whole-brain images from the two previously described time-frequency windows (temporal extent: -1500 to -1000 ms and -1000 to -500 ms prior to flanker stimulus onset; spectral extent: the respective entrainment frequency ± 0.25 Hz) within each participant for each entrainment frequency, and these maps were then used to identify the peak voxel of the respective entrainment response. MEG pre-processing and

imaging used the Brain Electrical Source Analysis (BESA version 6.1) software. Entrainment peak voxels were identified as the voxel with the highest response magnitude from the grand average of the entrainment maps. Peak voxel locations for the arrow stimulus alpha response were extracted from the voxel with the highest average pseudo-t across all conditions and participants.

Virtual sensor (i.e., voxel time series) data were computed by applying the sensor-weighting matrix derived through the forward computation to the preprocessed signal vector, which yielded a time series for each source vector centered in the voxel of interest. For the entrainment responses, time series were extracted across a frequency range of ± 0.25 Hz centered on the entrainment frequency of interest, to maximize the entrainment signal and reduce interference from competing responses (i.e., the lateral desynchronization). In contrast, the time series for the arrow stimuli response was extracted across a frequency range of 8-14 Hz, to both maximize the temporal precision of the dynamic neural signals being investigated, as well as to better represent the endogenous cortical oscillations that normally serve selective attention processing (*27*). It should be noted that, due to the temporal resolution needed to derive a reliable measure of the entrainment responses, the temporal resolution for the entrainment time series was reduced compared to the 8-14 Hz time series. These time series were in absolute units (not relative to baseline) and, after initial analyses did not suggest substantial laterality effects, were averaged across both hemispheres into one voxel time series per response (i.e., entrainment and arrow stimulus responses) per participant for the desired time interval (i.e., the time periods preceding and succeeding the presentation of the arrow stimuli).

Statistical Analyses

Once the peak voxel time series were extracted for the responses of interest (i.e., the entrainment and arrow stimuli responses), we used cluster-based permutation statistics to test our hypotheses. This method was selected due to the statistical non-independence of neural time series data (as neural activations are not expected to persist across only one time sample), as well as to account for the time-varying nature of attentional effects on steady-state responses (*28*). This statistical procedure is largely similar to that used in the sensor-level statistics. Briefly, clusters of temporally contiguous, significant relationships were identified using a two stage procedure to control for Type 1 error. In the first stage, effect-size statistics were computed for each data point and the output spectrogram of these values were thresholded at $p < .05$ to define time bins that were potentially significant across all participants. In stage two, time bins that survived were clustered with temporally neighboring bins that were also above the threshold, and a cluster value was derived by summing all of the effect size statistics of all data points in the cluster. Nonparametric permutation testing was then used to derive a distribution of cluster-values and the significance level of the observed clusters (from stage one) were tested directly using this distribution. For each comparison, 10,000 permutations were computed to build a distribution of cluster values, and a final cluster threshold of $p < .05$ was considered statistically significant. Time series permutation testing was performed using custom-built functions in Matlab, behavioral ANOVAs and Bayesian ANOVAs were computed in JASP (*29*), and linear regression modeling was performed in R (*30, 31*). All statistical tests were performed two-tailed, unless explicitly stated otherwise.

Results:

Effects of Entrainment Frequency and Arrow Congruency on Behavior

All participants performed well on the task (mean = 94.09% correct, SD = 2.94%) and we did not examine accuracy due to ceiling effects. A 2 x 2 (entrainment frequency by

flanker arrow congruency) repeated-measures ANOVA on reaction time (RT) revealed a significant main effect of congruency ($F(1,22) = 101.48$, $p < .001$), supporting decades of previous literature using similar selective attention paradigms. In addition, and supporting our primary hypothesis of alpha-frequency entrainment as an amplifier of active inhibition of the visual cortex, we observed an interaction between frequency and congruency ($F(1,22) = 18.70$, $p < .001$), such that the effect of congruency (i.e., the difference in RT between incongruent and congruent trials) was significantly reduced for the 10 Hz entrainment trials (mean ΔRT = 18.15), as compared to the 30 Hz entrainment trials (mean ΔRT = 37.76; Figure 2). To further probe the robustness of this effect, we also performed a repeated-measures Bayesian analysis to determine the relative evidence of the alternative hypothesis in reference to the null hypothesis (Bayes Factor; BF_{10}) while controlling for the individual effects of congruency and frequency in the null model. This

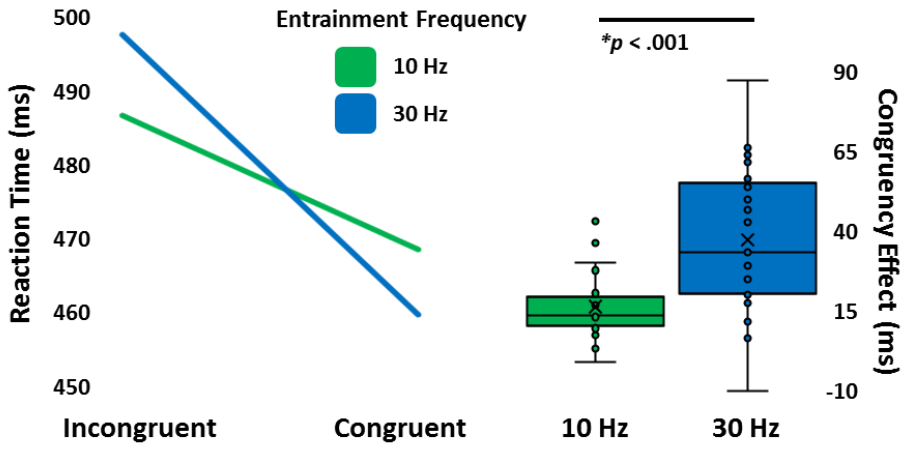

Figure 2. Reduction of the behavioral congruency effect by 10 Hz visual entrainment.

Visualization of the interaction term between the factors of entrainment frequency (10 or 30 Hz) and arrow congruency (incongruent or congruent) shows that participants exhibited a reduced effect of congruency in the 10 Hz entrainment condition, as compared to the 30 Hz condition. We propose that the 10 Hz entrainment increased alpha in visual regions corresponding to the flanking arrows, and that this increased alpha decreased local processing and thus decreased the impact of congruency between the flanking and central arrows. On the left, overall reaction time is denoted on the y-axis in milliseconds, while on the right, reaction time congruency differences (incongruent – congruent; in ms) are denoted on the y-axis.

analysis revealed an interaction term with an individual BF_{10} = 135.15, meaning that these data are ~ 135 times more likely to result from the alternative hypothesis than the null, which is considered very strong evidence for the alternative hypothesis. No significant main effect of entrainment frequency on reaction time was observed (p = .644).

Temporal-spectral Profile of Alpha-frequency Neural Oscillatory Dynamics

Before projecting our recorded neurophysiological signals into brain-space, we first needed to identify the temporal and spectral extent of our neural responses of interest (i.e., the entrainment and arrow stimulus responses). After decomposing the signal into time-frequency components across the entire array of sensors, we observed two distinct alpha-frequency neural responses, both consistent with previous reports (*16, 27*). In the 10 Hz entrainment condition, this analysis revealed a robust narrow-band synchronization at 10 Hz beginning almost immediately after the onset of the entrainment stimuli (1500 ms prior to the onset of the flanker arrow stimuli), and extending modestly into the presentation of the arrows. Further, we also observed a more broadband desynchronization in the alpha range (8 – 14 Hz) in both entrainment conditions, extending temporally from 200 to 550 ms after the onset of the arrow stimuli. A robust, narrow-band synchronization centered around 30 Hz was also observed in the 30 Hz entrainment condition, and this response also began 1500 ms prior to the onset of the flanker stimuli and extended slightly into the arrow presentation. These responses can be visualized in the data from a representative sensor (M2123) over the posterior occipital cortices in Figure 3.

To determine the cortical origins of these responses, each was subjected to an advanced source-reconstruction analysis (see Methods). In agreement with previous studies of visual entrainment and selective attention, the 10 Hz and 30 Hz narrow-band entrainment responses were found to originate from medial primary visual areas in the occipital cortex, while the 8 – 14Hz alpha desynchronization originated from slightly more

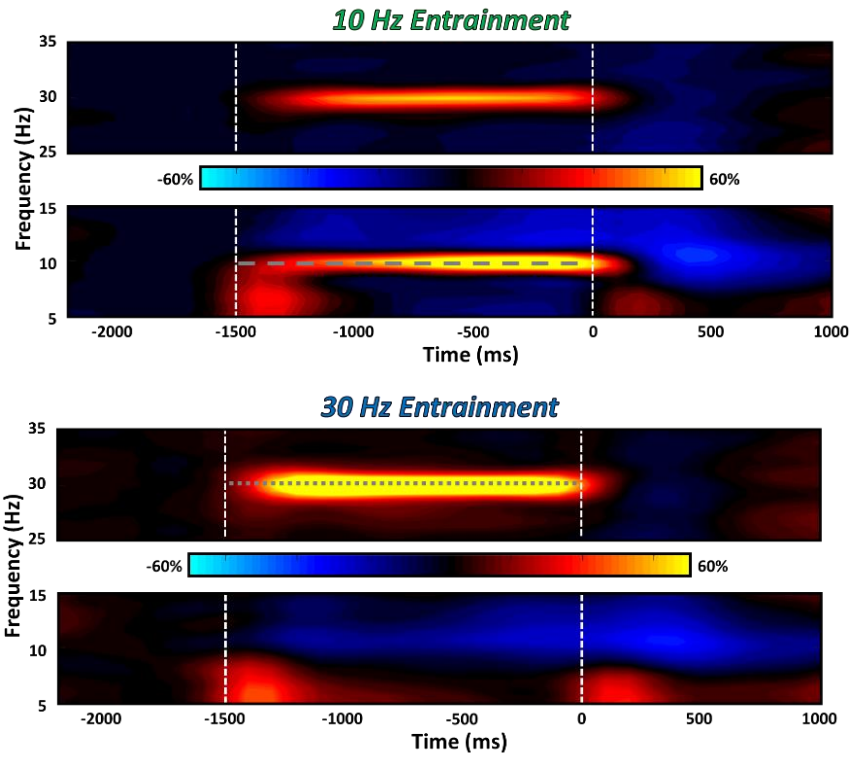

Figure 3. Temporal-spectral profile of visual entrainment dynamics.

The sensor plots display alpha and gamma frequency neural responses over occipital regions for the 10 Hz (top) and 30 Hz (bottom) entrainment conditions. Time (in milliseconds) is denoted on the x-axis at bottom, and frequency (in Hz) is denoted on the y-axis of each respective plot. The dashed white line at -1500 ms indicates the onset of the entrainment stimuli, and the dashed white line at 0 ms indicates the onset of the arrow stimuli. Entrainment frequency is denoted using a dashed grey bar for each condition. The color scale bar for percent change from baseline is displayed between the plots. These spectrograms represent group-averaged data from one posterior occipital gradiometer sensor (M2123) that was representative of the neural responses in this region.

lateral occipital regions. In order to better examine the distinct temporal profiles of each of these responses, we extracted peak voxel virtual sensor time-series from the 10 and 30 Hz entrainment conditions and the 8 – 14 Hz desynchronization peaks (in units of absolute power; nAm^2), and subjected the resulting frequency-specific power-envelopes to cluster-based permutation analyses to test our hypotheses.

Alpha Visual Entrainment Reduces the Effect of Distracting Stimuli

Providing robust support for our prediction that entrained alpha-frequency oscillations represent a form of active inhibition in visual cortex, time series permutation testing

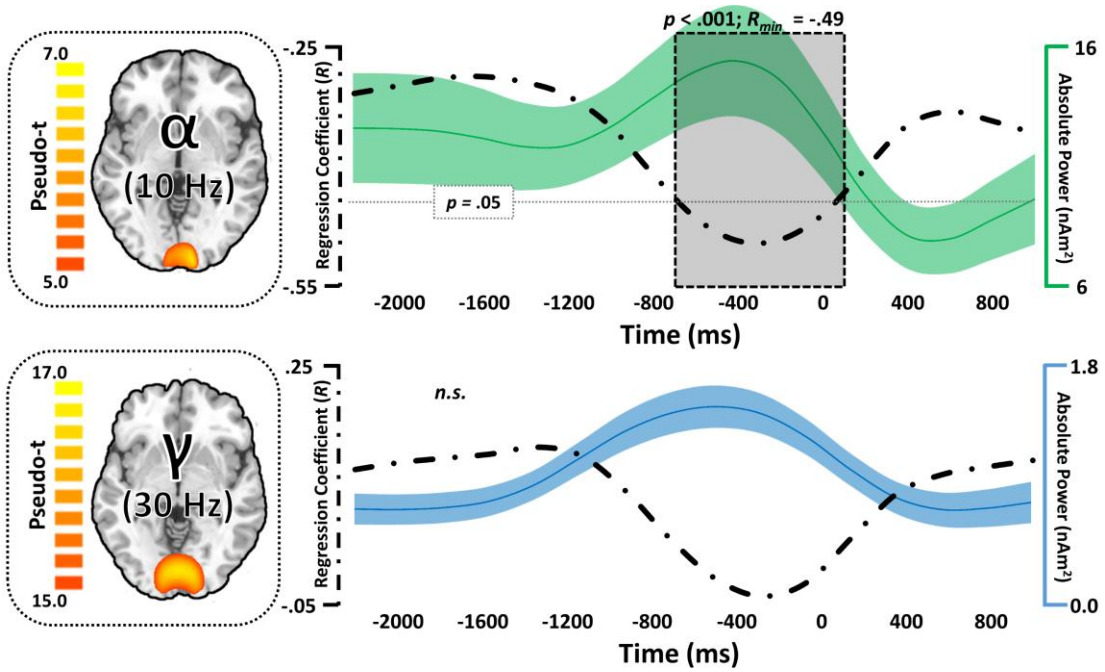

Figure 4. Power of visual entrainment at 10 Hz predicts congruency effects on behavior.

The source image maps (left) show the neural response to the 10 Hz (top) and 30 Hz (bottom) entrainment stimuli, with a color scale legend to the side representing group-averaged response amplitude (in pseudo-t values). Plots (right) are the power envelopes for the entrained medial occipital responses (green and blue lines) and the time-varying relationship between this respective entrainment response and the congruency effect on RT (dotted black lines). Time (in ms) is denoted on the x-axes, and the y-axes on the left and right display the relevant scales for the regression (in *R*) and power envelope (in nAm^2) time series, respectively. The shaded box indicates the temporal cluster identified as significant by permutation testing, with the peak regression effect size and cluster significance value denoted above. For reference, the horizontal gray dotted line indicates the initial cutoff of $p < .05$ used for the identification of potentially-significant clusters in the permutation analysis.

revealed that the power of the entrainment response at 10 Hz significantly predicted congruency differences in RT ($R_{min} = -.49$, $p_{cluster} < .001$; Figure 4, top), such that as the entrained response increased, the interference effect of the flanking arrows decreased. The predictive capacity of this signal increased steadily from the onset of the entrainment stimuli to the onset of the arrow stimuli, reaching significance in the peri-stimulus window for the presentation of the arrows (-600 to 200 ms). To enhance visualization and interpretation of this relationship, we averaged over this time window and plotted the resulting power values against congruency differences in RT (Figure 5). Additionally, although entrainment in the 30 Hz condition produced a robust neural response at 30 Hz (Figure 3), the power of this response did not predict the congruency effect on RT ($R_{max} =$

.12, R_{min} = -.004, no significant clusters; Figure 4, bottom), signifying that this effect is specific to the alpha-band, and not a general effect of visual entrainment.

Finally, due to the importance of neural congruency effects in lateral visual regions in the alpha-band (*27*), we hypothesized that the power of 10 Hz entrainment might be reflected in the difference values of the neural desynchronization responses to incongruent versus congruent trials. To test this hypothesis, we computed a timepoint-by-timepoint ratio of the alpha desynchronization response to the incongruent/congruent flanker stimuli. We then regressed the power of the 10 Hz entrainment response (averaged over the previously identified -600 to 200 ms time window) on these data, and corrected for multiple comparisons using a cluster-based permutation approach. This relationship was indeed significant from 75 to 325 ms (R_{max} = .48, $p_{cluster}$ < .001, one-tailed) after arrow onset, such that as the power of the entrainment response increased, the absolute power of the incongruent, relative to the congruent, response, also increased. Again, to enhance visualization, we averaged over this significant time window and plotted this relationship in Figure 6. In other words, since this response was a desynchronization from pre-stimulus levels of alpha (8-14 Hz) activity, the participants who exhibited stronger entrainment at 10 Hz tended to have a weaker response to the incongruent (relative to the congruent) stimuli. In contrast, those who did not entrain as strongly tended towards the more

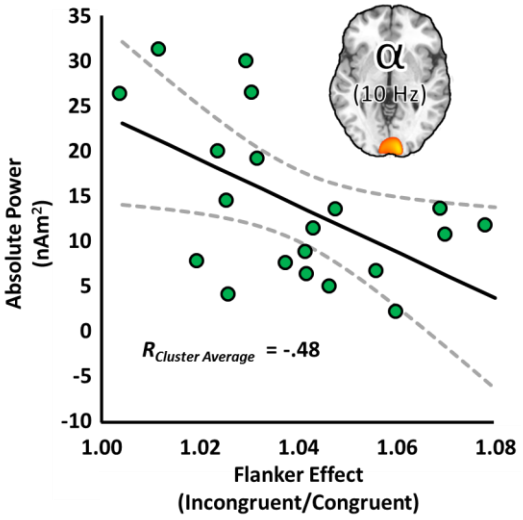

Figure 5. Relationship between the 10 Hz visual entrainment response and behavior.

This scatterplot shows the relationship between the 10 Hz visual entrainment response in primary visual cortex averaged across the significant time-window identified in the permutation analysis (denoted on the y-axis in nAm^2) and the effect of congruency on behavior (denoted on the x-axis as a ratio of incongruent RT/congruent RT). The line of best-fit and the regression coefficient for this relationship are overlaid on the plot in black. The grey dotted lines indicate the 95% confidence interval for this relationship.

prototypical pattern (*27*) of a stronger response to incongruent (relative to congruent) stimuli.

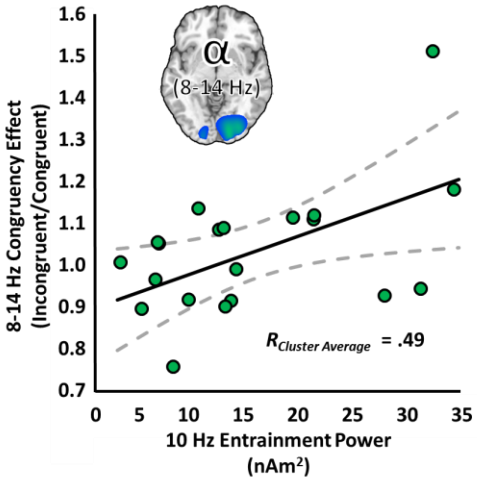

Figure 6. Relationship between entrained and endogenous visual alpha responses.

This scatterplot shows the relationship between the 10 Hz visual entrainment response in primary visual cortex averaged across the significant time-window identified in the permutation analysis (denoted on the x-axis in nAm^2) and the effect of congruency on the 8 – 14 Hz alpha desynchronization response (denoted on the y-axis as a ratio of incongruent response power/congruent response power). The line of best-fit and the regression coefficient for this relationship are overlaid on the plot in black. The grey dotted lines indicate the 95% confidence interval for this relationship.

Discussion:

Alpha-frequency oscillatory activity in the parieto-occipital cortices has been repeatedly connected to the active inhibition of irrelevant visual information (*1, 3, 5-9*), however causal links between neurophysiology and behavioral outcomes have been difficult to draw. Several studies have used visual stimuli that flicker at specific frequencies to systematically enhance occipital alpha oscillations and impair visual perception of target stimuli (*13-17, 19, 32*), but no study to date had investigated whether this effect could be extended to impair perception of distracting stimuli (i.e., for a net benefit). In this study, we used a modified arrow-based version of the classic Eriksen flanker selective attention paradigm (*33*), paired with frequency-targeted flickering stimuli and dynamic brain imaging using MEG to address these gaps in the scientific literature. By entraining visual cortex at 10 or 30 Hz only over the visual field of the to-be-presented distractor stimuli, we provide robust evidence for the role of pre-stimulus alpha entrainment in the active inhibition of visual cortex function, even when this inhibition is beneficial to task performance. These findings, as well as their broader implications, are discussed below.

Regarding our behavioral data, we had one primary hypothesis: that alpha-frequency (10 Hz) entrainment relative to 30 Hz entrainment would selectively reduce the congruency (i.e., flanker) effect of the interfering arrow stimuli, which was supported. Further, due to the literature suggesting substantial individual variability in neural responses to entraining stimuli (*34*), we hypothesized that the magnitude of the neural response to entrainment would predict this behavioral modulation, such that higher entrainment power at 10 Hz would predict a greater reduction in behavioral interference. Again this hypothesis was supported. Importantly, we found no main effect of entrainment frequency on overall reaction time (i.e., congruency-invariant RT), signifying that differences in entrainment did not differentially modulate general alertness on the task, but rather acted to specifically inhibit visual distractor information in the 10 Hz condition. The importance of this finding is two-fold. First, alpha entrainment of visual cortex has been found previously to inhibit visual perception, and these data provide additional support for this. Steady-state visual stimuli have been used for decades to “tag” stimuli in cognitive experiments using a purportedly inert/neutral frequency of entrainment, the representations of which (i.e., SSVEPs) could then be localized within relevant neural networks and used as markers of lateralization and other phenomena. The current study provides evidence that these stimuli are not only non-inert, but in some cases actually serve as potent modulators of very low-level cognitive processes (i.e., visual perception). Further, the finding that this effect was specific to the 10 Hz entrainment condition suggests a particular sensitivity of the occipital cortex to alpha-frequency rhythmic visual input. Through further research, it might be possible to use this knowledge to better understand low-level perceptual deficits in patient populations, or to enhance attention in cognitively demanding settings. Second, previous research on this topic has focused on impairing the perception of target stimuli, and until now it has remained uncertain whether this effect could be translated to the inhibition of distracting visual information. Our finding

that distracting information can also be compromised by 10 Hz visual entrainment notably strengthens the notion that the gating of information seen with alpha entrainment begins at visual perception. Interestingly, our findings also introduces the possibility of using alpha entrainment to positively modulate performance on selective attention tasks, by decreasing the negative effect of distracting environmental inputs.

In regards to our neural data, we hypothesized that the power of visual entrainment in the 10 Hz condition would significantly covary with the reduction of distractor inhibition discussed above. We observed such a relationship during the time-window prior to and encompassing the onset of the selective attention stimuli, further strengthening the link between alpha entrainment and visual inhibition. The 10 Hz entrainment response also covaried significantly with the effect of stimulus congruency on the occipital alpha desynchronization, which is a neural response that has previously been found to index the effect of flanker interference (*27*), as well as active visual processing more generally. The nature of this relationship was such that as 10 Hz entrainment in primary visual cortex increased, the difference in this response between incongruent and congruent trials was reduced, signifying a modulation of endogenous, perceptually relevant patterns of neural activity by 10 Hz entrainment. Finally, 30 Hz entrainment exhibited no relationship with task performance, indicating that these effects are frequency-specific, and not a general result of visual entrainment.

Of course, this research is not without limitations. First and foremost, due to the nature and focus of our experimental paradigm and hypotheses, the effect of other oscillatory frequencies was not explored. Neural oscillations in cortices other than occipital, and in frequencies other than alpha, have been found to be essential to selective attention processing (*27, 35*) and visual perception (*36-45*), and thus might have displayed interesting interactions with the occipital dynamics that we investigated, however the focus of this study was to examine the alpha-occipital dynamics in detail, and future research

will be needed to flesh out the effects of other oscillatory responses. Second, although we did find the hypothesized reduction in RT in the incongruent condition following 10 Hz, relative to 30 Hz, entrainment, we also observed the opposite effect in the congruent condition. In other words, it appears that in addition to decreasing RT on incongruent trials, 10 Hz entrainment also tended to increase RT on congruent ones. Although intriguing, this finding was unexpected, and future research is needed to understand its origin. Third, we made no attempt here to vary the delay between the end of the visual entrainment and the onset of the task stimuli (i.e., the arrows), as has been done in other studies (*16*). Thus, since we presented our task-stimuli at what would effectively be the "peak" of the entrained rhythm, it remains possible that our results would have been different if we had instead presented them at the "trough." Finally, it should be noted that since we only used one control entrainment condition that was "faster" than the 10 Hz condition (i.e., 30 Hz), it remains a possibility that the observed reduction in distractor effects was not alpha-specific. However, while theoretically plausible, this explanation is in direct conflict with the vast majority of literature on this topic, and would imply that the alpha-specific effects of entrainment previously observed on imperative stimuli do not persist when the stimuli are instead distracting. Thus, we remain convinced that alpha-specificity is the more parsimonious explanation.

Despite these limitations, this study provides new insight into the effects of alpha entrainment on visual perception, and supports the pivotal role of alpha oscillations in selective attention function. Further, these findings suggest that these signals might be used to enhance selective attention function in the presence of visual distractors. This is essential knowledge, which could potentially be leveraged to enhance selective attention abilities in cognitively taxing environments. These findings also provide novel information regarding the coding of visual saliency in the human visual cortex, and will hopefully motivate further study in this area.

CHAPTER 2: ALPHA-FREQUENCY INTERACTIONS BETWEEN VISUAL AND ATTENTION SYSTEMS

The material presented in this chapter was previously published in Wiesman and Wilson, 2019, Frontoparietal networks mediate the behavioral impact of alpha inhibition in visual cortex, Cerebral Cortex, 29(8):3505-3513.

Introduction:

The ability to rapidly perceive salient components of the visual environment is essential for normative cognitive function, and is thought to be supported by both "bottom-up" sensory (e.g., retinotopic activation in primary visual cortices) and "top-down" regulatory (e.g., activation in fronto-parietal attention networks) processes. Further, spectrally defined patterns of neural oscillatory activity have been found to play a key role in visual processing. In particular, alpha-frequency (8 – 13 Hz) rhythms in parietal and occipital cortices are thought to be essential for the active inhibition of irrelevant or distracting visual inputs (*1, 3, 4, 15, 16, 46*). Perhaps unsurprisingly then, alpha-band oscillations, both within and outside of parieto-occipital areas, have also been found to be essential to visual attention (*27, 47-53*) and are a potential spectral point of mediation between bottom-up sensory mechanisms and top-down regulatory systems in the human brain.

Unfortunately, experimental manipulation of alpha-frequency activity in the human brain is difficult in healthy individuals, making causal interpretations of the role of alpha oscillations problematic. To this end, many researchers have turned to noninvasive neurostimulation (*53-60*). For example, Capotosto et al. (*53*) used repetitive transcranial magnetic stimulation (rTMS) and EEG to systematically disrupt alpha oscillations in the right parietal and frontal cortices prior to the performance of a visual target identification task. They showed that the disruption of alpha oscillations impaired the participant's ability to identify subsequently-presented targets in the visual space. In addition, this impairment covaried significantly with the level of alpha-frequency disruption in parietal and occipital electrodes. These findings provide robust support for the involvement of alpha activity in

fronto-parietal networks in the perception of objects in the visual space. However, the experimental design precluded the authors from investigating other attention-network regions that may have been involved in this process, and also from examining whether signals from bottom-up systems interfered with attention networks.

Beyond neurostimulation, other studies have used flickering visual stimuli to systematically modulate endogenous rhythms in the human brain, by “entraining” activity in sensory cortices at targeted frequencies (*13, 15, 16, 34, 61, 62*). However, few experiments have investigated the interaction between exogenously entrained neural oscillatory activity in primary visual cortex and the endogenous patterns of rhythmic neural activity that support visual attention and perception. Because of this void, the mechanism by which rhythmic alpha activity in visual cortex exerts its functionally inhibitory effect remains unclear. On the other hand, studies have shown that visual alpha activity covaries with target perception (*3, 16, 49, 63*), is involved in the protection of stimulus representations during working memory maintenance, and is often correlated with accuracy and load on such working memory tasks (*4, 8, 64*). Alpha activity is also known to be widely-distributed across the human brain (*65*). In fact, prior studies using flickering stimuli have reported spatially widespread effects unique to alpha range entrainment (*61, 66, 67*). Thus, it seems likely that at least some part of this alpha-related modulation is taking place in top-down regulatory networks. If this is the case, it is important to understand (1) which specific cortical regions are implicated in this modulation, (2) whether modulation at these regions affects visual perception, and (3) to what extent this modulation statistically mediates the relationship between entrained dynamics in primary visual cortex and visual perceptual abilities.

In this study, we used 10 Hz visual entrainment to modulate the endogenous alpha oscillations in occipital cortices that are known to support visual processing, mapped the resulting neural perturbations using MEG, and delineated the effects of these neural

perturbations on visual perceptual abilities. Interestingly, previous studies have found that attentional deployment enhances the neural response at corresponding retinotopic areas to entraining visual stimuli, with the notable exception of alpha-frequency entrainment, where results have been less consistent, and attention often shows either a reduced or negative effect on entrainment power (*52, 66, 68*). Given these data, we did not hypothesize that entrainment to the 10 Hz flicker would necessarily be enhanced by attentional cueing, but we did expect the cueing effect (i.e., the degree to which cueing biased the neural response toward or away from the entraining stimuli) to covary with visual perception of the attended stimulus, as indexed by performance metrics on the task. Further, we hypothesized that this cueing effect on the 10 Hz entrainment response would covary with activity in top-down attention networks, signifying potential interference of processing in these networks by the 10 Hz entrainment signal. Finally, we expected that the relationship between this cueing effect and task performance would be mediated by activity in the same fronto-parietal regulatory networks, signifying an interfering effect of 10 Hz visual entrainment on attentional processing.

Methods:

Participants

Twenty-three healthy young adults were recruited for the study (M_{age} = 26.09; age range: 20-33 years; 16 males; 21 right-handed). Exclusion criteria included any medical illness affecting CNS function, any neurological or psychiatric disorder, history of head trauma, current substance abuse, and any non-removable metal implants that would adversely affect MEG data acquisition. All participants had normal or corrected-to-normal vision. The Institutional Review Board at the University of Nebraska Medical Center reviewed and approved this investigation. Written informed consent was obtained from

each participant following detailed description of the study. All participants completed the same experimental protocol.

MEG Experimental Paradigm and Behavioral Data Analysis

We used a modified version of the classic Posner cueing paradigm (*69*) to engage alpha-frequency networks related to the orienting of attention (Figure 7). Each trial began with a central fixation that was presented for a randomly-varied inter-stimulus interval of 2000-2400 ms. Participants were instructed to fixate centrally on this point of the screen for the entirety of the experiment. Subsequently, the fixation was replaced with an arrow-cue pointing towards the left or right. The centrally presented arrow-cue remained on the screen for 2000 ms and correctly predicted the side of the to-be-presented probe stimulus on 100% of trials. On each side of the cue was an entrainment stimulus (in the form of an outline of a box) that flickered at a frequency of 10 Hz. For clarity, both sides flickered in all trials, regardless of the cue direction. At the end of the entrainment period, the boxes stopped flickering and a small break appeared on either the top or bottom side of the box (cued side only) for 1000 ms. The presentation of this probe stimulus occurred at the same time relative to flicker offset for every trial, which aligned temporally with the peak of the ongoing 10 Hz phase of the entraining visual stimuli. Prior to starting the experiment, participants were instructed to respond as quickly and accurately as possible as to whether the break appeared on the top (index finger) or bottom (middle finger) of the cued box, using their right hand on a non-magnetic button pad. The entraining and probe stimuli occupied the same spatial areas of the visual field, so to entrain the visual cortex corresponding to the subsequently-presented probe stimulus. The 200 total trials were pseudo-randomized and equally split between each of the cue (left and right) and response (top and bottom) conditions. Correct responses were also pseudo-randomized, such that the same response was never repeated more than twice. Custom visual stimuli

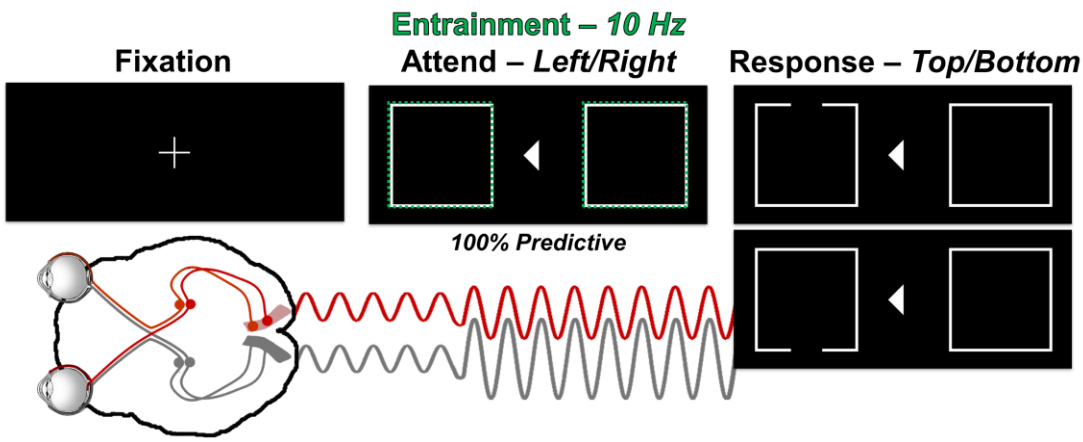

Figure 7. Visual entrainment Posner task paradigm and neurophysiological hypothesis.

Each trial began with a central fixation that was presented for 2200 ms (randomized jitter of ± 100 ms). After this, a 100% predictive arrow-cue pointing towards the left or right appeared centrally for 2000 ms. On each side of this cue was an entrainment stimulus (highlighted here by green dotted lines for clarity) that flickered at a frequency of 10 Hz. At the end of the entrainment period, the box stimuli ceased flickering, and a small break appeared on either the top or bottom side of the box on the cued side for 1000 ms. Participants responded as quickly and accurately as possible as to whether the break appeared on the top (index finger) or bottom (middle finger) of the cued box. The entraining and probe stimuli occupied the same spatial areas of the visual field, which ensured that the probe stimulus would be processed by entrained visual regions. The visual pathway and sine waves below reflect one of our neurophysiological hypotheses, which included a general increase in 10 Hz amplitude during the entrainment period, and either a negative or negligible effect of attention on the amplitude of this signal (red line), as has been reported in a number of previous studies. For clarity, although we did not predict a general effect of attention on entrainment across all participants, we did expect that the magnitude of attentional modulation on visual dynamics would affect task performance.

were programmed in Matlab (Mathworks, Inc., Massachusetts, USA) using *Psychophysics Toolbox Version 3* (*20*) and back-projected onto a semi-translucent nonmagnetic screen using a Panasonic PT-D7700U-K model DLP projector with a refresh rate of 60 Hz and a contrast ratio of 4000:1. Flickering stimuli were presented as a square-wave function with a frequency of 10 Hz (3 frames on/3 frames off; ~16.67 ms per frame), with a luminance contrast of 100% (white stimuli on a black background). Total MEG recording time was approximately 17 minutes. For each participant, accuracy data were computed as a percentage (correct/total trials). Reaction time (RT) data were also extracted for each individual trial, incorrect and no-response trials were removed, and outliers were then excluded based on a standard threshold of ± 2.5 standard deviations from the mean.

MEG Data Acquisition

All recordings were conducted in a one-layer magnetically-shielded room with active shielding engaged for environmental noise compensation. Neuromagnetic responses were sampled continuously at 1 kHz with an acquisition bandwidth of 0.1– 330 Hz using a 306-sensor Elekta MEG system (Helsinki, Finland) equipped with 204 planar gradiometers and 102 magnetometers. Participants were monitored during data acquisition via real-time audio-video feeds from inside the shielded room. Each MEG dataset was individually corrected for head motion and subjected to noise reduction using the signal space separation method with a temporal extension (*21*).

Structural MRI Processing and MEG Coregistration

Preceding MEG measurement, four coils were attached to the participant's head and localized, together with the three fiducial points and scalp surface, using a 3-D digitizer (Fastrak 3SF0002, Polhemus Navigator Sciences, Colchester, VT, USA). Once the participant was positioned for MEG recording, an electric current with a unique frequency label (e.g., 322 Hz) was fed to each of the coils. This induced a measurable magnetic field and allowed each coil to be localized in reference to the sensors throughout the recording session. Since coil locations were also known in head coordinates, all MEG measurements could be transformed into a common coordinate system. With this coordinate system, each participant's MEG data were co-registered with structural T1-weighted MRI data in BESA MRI (Version 2.0) prior to source-space analysis. Structural MRI data were aligned parallel to the anterior and posterior commissures and transformed into standardized space. Following source analysis (i.e., beamforming), each participant's 4.0 x 4.0 x 4.0 mm functional images were also transformed into standardized space using the transform that was previously applied to the structural MRI volume and spatially resampled.

MEG Preprocessing, Time-Frequency Transformation, and Sensor-Level Statistics

Cardiac artifacts were removed from the data using SSP, which was subsequently accounted for during source reconstruction (*22*). The continuous magnetic time series was then divided into 3500 ms epochs, with the baseline extending from -2500 to -2000 ms prior to the onset of the probe stimuli, which was defined as 0 ms. Epochs containing artifacts were rejected per participant using a fixed threshold method, supplemented with visual inspection. An average amplitude threshold of 1092.39 (SD = 212.86) fT and an average gradient threshold of 107.95 (SD = 38.84) fT/s was used to reject artifacts. Across the group, an average of 160.83 (SD = 8.72) trials per participant were used for further analysis.

The artifact-free epochs were next transformed into the time-frequency domain using complex demodulation, and the resulting spectral power estimations per sensor were averaged over trials to generate time-frequency plots of mean spectral density. These sensor-level data were normalized by each respective bin's baseline power, which was calculated as the mean power during the -2500 to -2000 ms time period. The time-frequency windows used for subsequent source imaging of the entrainment response were determined *a priori*, based on the duration and frequency of the entrained stimuli. The spectral window was defined as the frequency of entrainment (i.e., 10 Hz) ± 0.2 Hz, and the time window was defined from 750 to 0 ms prior to presentation of the probe stimulus. Although entrainment did elicit a neural synchronization beginning earlier (roughly 1500 ms prior to the onset of the probe stimulus, see below), only the time period that exhibited the strongest response (-750 to 0 ms) was used in order to maximize the signal-to-noise ratio of the subsequent source images.

MEG Source Imaging and Statistics

Cortical networks were imaged using the DICS beamformer (*26*), which applies spatial filters to time-frequency sensor data in order to calculate voxel-wise source power for the

entire brain volume. The single images are derived from the cross spectral densities of all combinations of MEG gradiometers averaged over the time-frequency range of interest, and the solution of the forward problem for each location on a grid specified by input voxel space. Following convention, we computed noise-normalized, source power per voxel in each participant using active (i.e., task) and passive (i.e., baseline) periods of equal duration and bandwidth. Such images are typically referred to as pseudo-t maps, with units (pseudo-t) that reflect noise-normalized power differences (i.e., active vs. passive) per voxel. MEG pre-processing and imaging used BESA (version 6.1) software. Left and right hemisphere entrainment peak voxels were identified as the voxel in occipital cortex with the highest average pseudo-t from grand-averaged whole-brain images across all participants. These bilateral peaks were then used to compute response values separately for the attended and unattended hemifields for each trial, based on the cue direction in that trial. For example, on a left-cued trial, the entrainment peak from the right (contralateral) primary visual cortex would represent the attended hemifield, while the peak from the left (ipsilateral) primary visual cortex would represent the unattended hemifield. To investigate hypothesized covariance between cueing effects and other metrics, a cueing ratio was derived from these peak values for each participant ((attended+100)/(unattended+100)). For interpretation, higher cueing effect values indicate an increased cueing bias of neural entrainment responses toward the attended hemifield, while lower values indicate biased neural entrainment away from the attended side. Note that a constant value of 100 was added prior to the division of these data, to account for any negative amplitude values.

Statistical Analysis

Pearson product-moment correlation coefficients were computed to test hypothesized covariance between metrics, with post-hoc control for multiple comparisons using

Bonferroni correction unless explicitly stated otherwise. To test hypothesized mediations, relevant metrics were extracted from behavioral and neurophysiological data, and the resulting values were used in stepwise linear regressions to determine whether an indirect effect was plausible. If the effect of the independent variable was reduced to the extent of no longer being significant, a nonparametric bootstrapping analysis with 10,000 simulations was used to test the significance of potential mediation (i.e., indirect) effects. Correlation coefficients, linear regressions, and mediation bootstrapping analyses were computed in R (*30, 31*). Finally, for whole-brain correlation maps, voxel-wise correlations were computed between neural activity in the participant-level whole brain maps and relevant continuous metrics (i.e., cueing effects on entrainment). For these maps, a stringent statistical threshold of $p < .0005$ was used, along with a cluster threshold (k) of at least 200 contiguous voxels. In addition, all peaks reported in this analysis also survived a stringent second-level correction using cluster-based permutation testing (initial threshold: $p < .0005$; 10,000 permutations).

Results:

Temporal-spectral Profile of 10 Hz Entrainment

Before projecting our recorded neurophysiological signals into brain-space, we first needed to identify the temporal and spectral extent of the neural responses of interest. After transforming the MEG signals into time-frequency space, we observed a robust, narrow-band synchronization centered at 10 Hz over occipital sensors. This synchronization began roughly 500 ms after the onset of the entrainment stimuli, and reached a maximum amplitude between 750 and 0 ms prior to the onset of the probe (Figure 8, top). To maximize the signal-to-noise ratio of the input data, the time window with the highest amplitude (750 to 0 ms before probe onset) was used for subsequent source imaging.

Effects of Entrainment on Behavior

Consistent with previous reports, the 10 Hz entrainment response was found to originate from bilateral sources in the primary visual cortices (Figure 8, top inlay). To investigate the general effect of entrainment (i.e., regardless of attentional cueing effects), we extracted peak voxel amplitude values from the 10 Hz entrainment response in each hemisphere for each participant, and averaged these values across bilateral primary visual cortices. This metric of cueing-invariant entrainment significantly correlated with accuracy on the task (r = .58, p = .004; Figure 8, bottom left), such that as alpha entrainment increased, accuracy improved. Although of interest in itself, this relationship was not the primary focus of our investigation, as it does not account for attentional cueing and likely reflects a more

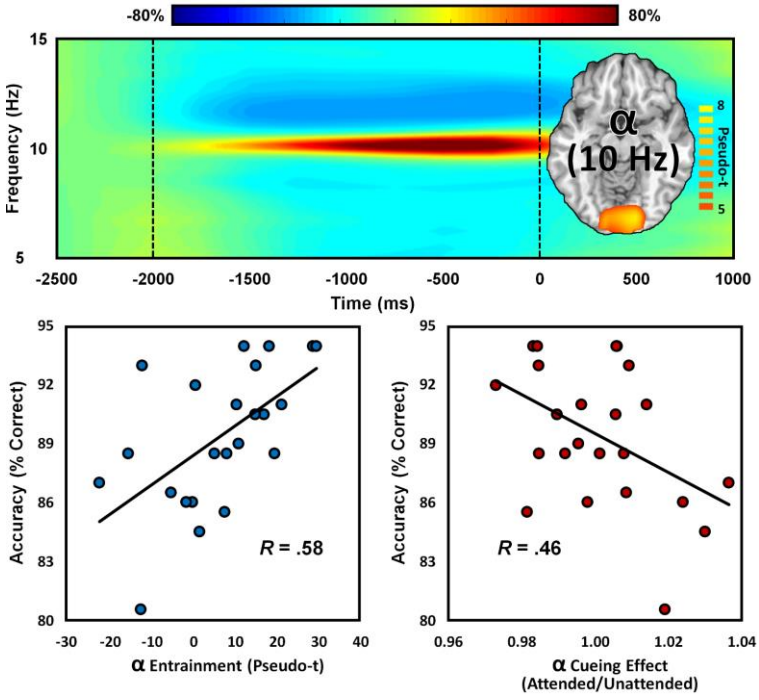

Figure 8. Spectral, temporal, and spatial definitions of neural responses to 10 Hz entrainment, and interactions with attention and behavior.

The MEG sensor spectrogram (top) displays alpha-frequency neural responses over occipital regions during the 10 Hz entrainment period, with time (in milliseconds) denoted on the x-axis and frequency (in Hz) denoted on the y-axis. The dashed black line at -2000 ms indicates the onset of the entrainment stimuli, and the dashed black line at 0 ms indicates the onset of the probe stimulus. The color scale bar for percent change from baseline is displayed above the plot. This spectrogram represents group-averaged data from one gradiometer sensor that was representative of the neural responses in occipital cortices. Inlaid on the far right is the source-imaged representation of this response, with the color scale bar to the right denoting response amplitude in pseudo-t units. The correlation plots below show the relationships between accuracy (on both y-axes, denoted in % correct trials) and bilaterally-averaged entrainment power (denoted on the x-axis in pseudo-t) on the left, and the cueing effect (denoted on the x-axis as a ratio of attended/unattended source amplitude) on the right. Lines of best-fit, as well as the relevant covariance coefficients, are overlaid on each plot.

general index of alertness when performing the task. To examine the effect of attentional cueing more directly, we used the same voxels described above and derived the amplitude values for 10 Hz entrainment responses corresponding to the attended and unattended hemifield separately, and then computed a ratio of these values for each participant (i.e., the *cueing ratio*; (attended+100)/(unattended+100)). For interpretation, higher cueing effect values indicate an increased cueing bias of neural entrainment responses toward the attended hemifield, while lower values indicate biased neural entrainment away from the attended side. Intriguingly, the effect of attentional cueing on the entrainment response also significantly covaried with accuracy (r = -.46, p = .029; Figure 8, bottom right). Confirming our primary hypothesis, this relationship was reversed in direction, such that greater entrainment on the attended (relative to the unattended) side was related to decreased performance on the task, indicating reduced visual perceptual abilities in that same visual space. In other words, regardless of the overall amplitude of visual entrainment, greater attentional "enhancement" of the 10 Hz entrainment in the cued hemifield (i.e., where the probe subsequently appeared) was associated with reduced performance.

Fronto-parietal Networks Covary with Attentional Modulation of 10 Hz Entrainment

To explore if any "higher-order" cortical regions were also affected by the 10 Hz entrainment, we next computed a whole-brain correlation between each participant's entrainment cueing ratio and voxel-wise amplitude values of neural activity during the entrainment period (-750 to 0 ms; Figure 9, top). Using stringent statistical thresholds, activity in a widespread network of regions was found to covary with the entrainment cueing effect, including nodes in the right dorsolateral prefrontal (r-dlPFC, r_{max} = -.72), right primary motor (r-M1, r_{max} = -.81), bilateral superior parietal (r-SPC, r_{max} = -.73; l-SPC, r_{max} = -.70), and midcingulate (MCC, r_{max} = -.70) cortices (all p's < 5 x 10^{-4}, cluster-corrected,

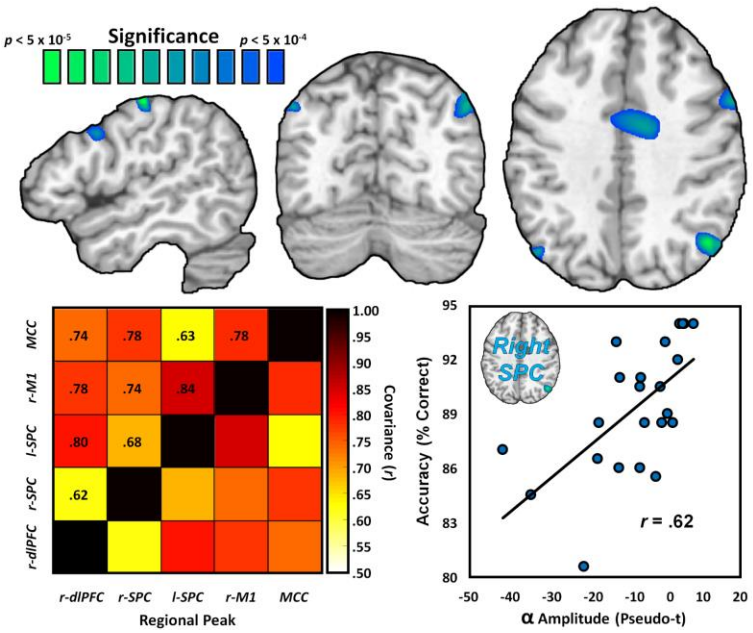

Figure 9. Fronto-parietal networks mediate the relationship between visual cueing effects and behavior.

(Top) Whole-brain covariance maps of the entrainment cueing effect and response amplitude, with significant peaks in the right dorsolateral prefrontal, right primary motor, mid-cingulate, and bilateral superior parietal cortices. A color scale bar depicting the statistical significance is displayed in the upper left. (Bottom left) Covariance matrix representing the intra-network covariance of all network nodes mentioned above. The correlation coefficient representing the amplitude relationship between each set of regional peaks is indicated by the scale bar on the right, and the individual effect size (*r*) for each relationship is overlaid on its appropriate square. (Bottom right) Correlation plot showing the relationship between accuracy (on the y-axis, denoted in % correct trials) and response amplitude in the right superior parietal region (denoted on the x-axis in pseudo-t). A line of best-fit and the covariance coefficient for the relationship are overlaid on the plot.

k = 200). The direction of this relationship was similar across all nodes, such that as entrainment in the attended (relative to the unattended) hemifield increased, the 10 Hz response in these other regions decreased (i.e., desynchronized). Such *decreases* from baseline levels of synchrony are well supported as being indicative of active neuronal processing at this (alpha) frequency (*1, 52, 70, 71*). Thus, this covariance should be interpreted as increased entrainment (i.e., interference) in visual cortex on the attended side leading to greater neural responses in fronto-parietal cortices. Interestingly, the peak voxel amplitude at all five of these nodes was robustly correlated, which further supports that these regions were functioning in concert (all *r*'s > .60 and all *p*'s < .05, Bonferroni-corrected; Figure 9). Finally, we investigated the behavioral relevance of these regions by correlating amplitude values extracted from each peak voxel with task accuracy. After Bonferroni correction, only activity in the r-SPC (*r* = .62, *p* = .005, Bonferroni-corrected; Figure 9) and l-SPC (*r* = .55, *p* = .035, Bonferroni-corrected) was found to significantly

predict accuracy on the task, such that a stronger neural response in these regions (i.e., a greater decrease from baseline) was related to worse task performance (i.e., lower accuracy).

Regions of the Fronto-parietal Network Mediate the Behavioral Impact of 10 Hz Entrainment

Since the above analyses indicated that the two superior parietal peaks were the most relevant nodes in this fronto-parietal network for task performance, we performed a mediation analysis in which each of these regions (i.e., left and right) was the prospective mediator between the entrainment cueing ratio and task accuracy. Upon addition of activity values from each of the superior parietal peaks, the relationship between cueing effects on entrainment and task performance became non-significant, indicating a full mediation. After testing each indirect effect with a statistically stringent bootstrapping procedure, activity in both the l-SPC (b = -.68, p = .029, 95% CI = -1.42, -0.07) and r-SPC (b = -.99, p = .008, 95% CI = -1.80, -0.25) was found to significantly mediate the relationship between the entrainment cueing ratio and visual perceptual abilities (i.e., task accuracy).

Discussion:

In this study, we used a modified Posner attention-cueing paradigm that included a 10 Hz flicker component to perturb visual perceptual networks during task performance, while simultaneously measuring the neural dynamics underlying these perturbations. *En masse*, our findings support both the role of alpha oscillations in functional inhibition of visual perception, as well as a powerful interference effect on fronto-parietal attention networks by 10 Hz entrainment. More specifically, we found that increased cue biasing of neural entrainment responses towards the attended hemifield was related to reduced task accuracy. In other words, participants with higher 10 Hz entrainment over the visual field

of the to-be-presented stimulus exhibited impaired visual perception. Additionally, this cueing effect covaried robustly with activity in a network of fronto-parietal regions, and activity in this network fully mediated the relationship between the entrainment cueing effect and visual impairment. In sum, these results support not only the functionally inhibitory role of 10 Hz activity in visual cortices, but also the ability of interfering inhibition in these visual networks to propagate to “higher-order” networks and thereby impair visual perception. Thus, these findings also provide direct support for a spectrally defined interaction between primary visual and fronto-parietal attention networks in the alpha band, which can be experimentally manipulated by means of artificially induced alpha-frequency visual entrainment.

Numerous studies have suggested that alpha-frequency oscillations in visual cortices reflect a functionally inhibitory signal (*1-3, 5-8, 15, 16, 49, 51, 52, 54*), and our data once again clearly support this conceptualization. Namely, when entrainment was stronger in the attended hemisphere, the participant was less accurate, signifying that attentional biasing towards entrainment in the attended hemifield interfered with subsequent visual perception of the probe stimulus. Importantly, the current framework provides a robust experimental and analytical method to test this relationship, as the normalization of the attended entrainment response to an unattended response within each participant removes the potentially confounding effects of differences in overall task-engagement. Supporting this, bilaterally-averaged entrainment amplitude (i.e., regardless of attentional cueing) exhibited a relationship with task accuracy in the opposite direction, suggesting that task engagement between participants also affected performance, as would be expected.

Although most studies have found visual gating by alpha inhibition to be beneficial for performance on higher-order cognitive tasks (e.g., working memory), a smaller subset have shown that enhancing alpha-frequency oscillatory activity at inopportune times can

also significantly impair behavior, which is in line with our findings. In particular, a number of experiments using flickering visual stimuli to entrain primary visual cortex have shown that alpha frequency entrainment impairs visual perceptual abilities (*15, 16*). However, the systems-level mechanism of this alpha interference effect has remained unclear until now. Although some part of this effect is potentially due to a modulation of endogenous rhythmic activity in occipital cortices, our results indicate that, at least in the case of an attentional manipulation, the negative relationship between alpha entrainment and visual perception is fully mediated by activity in extra-visual regions. More specifically, we found that activity in a set of frontal and parietal regions known to be involved in attention function exhibited substantial covariance with the entrainment cueing ratio, and these regions explained the entirety of the covariance between the cueing effects and task accuracy. The importance of these findings is twofold. First, previous studies reporting the widespread spatial distribution of alpha entrainment responses have lacked the spatial precision to identify the cortical generators of these signals reliably. Herein, we show that these generators are components of a well-established top-down regulatory system involved in attention: the fronto-parietal network. Second, the nature of this alpha-specific engagement of anterior cortices has remained elusive. Is it a compensatory mechanism to suppress the interfering effects of alpha entrainment on visual cortex, or evidence of a secondary interference effect that has “propagated” to higher-order regions from visual cortices, perhaps due to the pervasive functionality of alpha oscillations in visual attention networks across the human brain? Our data strongly support the latter, as the whole-brain analyses indicated that the increase in response amplitude within these regions was driven by attention accentuating entrainment, and was a strong negative predictor of task performance. Reinforcing this interpretation and providing new insight on the functional dissociation of the fronto-parietal network, our mediation analysis findings further showed

that the interfering effects of entrainment on behavior were entirely due to functional disruption in the superior parietal nodes of this network.

Despite the novelty of these findings, our experiment was not without limitations. For instance, the use of a 100% predictive cue during the entrainment period precluded us from examining any potentially unique effects of 10 Hz entrainment on the process of attentional re-orienting, which might provide additional insight into the mechanism of alpha entrainment interference. Further, we did not investigate the potential impact of entrainment-stimulus phase on these dynamics. The relative phase of ongoing alpha-frequency entrainment has been found to influence visual perceptual abilities (*16*), and thus presenting our probe stimuli at the trough rather than the peak of the entraining alpha phase might have yielded different results. Future exploration of this possibility is warranted and would help clarify the impact of each parameter. Future studies might also consider the use of complementary neuroimaging and neurostimulation modalities to expand upon these findings. For instance, it would be intriguing to see if these effects could be replicated using alpha-frequency transcranial alternating current stimulation (tACS) over the occipital cortices. Finally, in light of previous findings in the field, this study investigated only the effects of 10 Hz entrainment on visual perception and attention processes, however it remains possible that other frequencies of entrainment might also interfere with higher-order systems. Adding further nuance, frequency variability even *within* the alpha range might influence these effects. For instance, it appears that attention to stimuli flickering in the lower alpha-frequency range (e.g., 8 – 10 Hz) commonly results in a null or negative effect on the amplitude of the entrainment response (*52, 66, 68*), while the reverse effect (i.e., an enhancement of the response by attention) appears to occur when stimuli flicker at higher alpha-frequencies (e.g., 10 - 14 Hz; *66, 72, 73, 74*). Additionally, variation in the individual alpha peak frequency between participants has been found to covary with entrainment effects on visual perception (*15*), which could also

potentially influence the effect of visual alpha entrainment at set frequencies. Regardless of these limitations, our findings provide a new understanding of how alpha-frequency visual entrainment affects visual perception, and enhance our knowledge of the functional importance of fronto-parietal networks in visual attention.

CHAPTER 3: ATTENTION EFFECTS ON OSCILLATORY SOMATOSENSORY SYSTEMS

The material presented in this chapter was previously published in Wiesman and Wilson, 2020, Attention modulates the gating of primary somatosensory oscillations, NeuroImage, 211:116610.

Introduction:

Sensory gating (SG) is a robust phenomenon whereby neural responses to identical stimuli are reduced when presented in rapid succession. This phenomenon has been widely studied in the auditory (*75-77*) and somatosensory (*78-84*) systems, and is commonly interpreted as representing the "filtering" of redundant stimulus features at an early level of processing. Traditionally, SG has been considered a pre-attentive process in the human brain (*85*). Despite this consideration, very few studies have examined whether differences in attentional state directly modulate SG. This is surprising, as a number of studies have reported robust interactions between neuropsychological measures of attention function and SG, such that reduced attentional capacity is related to reductions in SG. For instance, stronger sensory gating has been linked with reduced distractibility and faster reaction times on the continuous performance task of sustained attention (*86-88*), as well as enhanced performance on the Posner attentional orienting task (*87*), the Stroop cognitive interference task (*89*), and the Attention Network Task (*88, 89*). Beyond these indirect links to neuropsychology, only a handful of studies (*90-93*) have examined the neural dynamics of SG across differing attentional states. Generally, these studies have found no significant effect of attention on the gating of primary sensory responses, however, none of these studies have examined this potential effect in the somatosensory domain or comprehensively examined the role of neural oscillations. An enhanced understanding of the potential effects of attention on SG is essential to better understand the basic neurophysiology of attention function in the human brain, as well as to aid in interpretation of aberrant SG in patient populations.

It also remains unknown whether the gating of the evoked (i.e., phase-locked) and multi-spectral oscillatory neural responses serving somatosensory processing (*80, 83, 94-104*) are differentially impacted by attention. In general, early-latency evoked and low-frequency theta synchronizations are thought to index the processing of incoming somatosensory stimulus information in a "bottom-up" manner (*80, 83, 84, 100-105*). In contrast, later-latency desynchronizations in the alpha and beta frequencies following somatosensory stimulation have been robustly tied to the "top-down" processing of this information in relation to context-specific task demands, and appear to be modulated by the direction of attention towards the somatosensory domain (*94-99, 106, 107*). In light of these previous findings, it seems likely that the gating of these differing responses would be affected by attention in opposing directions. In addition, the direction of such effects would provide clarification regarding the functional nature of these responses.

A significant volume of research has also been devoted to the study of SG in clinical populations and as a function of healthy aging. Perhaps most auspiciously, both auditory and somatosensory gating have been found to be aberrant in patients with schizophrenia (*77, 83, 108-110*), and somatosensory gating deficits have been reported in cerebral palsy (*79*) and HIV-associated cognitive dysfunction (*78*). These aberrations have widely been interpreted to represent an inability by these patients to suppress non-salient sensory information, which could then lead to common disease sequelae such as degraded perception and even hallucinations. In addition, somatosensory gating is often found to decrease as age increases in healthy adults (*81, 82, 111, 112*), suggesting a degradation of somatosensory processing as age progresses. Importantly, in the majority of clinical populations commonly studied with SG paradigms (*78, 79, 113-115*), attentional deficits are also consistently reported. This is problematic, as the effects of directed attention on SG are not well studied, particularly in the somatosensory domain.

In this study, we investigate the interaction between directed attention and somatosensory gating, as measured with MEG. Twenty-six healthy young adults performed a novel somato-visual paradigm designed expressly for this purpose during an MEG recording, whereby alertness was held constant and attention was either directed towards or away from a paired-pulse somatosensory stimulation applied to the left median nerve. We hypothesized that SG would be significantly altered when attention was directed away from the somatosensory stimuli, relative to when it was directed towards the stimuli. Specifically, we predicted that attention would enhance SG of neural somatosensory responses that are known to index early, "bottom-up" stimulus processing, including the initial evoked broadband and early theta-frequency responses (*75, 83, 100, 101, 103, 104, 116*). Conversely, we predicted that attention would reduce SG of somatosensory responses thought to represent "top-down" integration with executive systems, and in particular neural activity in the alpha and beta bands, where attention has been repeatedly found to have a robust influence (*94-99, 106, 107*). Along these lines, we also expected that coherent neural activity in the alpha and beta frequency bands might facilitate communication between prefrontal attention cortices and primary somatosensory cortex.

Methods:

Participants

We enrolled 26 healthy young adults (mean age = 24.04 years; SD = 3.22 years; range = 19-31 years; 12 males/14 females) for participation in this study. Exclusionary criteria included any medical illness affecting CNS function, any neurological disorder, history of head trauma, any non-removable metal implant that would adversely affect data acquisition, and current substance abuse. The Institutional Review Board at the University of Nebraska Medical Center reviewed and approved this investigation. After complete

description of the study, written informed consent was acquired from each participant. All participants had normal or corrected-to-normal vision. All participants completed the same experimental protocol.

Experimental Paradigm

Participants were seated in a custom-made nonmagnetic chair with their head positioned within the MEG sensor array. During the scan, participants performed a novel somato-visual oddball paradigm, aimed at systematically dividing attention between the somatosensory and visual domains during paired-pulse somatosensory stimulation (Figure 10). Stimuli from these two sensory modalities were presented in alternation, and a small proportion of the stimuli from each modality were temporal "oddballs," which were utilized to monitor behavior and ensure that attention was directed towards either the visual or somatosensory domain. The visual stimulus consisted of a right-lateralized circle

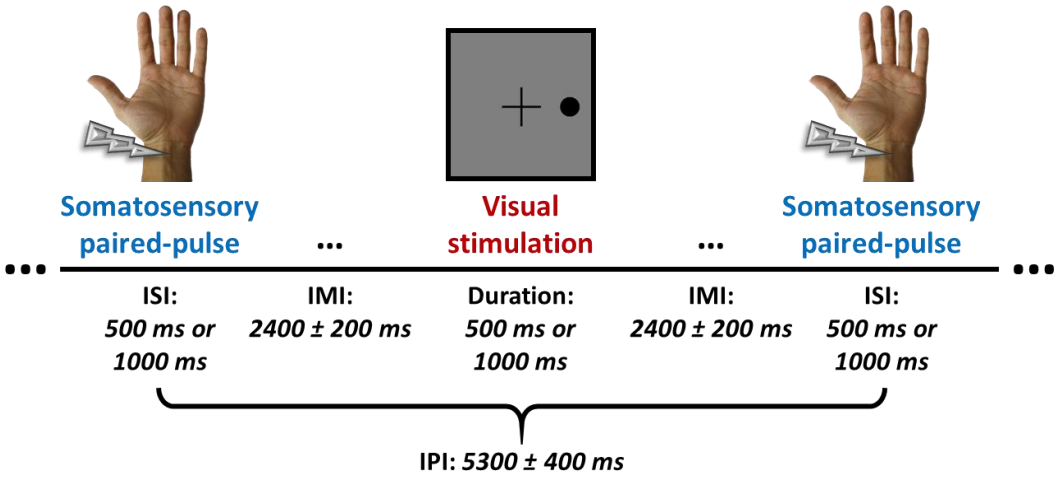

Figure 10. Somato-visual directed attention task paradigm.

Each participant performed one counterbalanced block of the experiment per attention condition (i.e., 88 somatosensory and 88 visual trials/block, 352 total trials). The task consisted of interspersed somatosensory paired-pulse (inter-stimulus interval (ISI): 500 ms) and visual stimuli (duration: 500 ms), separated by a variable inter-modality interval (IMI) of 2400 ± 200 ms. Eight of the total 88 stimuli per modality were oddballs (somatosensory ISI: 1000 ms; visual duration: 1000 ms), and participants only responded to oddballs in one modality per block, depending on the condition. These conditions only differed in the instructions given (i.e., "respond to the somatosensory oddballs" versus "respond to the visual oddballs"), and the visual fixation was present for the entire duration of the task. IPI: interpair interval.

centered on the horizontal axis and to the right of a centrally-presented fixation crosshair. In 80 of the 88 total visual trials, this stimulus was presented for a duration of 500 ms, and for the other eight “oddball” trials it was presented for 1000 ms. The somatosensory stimulus consisted of a paired-pulse delivered using unilateral electrical stimulation to the median nerve of the left hand. For each participant, 80 paired-pulse trials were collected per block using an inter-stimulus interval of 500 ms, while the remaining eight “oddball” somatosensory trials used an inter-stimulus interval of 1000 ms. Visual and somatosensory trials were presented in alternation for a total of 160 non-oddball trials in a single block (i.e., 80 somatosensory and 80 visual). The inter-pair interval (IPI) between somatosensory paired-pulses was 5300 ± 400 ms (randomly jittered to prevent anticipatory effects; not accounting for the additional 500 ms present on the eight oddball trials out of the total 88 visual trials) and the inter-modality interval (IMI) between visual and somatosensory stimuli was 2400 ± 200 ms. Each participant performed two blocks of the experiment (i.e., 352 total trials, including 32 oddball trials), and the only difference between the two blocks was the instructions given (i.e., “respond to somatosensory oddballs” versus “respond to visual oddballs”). In the “visual” block, participants responded to only the visual oddballs, and were told to ignore the task-irrelevant somatosensory stimuli. Conversely, in the “somatosensory” block, participants were told to respond only to the somatosensory oddballs, and to ignore the task-irrelevant visual stimuli. Importantly, participants were required to fixate on the centrally-presented crosshair and keep their left arm still for the entirety of both blocks. The order of the blocks was counterbalanced across participants. Participants used a MEG-compatible five-finger response pad to respond to the occurrence of the oddball stimuli, using their right index finger. Total MEG recording time was approximately 20 minutes per participant.

For the somatosensory stimuli, mild electrical stimulation was delivered using external cutaneous stimulators connected to a Digitimer DS7A constant-current stimulator system

(Digitimer Limited, Letchworth Garden City, UK). Each pulse was comprised of a 0.2 ms constant-current square wave that was set to 10% above the motor threshold required to elicit a subtle twitch in the thumb, and the same stimulation amplitude was used in both blocks for each participant. A 500 ms inter-stimulus interval (ISI) between the pulses was chosen, as this is the interval most commonly used in previous research, and is known to elicit robust SG responses (*77-81, 84, 117, 118*). Custom visual stimuli were programmed in Matlab (Mathworks, Inc., Massachusetts, USA) using Psychophysics Toolbox Version 3 (*20*) and back-projected onto a semi-translucent non-ferromagnetic screen at an approximate distance of 1.07 meters, using a Panasonic PT-D7700U-K model DLP projector with a refresh rate of 60 Hz and a contrast ratio of 4000:1.

MEG Data Acquisition

All recordings were conducted in a one-layer magnetically-shielded room with active shielding, based on measurements taken from several magnetometers within the MEG array, engaged for environmental noise compensation. Neuromagnetic responses were sampled continuously at 1 kHz with an acquisition bandwidth of 0.1– 330 Hz using a 306-sensor Elekta/MEGIN MEG system (Helsinki, Finland) equipped with 204 planar gradiometers and 102 magnetometers. Participants were monitored during data acquisition via real-time audio-video feeds from inside the shielded room. Each MEG dataset was individually corrected for head motion and subjected to noise reduction using the signal space separation method with a temporal extension (correlation limit: .950; correlation window duration: 6 seconds; *21*). Only data from the gradiometers were used for further analysis.

Structural MRI Processing and MEG Coregistration

Preceding MEG measurement, four coils were attached to the participant's head and localized, together with the three fiducial points and scalp surface, using a 3-D digitizer

(Fastrak 3SF0002, Polhemus Navigator Sciences, Colchester, VT, USA). Once the participant was positioned for MEG recording, an electric current with a unique frequency label (i.e., 293, 307, 314, and 321 Hz) was fed to each of the coils. This induced a measurable magnetic field and allowed each coil to be localized in reference to the sensors throughout the recording session. Since coil locations were also known in head coordinates, all MEG measurements could be transformed into a common coordinate system. With this coordinate system, each participant's MEG data were co-registered with structural T1-weighted MRI data using BESA MRI (Version 2.0) prior to source-space analysis. Structural MRI data were aligned parallel to the anterior and posterior commissures and transformed into Talairach space. Following source analysis (i.e., beamforming), each participant's 4.0 x 4.0 x 4.0 mm functional images were also transformed into Talairach space using the transform that was previously applied to the structural MRI volume and spatially resampled.

MEG Preprocessing, Time-Frequency Transformation, and Sensor-Level Statistics

Cardiac and blink artifacts were removed from the data using SSP, which was subsequently accounted for during source reconstruction (Uusitalo and Ilmoniemi 1997). The continuous magnetic time series was then filtered between 0.5 – 200 Hz plus a 60 Hz notch filter, and divided into 2500 ms epochs, with the baseline extending from -500 to 0 ms prior to the onset of the somatosensory paired-pulse stimuli. It should be noted that only the "short" duration (i.e., 500 ms) paired pulse somatosensory trials were considered in this analysis, and the oddball trials were excluded entirely. The visual stimulation trials were also excluded. Epochs containing artifacts were rejected using a fixed threshold method, supplemented with visual inspection. Briefly, in MEG, the raw signal amplitude is strongly affected by the distance between the brain and the MEG sensor array, as the magnetic field strength falls off sharply as the distance from the current source increases.

To account for this source of variance across participants, as well as actual variance in neural response amplitude, we used an individually-determined threshold based on the signal distribution for both signal amplitude and gradient to reject artifacts. Across all participants, the average amplitude threshold was 947.79 (SD = 157.74) fT and the average gradient threshold was 135.42 (SD = 35.01) fT/s. Across the group, an average of 71.48 (SD = 1.93) trials per participant per condition (out of 80 possible trials) were used for further analysis. Importantly, none of our statistical comparisons were compromised by differences in trial number nor artifact thresholds, as none of these metrics significantly differed across attention conditions (trial number: p = .479, BF_{01} = 3.81; amplitude threshold: p = .291, BF_{01} = 2.86; gradient threshold: p = .404, BF_{01} = 3.48).

The epochs remaining after artifact-rejection were averaged across trials to generate a mean time series per sensor, and the specific time windows used for subsequent source analysis were determined by statistical analysis of the sensor-level time series across all conditions and the entire array of gradiometers. Each data point in the time series was initially evaluated using a mass univariate approach based on the general linear model. To reduce the risk of false positive results while maintaining reasonable sensitivity, a two-stage procedure was followed to control for Type 1 error. In the first stage, paired-sample t-tests were conducted to test for differences from baseline at each data point and the output time series of t-values was thresholded at $p < .001$ to define time-points containing potentially significant responses across all participants. In stage two, the time points that survived the threshold were clustered with temporally and/or spatially neighboring time points that were also above the threshold ($p < .001$), and a cluster value was derived by summing all of the t-values of all data points in the cluster. Nonparametric permutation testing was then used to derive a distribution of cluster-values and the significance level of the observed clusters (from stage one) were tested directly using this distribution (Ernst 2004; Maris and Oostenveld 2007). For each comparison 10,000 permutations were

computed to build a distribution of cluster values, and the time windows of phase-locked, time-domain data that were non-exchangeable with baseline across all participants according to these permutation analyses were used to guide subsequent time domain source level analysis.

To investigate the oscillatory responses commonly associated with somatosensory processing, we next transformed the same post-artifact-rejection epochs into the time-frequency domain using complex demodulation (*23, 119, 120*). Briefly, complex demodulation works by first transforming the signal into the frequency space, using a Fast Fourier Transform (FFT). This results in a frequency spectrum, inherently containing the same power and cross spectrum information as the original signal. From here, this frequency spectrum is (de)modulated in a step-wise manner to adopt the center frequency of a series of complex sinusoids with increasing carrier frequencies, in a process termed "heterodyning." These resulting signals are then low-pass filtered to reduce spectral leakage, and thus the nature of this filter inherently determines the time and frequency resolution of the resulting data. For this study, the time-frequency analysis was performed with a frequency-step of 2 Hz and a time-step of 25 ms between 4 and 100 Hz, using a 4 Hz lowpass finite impulse response (FIR) filter with a full-width half maximum (FWHM) in the time domain of ~115 ms. Importantly, prior to this time-frequency transformation, we regressed out the time-domain averaged evoked signal from the single-trial data, in order to avoid any “contamination” of the oscillatory data by the evoked response, which is the focus of the time-domain analysis. The resulting spectral power estimations per sensor were averaged over trials to generate time-frequency plots of mean spectral density, which were normalized by the baseline power of each respective bin, calculated as the mean power during the -500 to 0 ms time period. The time-frequency windows used for the time-frequency domain source analysis were again determined by means of a paired-sample cluster-based permutation test against baseline across all participants and the entire

frequency range (4 – 100 Hz), with an initial cluster threshold of $p < .001$ and 10,000 permutations.

MEG Source Analysis

Time domain source images were computed using standardized low resolution brain electromagnetic tomography (sLORETA; regularization: Tikhonov .01%; *121*). The resulting whole-brain maps were 4-dimensional estimates of current density per voxel, per time sample across the experimental epoch. These data were normalized to the sum of the noise covariance and theoretical signal covariance, and thus the units are arbitrary. Using the temporal clusters identified in the sensor-level analysis, these maps were averaged over time following each somatosensory stimulation (i.e., 25 – 70 ms and 525 – 570 ms after the onset of the first stimulation) and across both attention conditions. The resulting maps were then grand-averaged across the two stimulations to determine the peak voxel of the time-domain neural response to the stimuli across participants. From this peak, the sLORETA units were extracted per stimulation and attention condition to derive estimates of the time-domain response amplitude for each participant.

Time-frequency resolved beamformer source images were computed using the DICS (regularization: singular value decomposition .0001%; *26*) approach, which uses the time-frequency averaged cross-spectral density to calculate voxel-wise estimates of neural power and/or coherence. Following convention, we computed noise-normalized, source power per voxel in each participant using active (i.e., task) and passive (i.e., baseline) periods of equal duration and bandwidth. Such images are typically referred to as pseudo-t maps, with units (pseudo-t) that reflect noise-normalized power differences (i.e., active vs. passive) per voxel. This approach generated three-dimensional participant-level pseudo-t maps per attention condition and stimulation (i.e., the first or second stimulation in the pair), for each time-frequency cluster identified in the sensor-level analysis. As with

the time-domain source analysis, the resulting images were next grand-averaged (i.e., across attention condition and stimulation number) and used to derive peak voxel locations for each time-frequency response. Using these peak voxel locations, virtual sensor data were computed by applying the sensor-weighting matrix derived through the forward computation to the preprocessed signal vector, which yielded a time series corresponding to the location of interest. These virtual sensor data were then decomposed into time-frequency space and averaged across the previously identified time-frequency extents (i.e., used in the beamformer analysis) for each response, within each attention condition. This resulted in amplitude estimates of each time-frequency domain response per participant.

To address hypotheses regarding fronto-somatosensory connectivity in the time-frequency domain, peak voxels identified in the DICS power analysis were used as seeds for computation of whole-brain cortico-cortical coherence (again using DICS), reflecting time-frequency-resolved connectivity between these seeds and all other voxels in the brain. Similarly to the power analysis, coherence maps computed from active periods were normalized to coherence maps from passive periods, resulting in whole-brain estimates of percent-change in coherence from baseline for each participant, stimulation, and attention condition. These whole-brain cortico-cortical coherence images were compared voxel-wise, and corrected for multiple comparisons using a similar cluster-based permutation approach as detailed in the *Sensor-Level Statistics* section (i.e., initial cluster threshold of $p < .001$; 10,000 permutations). Importantly, due to the persistent concern regarding amplitude confounds in MEG measures of functional connectivity (e.g., coherence; *122*), we also used peak-voxel data from these coherence maps to compute repeated-measures ANOVAs of the same conditional connectivity differences, above and beyond the effects of amplitude at both sources. All reported clusters for the coherence analysis are thus significant above and beyond the effects of amplitude.

Statistical Analyses and Software

To examine the effects of attention condition on SG, a gating ratio (stimulation 2/stimulation 1) was derived per participant for each attention condition, and a repeated-measures ANOVA model was used to test for significant differences in this ratio (i.e., as [1] a function of attention condition and [2] neural response). It is important to note that this ratio was used to test hypotheses, rather than modeling somatosensory gating as a within-participant contrast, since such a model would test the effect of gating as (S2 – S1), rather than (S2/S1). The prior is problematic for two reasons: (1) it is less comparable to previous literature in the field that typically uses the ratio instead, and (2) it biases participants with a higher overall amplitude of response (regardless of stimulation) towards artificially-high gating estimates, whereas the ratio provides a better control for this confound. Simple effects testing for differences in gating ratio between attention conditions for each response was then used to guide interpretation of the initial RM-ANOVA results (Bonferroni correction: p = .050/4 responses = .0125). For similar reasons, significant effects of gating (i.e., regardless of attention condition) were tested on these data using one-sample t-tests against the null hypothesis of stimulation 2/stimulation 1 = 1. This gating analysis was performed on each of the four responses (i.e., one time domain and three time-frequency domain). Additionally, since this initial analysis suggested no effect of attention on SG in the time domain response identified at the sensor-level, an exploratory analysis was conducted whereby time-varying estimates of evoked response amplitude across the epoch were extracted from the peak voxel identified by the sLORETA analysis described above. Using these data, time-varying estimates of SG were computed (stimulation 2/stimulation 1), and cluster-based permutation testing was used to determine whether a significant effect of attention was present during any time window across the time period ranging from 0 to 400 ms post-stimulation using a liberal threshold (initial

cluster threshold: $p < .500$; final significance threshold: $p < .200$; 10,000 permutations). To test whether attention condition significantly modulated connectivity between the primary somatosensory cortex and other cortical regions during sensory processing, we averaged the cortico-cortical coherence images across stimulations 1 and 2 within each attention condition and participant, and tested these images against each other using voxel-wise paired-samples t-tests corrected for multiple comparisons using cluster-based permutation testing (10,000 permutations). All primary data preprocessing, coregistration, and sensor- and source-level analyses were performed in the BESA software suite (BESA Research v6.1 and BESA MRI v2.0). Cluster-based permutation testing on sensor-array and whole-brain cortico-cortical coherence data was performed in BESA Statistics (v2.0), and all parametric statistics were computed in *JASP* (*123*). Multiple comparisons correction for parametric statistics used the Bonferroni approach, with a corrected significance threshold set to $p = .0125$ ($p = .050/4$ tests). To complement our initial frequentist statistical approach, Bayesian analysis was also performed in *JASP*, using a zero-centered Cauchy distribution with a default scale of 0.707.

Results:

All participants performed well on the somato-visual oddball task (Figure 10), with a mean accuracy of 95.19% correct overall (SD = 7.14%; 95% CI: [92.45, 97.93]). Performance did not significantly differ by attention condition (attend somatosensory: mean = 96.63%, SD = 6.66%; attend visual: mean = 93.27%, SD = 10.14%; $p = .090$, $BF_{01} = 1.25$). Importantly, no participant identified the oddball stimuli at a rate of <65%, indicating that attention was being effectively directed towards the relevant stimulus modality across all participants.

Neural responses to paired-pulse stimulation

Prior to determining the spatial origin of the neural responses to each stimulation, we first identified significant neural responses to the somatosensory stimuli. In the time domain, this revealed one temporally defined (25 – 70 ms post-stimulus; $p < .001$) cluster after each somatosensory stimulation in sensors over right somato-motor regions (Figure 11A). For the time-frequency data, three spectrally- and temporally-distinct clusters were identified following each somatosensory stimulation. These included an early increase in theta activity (4 – 8 Hz, 0 – 250 ms post-stimulus; $p < .001$), and later decreases in both alpha (8 – 14 Hz, 175 – 475 ms post-stimulus; $p < .001$) and beta (20 – 26 Hz, 100 – 350 ms post-stimulus; $p < .001$) activity (Figure 11B). From these source-level images, peak voxel time series data were then extracted and averaged over the same time/time-frequency windows per stimulation and attention condition for subsequent hypothesis testing (i.e., for effects of gating and attention).

Interactions between SG and directed attention on primary somatosensory neural responses

Source reconstruction of each of these neural responses indicated that all four were centered on the primary somatosensory cortex. Next, we examined the SG effect (stimulation 2/stimulation 1) on each of these source-level responses, as well as the impact of directed attention (i.e., toward or away from the somatosensory stimuli) on this gating. The evoked (i.e., phase-locked) response exhibited significant gating ($t(25) = -10.40$, $p < .001$), such that the amplitude was reduced in response to the second stimulation. The theta ($t(25) = -6.38$, $p < .001$; $BF_{10} = 16{,}087.22$, error % = 5.23×10^{-8}) and beta ($t(25) = 2.95$, $p = .007$; $BF_{10} = 6.51$, error % = 7.26×10^{-4}) responses, but not the

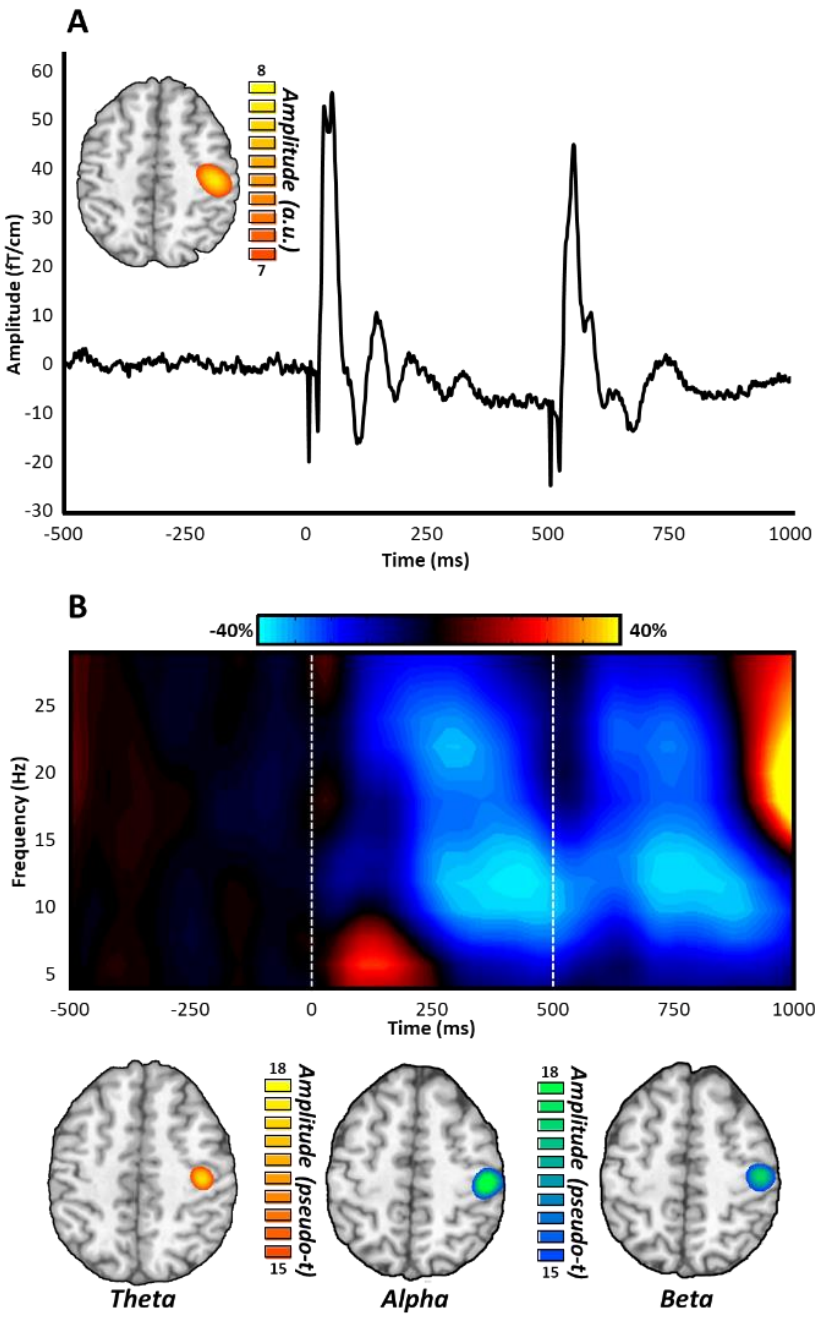

Figure 11. Neural responses in primary somatosensory cortex.

(A) The time domain average of data from a representative sensor over right somato-motor cortices (MEG1132), with a time domain source image averaged across both stimulations and attention conditions overlaid on the plot. (B) A grand-averaged spectrogram from the same sensor (MEG1132). Note that the phase-locked (evoked) signal has been regressed out. Time is indicated in ms on the x-axis and frequency is indicated in Hz on the y-axis, with percent change from baseline indicated by the color bar above. The white dashed lines represent the onset of each of the two stimulation pulses. Below this plot are frequency-resolved source images of each time-frequency cluster identified in the sensor-level data (again grand-averaged over stimulations and attention conditions). The response amplitude (in pseudo-t) for each cluster is indicated by the color scale bars in between.

alpha response ($t(25) = -1.77$, $p = .090$; $BF_{01} = 1.25$, error % = 3.65×10^{-5}), also exhibited significant SG when collapsing across both attention conditions. Similar to the evoked response, the absolute amplitude of theta activity decreased in response to the second stimulation of the pair. For the beta response, this effect was reversed, such that the absolute amplitude was higher in response to the second stimulation as compared to the first. However, it should be noted that since the beta response was a *desynchronization* (i.e., decrease from pre-stimulus levels), this SG effect should be interpreted as a weakened response to the second stimulation relative to the first, which again would be interpreted as a gating effect.

A two-way repeated-measures ANOVA (within-participants contrasts of *response* [4 levels] and *attention condition* [2 levels]) indicated significant main effects of condition ($F(1,25) = 6.45$, $p = .018$) and frequency ($F(3,75) = 58.56$, $p < .001$), as well as a significant condition by response interaction ($F(3,75) = 4.032$, $p = .010$), on SG. Post-hoc simple effects testing indicated that

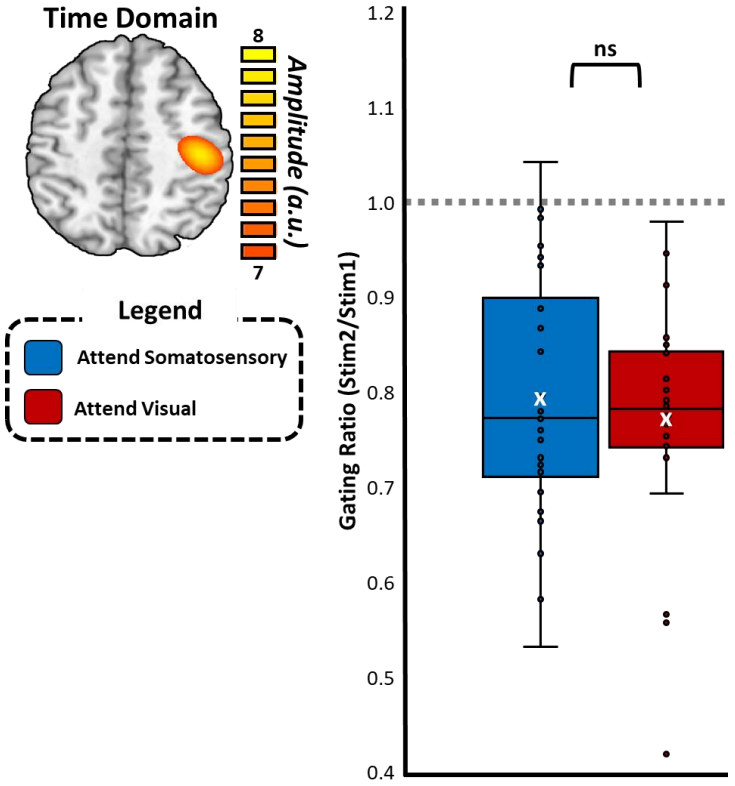

Figure 12. Phased-locked somatosensory responses are gated and attention-invariant.

The gating of time domain responses was not modulated by attention. Box and whisker plots represent the gating ratio (stimulation 2 amplitude/stimulation 1 amplitude) per attention condition (red and blue). Each plot includes the individual data points, median (horizontal line), mean (white x), first and third quartile (box), and local minima and maxima (whiskers). Points falling outside of the whiskers are more than 1.5 times the interquartile range above or below the third and first quartiles, respectively, and are plotted as such for visualization purposes. These data were included in all analyses.

gating of the evoked response was not significantly affected by attention condition ($t(25) = -0.89$, $p = .380$; Figure 12). Post hoc Bayesian analysis of this effect gave moderate evidence for the null hypothesis, suggesting that gating of the evoked response is indeed attention-invariant ($BF_{01} = 3.36$, error % = 0.03).

Interestingly, the SG of all three oscillatory responses was altered by directed attention (Figure 13). Specifically, the theta response exhibited lower SG ratios when attention was directed toward the somatosensory stimuli, relative to when it was directed away ($t(25) = -3.03$, $p = .006$; $BF_{10} = 7.74$, error % = 4.25×10^{-4}). The direction of this effect indicates that theta response gating was stronger when attention was directed towards the somatosensory domain. Similarly, attention towards somatosensory stimulation resulted in significantly lower alpha ($t(25) = -2.98$, $p = .006$; $BF_{10} = 6.98$, error % = 5.90×10^{-4}) and beta ($t(25) = -3.04$, $p = .005$; $BF_{10} = 7.89$, error % = 4.00×10^{-4}) SG ratios relative to when attention was directed away. However, note that since these alpha and beta responses were desynchronizations (i.e., *decreases* relative to baseline), lower SG values reflect reduced gating, or even *response enhancement*. Importantly, no significant main effect of attention was found on the neural response amplitude to the stimulations for any of the four neural responses (evoked: $p = .981$, $BF_{01} = 4.83$; theta: $p = .618$, $BF_{01} = 4.29$; alpha: $p = .949$, $BF_{01} = 4.82$; beta: $p = .256$, $BF_{01} = 2.63$).

The direction of attention effects on the gating of these multi-spectral responses suggested that the early theta component may be an early, “bottom-up” response, while the later alpha and beta oscillations were potentially modulated by “top-down” control. Essentially, since the somatosensory stimulus was only task-relevant in the “attend somatosensory” condition, a declining response to the second stimulus during directed attention (such as in the theta response) indicates an earlier alerting component of stimulus processing. In contrast, an increasing response to the second somatosensory stimulus during directed attention (such as in the alpha and beta responses) indicates

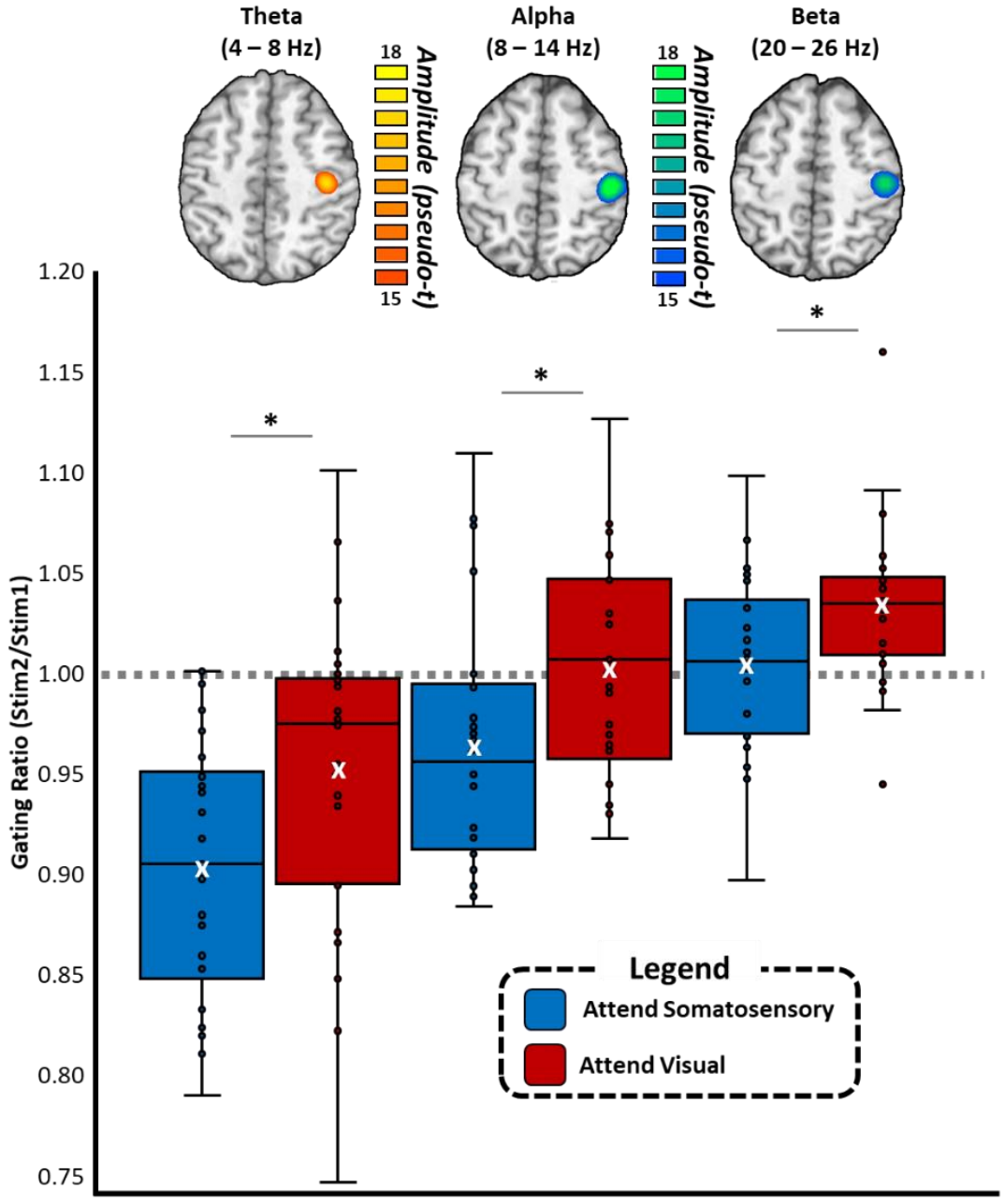

Figure 13. Directed attention modulates the gating of somatosensory oscillations.

Box and whisker plots represent the sensory gating ratio (stim 2 amplitude/stim 1 amplitude) per attention condition. Each plot includes the individual data points, median (horizontal line), mean (white x), first and third quartile (box), and local minima and maxima (whiskers). Points falling outside of the whiskers are more than 1.5 times the interquartile range above or below the third and first quartiles, respectively, and are plotted as such for visualization purposes. These data were included in all analyses. It should be noted that for the theta synchronization response, higher values indicate reduced gating, whereas for the alpha and beta desynchronization responses higher values indicate enhanced gating. Thus, directing attention toward somato-sensation enhanced theta-band SG, while the opposite was true for both alpha and beta oscillations. *$p < .01$

heightened processing of this relevant stimulus. To test this possibility further, we computed whole-brain cortico-cortical coherence maps for each oscillatory response, attention condition, and stimulation in each participant, and averaged these maps across stimulations to derive voxel-wise coherence estimates per attention condition and oscillatory response per participant. These maps represent whole-brain coherence between the neural response of interest (e.g., the primary somatosensory alpha response) and the activity across the rest of the brain within the same time-frequency window. We then tested these whole-brain maps for effects of attention condition on coherence in both the alpha and beta frequencies, and corrected for multiple comparisons using cluster-based permutation testing (initial cluster threshold: $p < .001$; final significance threshold: $p < .025$; 10,000 permutations). Intriguingly, coherence between the primary

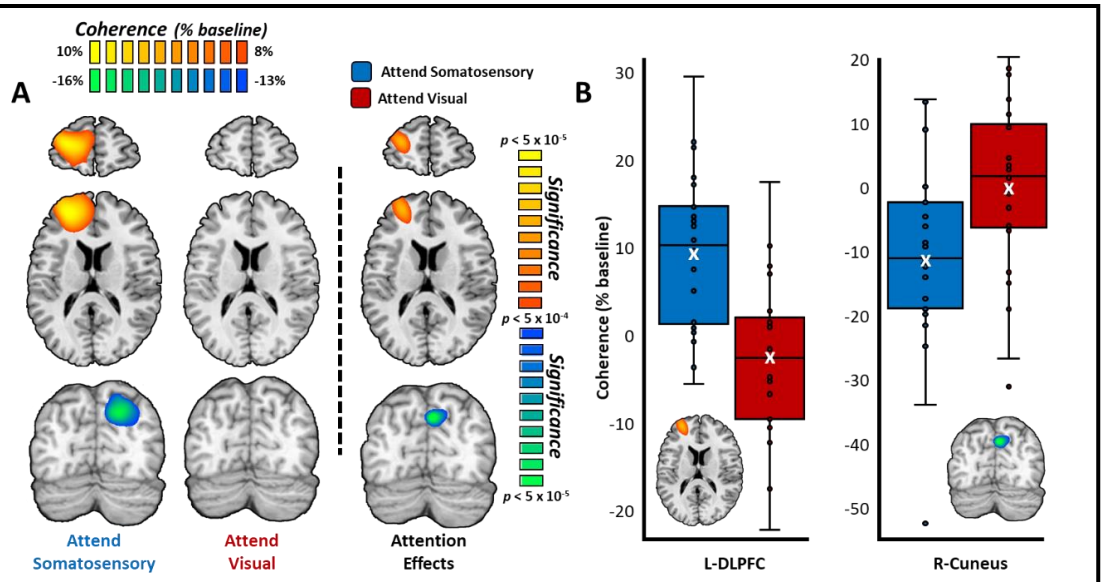

Figure 14. Directed attention modulates inter-regional somatosensory alpha coherence.

The images on the left of the dashed line in (A) represent whole-brain alpha-band coherence (in % change from baseline) with the primary somatosensory cortex as the seed for each attention condition. Scale bars are shown above the maps. Maps on the right of the dashed line represent a voxel-wise paired-samples t-test of this alpha coherence between the two attention conditions (Left-DLPFC: $p = .008$, corrected; Right-Cuneus: $p = .010$, corrected), with the color bars to the right indicating uncorrected voxel-wise significance. The box and whisker plots on the far right represent the condition-wise coherence differences at the peak difference voxel from the overlaid maps (bottom). The features of each plot matches those in the box and whisker plots above. These data were included in all analyses. We found that coherence between somatosensory and prefrontal cortices was sharply increased during the attend somatosensory condition, while such coherence was sharply decreased between the cuneus and somatosensory cortices in the same condition.

somatosensory alpha response and the left dorsolateral prefrontal cortices was significantly increased when attention was directed towards the somatosensory stimuli, relative to when it was directed away (Figure 14; p = .004). Further, alpha coherence between the primary somatosensory response and the right cuneus was also modulated by attention, such that connectivity between these regions decreased when attention was directed toward the somatosensory domain (p = .021). No significant cortico-cortical coherence differences were observed for the beta response.

Discussion:

In this study, we used a novel somato-visual oddball task and whole-brain MEG to investigate the impact of directed attention on SG in the somatosensory domain. We found that attention toward somatosensation significantly altered the gating of all three population-level neural oscillatory responses to the paired-pulse stimuli, and that this gating effect differed according to the spectro-temporal profile of the response. Specifically, SG of the early theta response was increased when attention was directed towards the somatosensory domain, while gating of the alpha and beta responses was decreased in the same attentional state. Importantly, this attention effect on SG was not present for the evoked (i.e., phase-locked) somatosensory response. Further, all of these attentional effects were the most robust in frequencies strongly tied to somatosensory processing in previous studies (*94-99, 106, 107*). These findings, as well as their implications and future directions for study, are discussed at length below.

The current findings have important implications for understanding the basic functional role of the spectrally distinct somatosensory responses. Alpha and beta oscillations in the primary somatosensory cortices have been tied to anticipatory and attentional processing (*94, 95, 97-99, 106*), and so it is unsurprising that SG in these frequencies was robustly affected by directed attention. What is perhaps more surprising, is that the effects of

attention on the gating of neural oscillatory responses reversed direction depending on the spectro-temporal profile of the response in question. While attention enhanced gating of the early theta response, it decreased gating of the later alpha and beta responses. This broadly supports the conceptualization of this early theta component as representing low-level stimulus recognition and feature encoding (*80, 100-102, 105*). Essentially, as such gating is thought to represent the "filtering" of irrelevant stimulus information at an early stage, it is intuitive that enhanced attention towards this stimulus would translate to more effective gating. In other words, since the stimulus properties (e.g., amplitude, pulse-width) were identical for both stimulations, additional processing of these properties would be unnecessary or even detrimental, and this effect would only be accentuated when the *timing* (but not the stimulus properties themselves) were relevant. On the other hand, the reduction in gating of the later beta and alpha responses as a function of directed attention indicates that these responses are representative of modulatory feedback and (at least in this case) temporal processing, as the timing of the second stimulus was more salient in the "attend somatosensory" condition.

Further supporting this notion, alpha coherence between the prefrontal cortex and the primary somatosensory cortices was higher when attention was directed towards the somatosensory domain. This points to a prefrontal modulator of the alpha-somatosensory response and, interestingly, this effect was specific to this frequency band. This finding is in line with previous reports of a prefrontal modulator of somatosensory processing (*124-126*), but importantly, to our knowledge is the first empirical evidence of direct prefrontal-somatosensory modulation (i.e., prior studies showed only co-activation). Somatosensory alpha coherence with the right cuneus was also significantly decreased when attention was directed towards the somatosensory domain. This finding is in line with a vast literature supporting parieto-occipital alpha desynchronizations as an active dis-inhibition of visual processing circuits during specific visual tasks (*1, 4, 14, 49, 50, 64, 127-129*).

Given these previous findings, the relative decrease in somato-visual connectivity observed during the attend somatosensory condition represents a “decoupling” of the somatosensory and visual processing circuits, in order to facilitate more effective performance on the somatosensory task.

The evidence provided herein for no attentional effect on SG of phase-locked (i.e., evoked) primary somatosensory responses is also highly informative. Although more recent studies have begun to focus on the oscillatory neural dynamics of SG (78-82), historically, the vast majority of this literature has centered around time domain analysis of the evoked components. While these studies have provided a foundational understanding of the neurophysiological bases of SG, it is clear from this study and others that SG of evoked responses is only one part of a complex series of neurophysiological phenomena at play. Indeed, our findings align well with previous investigations that often find no significant effect of attention on SG of early evoked responses (*91-93*). Our study expands this into the somatosensory domain, and provides the *first evidence for the null hypothesis* of no attentional effect, using post hoc Bayesian analysis.

In addition to the significance for understanding the population-level neurophysiology of somatosensory processing, the implications of this research for previous and future studies of clinical populations should also be addressed. Given the vast number of studies that have reported SG alterations in patient groups, the fact that most of these studies did not control for attentional state across participants raises important concerns. Basically, we systematically modulated attention and found robust effects on SG across three well-documented oscillatory somatosensory responses. Thus, it is possible, perhaps even probable, that the known attentional differences in many psychiatric and neurologic disorders may have incidentally affected previous findings. Supporting the likelihood that attentional differences might be partly responsible for these effects, SG has been repeatedly tied to neuropsychological tests of attention function (*86, 87, 89*), and select

components of auditory SG have been found to be modulated by attention (*90-93*). The current results extend this potential confound into the somatosensory domain, and also provide evidence for spectrally-specific differences in the nature of the attention effect on SG. Future studies are certainly warranted to better understand the actual impact of attentional differences on SG. Further, future studies investigating SG in populations which vary in attentional abilities (e.g., patient populations or aging samples) should attempt to either control for these potential confounds, or to investigate the impact of attentional abilities on key SG metrics. With all of this said, it is notable that many previous patient-based studies have focused on evoked responses, which to at least some degree should be reassuring, as we did not observe attentional effects on these responses.

Despite its novelty, this study is not without limitations. First, although we were successful in directing participant's attention towards and away from the somatosensory domain, the attentional load required for this task was likely only moderate. Future studies might systematically increase the attentional load towards the somatosensory domain in a step-wise manner, which would show whether the attentional effects on SG observed here reach any type of functional plateau. Second, although participants did respond to the stimuli presented in this study, these responses were only to the oddball stimuli, and thus there was not enough behavioral data for a thorough analysis. Additional research is necessary to determine how these attentional effects might affect perception and discrimination of somatosensory stimuli. Third, although we found sufficient evidence for no effect of attention on the gating of somatosensory responses in the *primary* somatosensory cortex, we are not as confident that such an effect does not exist in secondary somatosensory regions (SII). Initial exploratory analyses indicated no such effect in the later evoked components usually attributed to this region, and no distinct SII peak could be identified using our methods, however, it remains a possibility that such an effect might be identified using more targeted methodologies and analytical approaches.

Indeed, MEG has even been suggested to be a poor method for measurement of SII activity, which is highly variable between participants (*80, 84, 101, 130*). Finally, we were able to identify a prefrontal modulator of somatosensory dynamics in this study, supporting our hypothesis that the later alpha response represents “top-down” processing of the stimulus. However, conversely, we would also predict that a similar pattern of coherence with “bottom-up” regions would exist for the earlier theta response (i.e., from thalamic inputs). We found no such pattern of coherence, and though it is possible that this connectivity does not exist, it seems more likely that the limited sensitivity of MEG to deeper brain structures might have played a limiting role. Regardless, these findings have important implications for advancing our basic understanding of somatosensory neurophysiology, as well as for our interpretation of previous research in clinical and aging populations.

CHAPTER 4: ATTENTION AND INTERFERENCE EFFECTS ON OSCILLATORY MOTOR SYSTEMS

The material presented in this chapter was previously published in Wiesman, Koshy, Heinrichs-Graham, and Wilson, 2020, Beta and Gamma Oscillations Index Cognitive Interference Effects Across a Distributed Motor Network, NeuroImage, in press.

Introduction:

The ability to effectively prepare and execute an efficient motor plan is essential to normative function. However, this seemingly simple concept belies an extremely complex set of cognitive processes, known to involve a network of cortical regions distributed across the frontal and parietal lobes. For example, the so-called “motor-strip” of the precentral gyrus has been established as the source of population-level vector-codes for directed motor plans, with a clearly defined homuncular organization. Directly anterior to this primary motor (M1) region is the premotor cortex, which has been found to be essential to the planning and execution of complex motor directives, as well as the observation and interpretation of motor actions in others (*131, 132*). The posterior parietal cortices have also been implicated in goal-directed movements, and are thought to be extremely important in the integration of motor plans with information from stimuli in the visual environment (*132-134*).

In addition to these well-studied spatial/anatomical characteristics, the spectral and temporal properties of the neural responses serving movement are becoming increasingly understood. Among the most important spectral features are neural oscillatory responses in the beta (~14 – 30 Hz) and gamma (> 30 Hz) frequency-bands. Decreases in spontaneous beta synchrony from baseline levels typically begin several hundred milliseconds prior to the onset of a movement, and quickly dissipate shortly after the movement is terminated. Thus, this response has been termed the peri-movement beta event-related desynchronization, or beta ERD (*135-144*). The beta ERD is most commonly localized to the M1 region contralateral to movement, however robust beta ERDs have

also been observed in the ipsilateral M1, parietal areas, premotor cortices, supplementary motor area, and cerebellum (*135-137, 140, 145-149*). The function of this response has been a topic of intense study for decades, and relevant research generally supports the notion that the beta ERD is essential for movement planning. For instance, the amplitude of the beta ERD has been found to be altered by cue-related factors (*145*), movement certainty (*150-152*) and complexity (*136*), and the similarity between potential movement options (*153, 154*). In contrast, oscillatory movement-related gamma synchronizations (MRGS) are commonly reported in the 60 – 90 Hz range, are much more temporally-constrained than their beta-band counterparts, and are almost exclusively located in the contralateral M1 region (*148, 155-160*). As the name suggests, MRGS responses are also *increases* in synchrony from baseline levels. Due to its relative spatial and temporal discreteness, the MRGS has long been interpreted as a neural signature of movement execution, however very few studies to date have investigated the potential for this signal to be modulated by "higher-order" task demands, such as attentional load and cognitive interference.

Cognitive interference occurs when there is an attentional conflict between two opposing stimuli or cognitive domains, such that behavior is impaired in some measurable way. Importantly, the resolution of this interference requires the attentional selection of one stimulus or domain and the inhibition of the other. The two most thoroughly studied subtypes of cognitive interference are conflicts at the stimulus perception (i.e., stimulus-stimulus) and response selection (i.e., stimulus-response) stages. To study these different forms of interference, a number of cognitive tasks have been developed. Among the most established are the Eriksen "flanker" task (see also *Chapter 1*), where the presence of irrelevant distractor stimuli flanking the target stimulus have been found to impair performance (stimulus-stimulus interference), and the Simon task, where the spatial

location of the target stimulus conflicts with the mapping of pre-potent motor responses (stimulus-response interference).

Despite a substantial literature exploring the effects of attention and the resolution of cognitive interference on non-motor neural dynamics (*27, 129, 161-169*), very little research has examined the impact of such interference on the neural dynamics of movement. Further, only three studies to date have examined the effects of cognitive interference on the oscillatory neural responses that are known to serve motor function. Two of these studies (*156, 170*) examined the effects of stimulus-stimulus interference on the beta ERD and MRGS using a flanker task, and both found that the amplitude of the beta ERD was greater on trials with attentional distractors present (i.e., higher cognitive interference). Interestingly, regarding the MRGS, one found a modulation of only the amplitude of this response (*170*), while the other found only a modulation of the peak frequency (*156*). However, this discrepancy is likely accounted for by the fact that the first study did not examine peak frequency, nor fully account for the potential influence of differences in reaction time (RT) between task conditions on the MRGS amplitude. A third study (*158*) used the classical version of the established multi-source interference task (MSIT) to investigate the influence of subtype-nonspecific cognitive interference on the MRGS. Although this study found a modulation of the MRGS amplitude by cognitive interference load, like (*170*) they did not account for the potential confounding influence of reaction time differences by condition. While all three of these studies provided essential information regarding the effects of cognitive interference on motor-related oscillatory dynamics, it remains uncertain how different subtypes of interference might play a role. It may be the case that differing subtypes of cognitive interference influence motor oscillations differentially, which would provide important and novel information regarding the functional significance of these neural responses. Alternatively, it seems equally likely that the interference subtypes will not differentially affect these motor oscillations,

signifying that these neural responses are important in the resolution of cognitive interference in general, but are subtype invariant. Finally, since the previous studies examined either only one subtype of interference in isolation (*156, 170*), or two subtypes presented simultaneously (*158*), the potential for divergent and superadditive effects of cognitive interference subtypes on these neural dynamics remains uncertain, as such effects could not be examined given the task design in these previous investigations. This is particularly important, as the existence of any shared neural resource for the resolution of cognitive interference subtypes in the motor system would provide direct evidence for a point of interaction between “higher-order” attention networks and “lower-order” motor systems.

In the current study, we use MEG to investigate the potential for divergent and superadditive effects of cognitive interference on the neural dynamics supporting movement; namely the beta ERD and MRGS responses. Towards this goal, we have developed a novel adaptation of the MSIT (Figure 15; see also *161, 169, 171*) that consists of four trial conditions including Flanker (stimulus-stimulus), Simon (stimulus-response), and Multi-Source (combined stimulus-stimulus *and* stimulus-response) interference, as well as a control (no interference) condition. We hypothesized that increased interference would lead to enhanced beta ERD responses in key motor regions, aligning with previous studies on this topic. Although the stimulus-response subtype might be expected to preferentially interfere with motor oscillations, previous reports have found that stimulus-stimulus interference also affects these neural responses robustly. Thus, we did not have specific hypotheses regarding whether differing subtypes of interference would differentially impact this response. However, given our previous findings (*169*), we did expect that superadditive effects of Multi-Source interference would manifest in the form of an increased MRGS.

Methods:

Participants

Twenty-three healthy young adults were recruited (M_{age} = 26.09; age range: 20-33 years; 16 males; 21 right-handed). Exclusion criteria included any medical illness affecting CNS function, any neurological or psychiatric disorder, history of head trauma, current substance abuse, and any non-removable metal implants that would adversely affect MEG data acquisition. All participants had normal or corrected-to-normal vision. The Institutional Review Board at the University of Nebraska Medical Center reviewed and approved this investigation. Written informed consent was obtained from each participant following detailed description of the study. All participants completed the same experimental protocol.

MEG Experimental Paradigm and Behavioral Data Analysis

We used a modified version of the MSIT (*169*) to engage cognitive interference networks (Figure 15). Briefly, each trial started with a central fixation cross presented for an inter-stimulus interval of 2000-2400 ms that was randomly-varied across trials. A vertically-centered row of three equally-spaced integers from 0 to 3 then replaced the fixation, and these stimuli were presented for 1500 ms. Two of the number stimuli were always identical (task-irrelevant), and the third unique to that trial (task-relevant). Prior to beginning the experiment, participants were given a five-finger button pad and instructed that the index, middle, and ring finger locations represented the integers 1, 2, and 3, respectively. Participants were then instructed that on each trial they would be presented with a horizontal row of three integers, and that the objective was to indicate the “odd-number-out” by pressing the button corresponding to its numerical identity (and *not* its spatial location). The importance of speed and accuracy was also stressed to the participant at this point. Using these stimuli, four interference conditions were possible: (1)

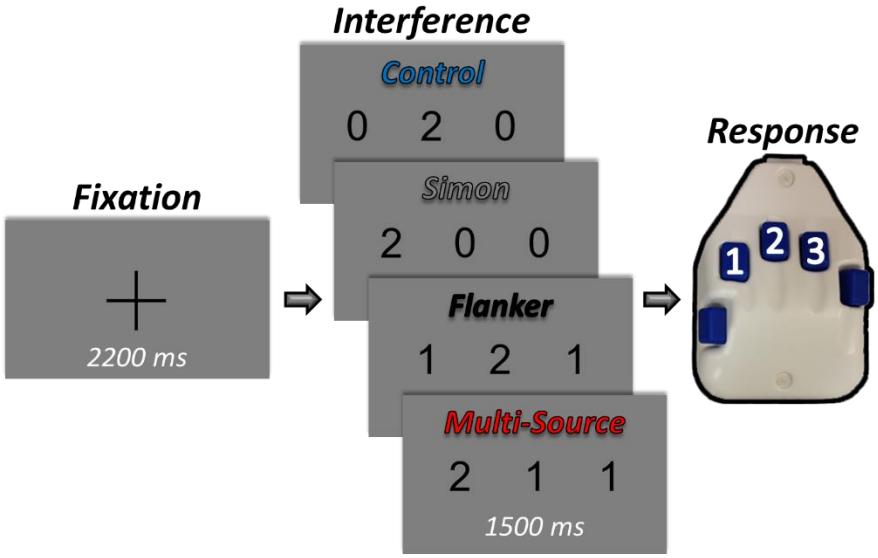

Figure 15. Multi-source interference task paradigm.

Each trial started with a central fixation cross presented for an inter-stimulus interval of 2000-2400 ms. A row of three equally-spaced integers between 0 and 3 then replaced the fixation, and these stimuli were presented for 1500 ms. Two of the number stimuli were always identical (task-irrelevant), and the third unique to that trial (task-relevant). Participants were given a five-finger button pad and instructed that the index, middle, and ring finger locations represented the integers 1, 2, and 3, respectively. Participants were instructed that on each trial they would be presented with a row of three integers, and that the objective was to indicate the "odd-number-out" by pressing the button corresponding to its numerical identity (and not its spatial location). Using these stimuli, four interference conditions were possible: (1) Control (no interference), (2) Simon (stimulus-response interference), (3) Flanker (stimulus-stimulus interference), and (4) Multi-Source.

Control (no interference; e.g., 0 2 0), (2) Simon (stimulus-response interference; e.g., 2 0 0), (3) Flanker (stimulus- stimulus interference; e.g., 1 2 1), and (4) Multi-Source (e.g., 2 1 1). Trial types and responses were pseudo-randomized over the course of the experiment, such that no interference condition nor any response was repeated more than twice in a row. Participants completed 100 trials of each interference condition, for a grand total of 400 trials, and a total recording time of ~24 minutes. Custom visual stimuli were programmed in Matlab (Mathworks, Inc., Massachusetts, USA) using *Psychophysics Toolbox Version 3* (*20*) and back-projected onto a nonmagnetic screen. For each participant, accuracy data were computed as a percentage (correct/total trials). Reaction time (RT) data were also extracted for each individual trial and incorrect and no-response

trials were removed. Outliers were excluded based on a standard threshold of ± 2.5 standard deviations from the mean, and subsequently mean RT values were computed for each participant. These metrics (i.e., accuracy and RT) were analyzed for main effects of interference condition using two four-way repeated measures ANOVAs, implemented in JASP (*123*). We next tested for superadditive effects of Multi-Source cognitive interference on behavior. To this end, we first computed the *interference effect* of each interference condition within each participant (i.e., the Flanker, Simon, and Multi-Source conditions) by subtracting each behavioral metric in the Control condition from the same metric in each condition (e.g., Simon RT - Control RT). From this, we were left with participant-level accuracy and RT values reflecting the difference in task performance caused by each type of interference. To test for superadditivity, we computed paired-samples t-tests separately for accuracy and RT between the Multi-Source interference condition and the summed effects of interference from the Simon and Flanker conditions, added within each participant. Using these tests, a rejection of the null hypothesis would indicate that the simultaneous presentation of two interference types (Multi-Source) affects task performance at a different magnitude than what would be expected by an additive model (Simon + Flanker).

MEG Data Acquisition

All recordings were conducted in a one-layer magnetically-shielded room with active shielding engaged for environmental noise compensation. Neuromagnetic responses were sampled continuously at 1 kHz with an acquisition bandwidth of 0.1– 330 Hz using a 306-sensor Elekta MEG system (Helsinki, Finland) equipped with 204 planar gradiometers and 102 magnetometers. Participants were monitored during data acquisition via real-time audio-video feeds from inside the shielded room. Each MEG

dataset was individually corrected for head motion and subjected to noise reduction using the signal space separation method with a temporal extension (tSSS; *21*).

Structural MRI Processing and MEG Coregistration

Preceding MEG measurement, four coils were attached to the participant's head and localized, together with the three fiducial points and scalp surface, using a 3-D digitizer (Fastrak 3SF0002, Polhemus Navigator Sciences, Colchester, VT, USA). Once the participant was positioned for MEG recording, an electric current with a unique frequency label (e.g., 322 Hz) was fed to each of the coils. This induced a measurable magnetic field and allowed each coil to be localized in reference to the sensors throughout the recording session. Since coil locations were also known in head coordinates, all MEG measurements could be transformed into a common coordinate system. With this coordinate system, each participant's MEG data were co-registered with structural T1-weighted MRI data in BESA MRI (Version 2.0) prior to source-space analysis. Structural MRI data were aligned parallel to the anterior and posterior commissures and transformed into standardized space. Following source analysis (i.e., beamforming), each participant's 4.0 x 4.0 x 4.0 mm source-level MEG images were also transformed into standardized space and spatially resampled.

MEG Preprocessing, Time-Frequency Transformation, and Sensor-Level Statistics

Cardiac and ocular artifacts were removed from the data using SSP, and the projection operator was subsequently accounted for during source reconstruction (*22*). The continuous magnetic time series was then divided into 3500 ms epochs, with the baseline extending from -1600 to -1100 ms prior to movement onset (i.e., button press). Importantly, this time window always fell within the visual fixation period, and thus our results were not biased by visual differences in the baseline period. Epochs containing artifacts were rejected using a fixed threshold method, supplemented with visual

inspection. An average of 345.52 (SD = 12.71) trials per participant were used for further analysis. The number of accepted trials did not differ across the four conditions ($p > .90$).

The artifact-free epochs were next transformed into the time-frequency domain using complex demodulation (*23*), with a frequency range of 4 to 100 Hz, and a time-frequency resolution of 2 Hz/25 ms. The resulting spectral power estimations per sensor were then averaged over trials to generate time-frequency plots of mean spectral density. These sensor-level data were normalized by each respective bin's baseline power, which was calculated as the mean power during the -1600 to -1100 ms time period. The specific time-frequency windows used for subsequent source imaging were determined by statistical analysis of the sensor-level spectrograms across all conditions and the entire array of gradiometers. Each data point in the spectrogram was initially evaluated using a mass univariate approach based on the general linear model. To reduce the risk of false positive results while maintaining reasonable sensitivity, a two stage procedure was followed to control for Type 1 error. In the first stage, paired-sample t-tests against baseline were conducted on each data point and the output spectrogram of t-values was thresholded at $p < 0.05$ to define time-frequency bins containing potentially significant oscillatory deviations across all participants. In stage two, the time-frequency bins that survived the threshold were clustered with temporally and/or spectrally neighboring bins that were also above the threshold ($p < 0.05$), and a cluster value was derived by summing all of the t-values of all data points in the cluster. Nonparametric permutation testing was then used to derive a distribution of cluster-values and the significance level of the observed clusters (from stage one) were tested directly using this distribution (*24, 25*). For each comparison, 1,000 permutations were computed to build a distribution of cluster values. Based on these analyses, the time-frequency windows that contained significant oscillatory events across all participants were subjected to a beamforming analysis.

MEG Source Imaging and Statistics

Cortical oscillatory activity was imaged using DICS (*26*), which applies spatial filters to time-frequency sensor data in order to calculate voxel-wise source power for the entire brain volume. The single images are derived from the cross spectral densities of all combinations of MEG gradiometers averaged over the time-frequency range of interest, and the solution of the forward problem for each location on a 4.0 x 4.0 x 4.0 mm grid specified by input voxel space. Following convention, we computed noise-normalized, source power per voxel in each participant using active (i.e., task) and passive (i.e., baseline) periods of equal duration and bandwidth. Such images are typically referred to as pseudo-t maps, with units (pseudo-t) that reflect noise-normalized power differences (i.e., active vs. passive) per voxel. This generated participant-level pseudo-t maps for each time-frequency-specific response identified in the sensor-level cluster-based permutation analysis. MEG pre-processing (including artifact rejection, SSP of cardiac and ocular artifacts, and data epoching), time frequency analysis, and imaging used the BESA (version 6.1) software suite.

To initially investigate the spatial location of each time-frequency-specific neural response to the task, we computed grand-average maps for each, collapsing across all interference conditions. These grand-average maps were used to discern the nature of each response, and thus ensure that all responses used for further analysis were of a motor origin. Importantly, we focus our interpretation here on those statistical effects that occurred in motor-related cortical regions, as this was where our neural responses of interest (i.e., the beta ERD and MRGS) were most robust. To examine interference-related differences in frequency-specific neural activity, we then computed whole-brain repeated-measures ANOVAs for each time-frequency response of interest (beta and gamma). From the resulting significant clusters, pseudo-t values per participant were extracted from the

peak voxel of each cluster, and these were used in post-hoc testing. Post-hoc testing consisted of two levels. First, we performed paired-samples t-tests between conditions on data from regions exhibiting a significant ANOVA effect, in order to better interpret the directionality and statistical significance of these effects. Next, to better understand the relative evidence for our effects, including those that did not meet the traditional criteria for rejecting the null hypothesis (i.e., $p < .05$), we computed Bayesian t-tests between these conditions to examine whether they presented evidence for or against the null hypothesis. Briefly, as opposed to a frequentist statistical approach, where one simply rejects or fails to reject the null hypothesis using arbitrary cutoffs (i.e., *p*–values), Bayes Factors (BF_{10}) represent the likelihood of the alternative hypothesis producing the same observed pattern in the data as compared to the null hypothesis, and thereby facilitates the interpretation of effects that seem to *support* the null hypothesis (rather than simply fail to reject it).

Finally, we computed whole-brain statistical maps investigating the potential for superadditivity of Multi-Source interference on the neural dynamics, similar to the comparisons made to test for superadditivity in the behavioral metrics (see above). For this analysis, we first performed a voxel-wise subtraction of the control condition map from each of the three interference condition maps for each participant per time-frequency component (i.e., beta and gamma). This produced participant-level whole-brain *interference effect* maps for each of the Simon, Flanker, and Multi-Source conditions. We then summed the voxel-wise values of the Simon and Flanker interference effect maps to produce a whole-brain map (per participant, per neural response), which represented the null hypothesis of an additive model. To then test the potential for superadditivity statistically, whole-brain paired-samples t-tests were computed between the Multi-Source interference model maps and these additive-model maps. It is important to note that these tests were performed one-tailed, since a two-tailed test would also investigate significant

sub-additive effects, and such an analysis was not justified by the behavioral data. The end result of this analysis was two spectrally-defined (i.e., one beta and one gamma) whole-brain statistical maps showing the cortical regions that exhibited a significantly larger interference effect in the Multi-Source condition than what would be expected from the additive model (H_1: Multi-Source > Simon+Flanker). Once again, pseudo-t values per participant were extracted from the peak voxel of each cluster in these maps for further testing. To account for multiple comparisons, a significance threshold of $p < .01$ was used for the identification of significant clusters in all whole-brain statistical maps, accompanied with a cluster (k) threshold of at least 200 contiguous voxels.

Results:

Spectral, Temporal, and Spatial Definitions of Neural Responses to the Task

Prior to testing for main effects of cognitive interference, we first needed to determine the temporal, spectral, and spatial locations of motor-related neural responses to the task, regardless of condition. We first transformed the data into time-frequency space, and observed robust neural activity in the beta and gamma bands (Figure 16) in sensors near the sensorimotor cortices. Specifically, a significant desynchronization was observed in the beta band (18 – 26 Hz) from 400 ms before movement to 100 ms after movement onset. In addition, we observed a significant synchronization from baseline in the gamma band (64 – 84 Hz) beginning 200 ms before movement and persisting until 100 ms after movement. Note that we did not image the post-movement beta rebound response (red area in top spectrogram) for two reasons. First, this task was ill-designed to investigate interference effects on this response, as the temporal offset of the visual stimuli occurred during the response and varied trial-to-trial due to variation in RT. Second, this response occurred well after movement and we were primarily interested in interference and attention effects on the planning and execution of movement.

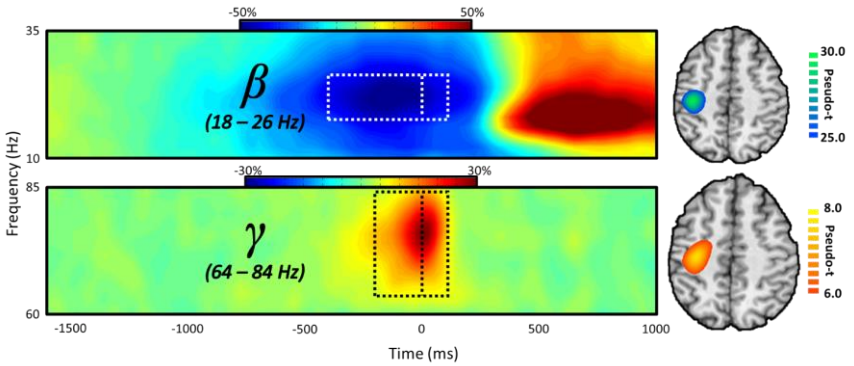

Figure 16. Spectral, temporal, and spatial definitions of oscillatory motor responses.

The representative MEG sensor–level spectrograms (top: beta – M0442; bottom: gamma – M0432) show the time-frequency representations of neural responses identified by cluster-based permutation analysis (see Methods). Time (in ms) is denoted on the x-axis, frequency (in Hz) is denoted on the y-axis, and the dashed line at 0 ms indicates the motor response. The dashed rectangle surrounding this line indicates the time-frequency definitions identified for source imaging by the cluster-based permutation test. The color scale bar for percent change from baseline is displayed above each plot. Each spectrogram represents group-averaged data across all conditions from one gradiometer sensor that was representative of these oscillatory neural responses. On the far right is the source-imaged representation of each response (beta ERD and MRGS), averaged across all conditions and participants, with the color scale bar to the right denoting response amplitude in pseudo-t units.

Effects of Cognitive Interference on Task Performance

Participants performed well on the task, with a mean accuracy of 96.49% (SD = 2.29%) and a mean reaction time (RT) of 739.32 ms (SD = 116.80 ms). Repeated-measures ANOVAs revealed a significant effect of interference condition on both accuracy ($F(3,66) = 22.37$, $p < .001$) and RT ($F(3,66) = 195.10$, $p < .001$; Figure 17). Post-hoc comparisons for accuracy revealed that participants were significantly less accurate in the Simon ($t(22) = -4.56$, $p < .001$) and Multi-Source ($t(22) = -5.43$, $p < .001$) conditions than in the Control condition. Further, participants were significantly less accurate in the Multi-Source condition than both the Simon ($t(22) = -2.60$, $p = .016$) and Flanker ($t(22) = -6.49$, $p < .001$) conditions. Finally, participants were significantly less accurate in the Simon condition compared to the Flanker condition ($t(22) = -4.53$, $p < .001$). The results of the post-hoc

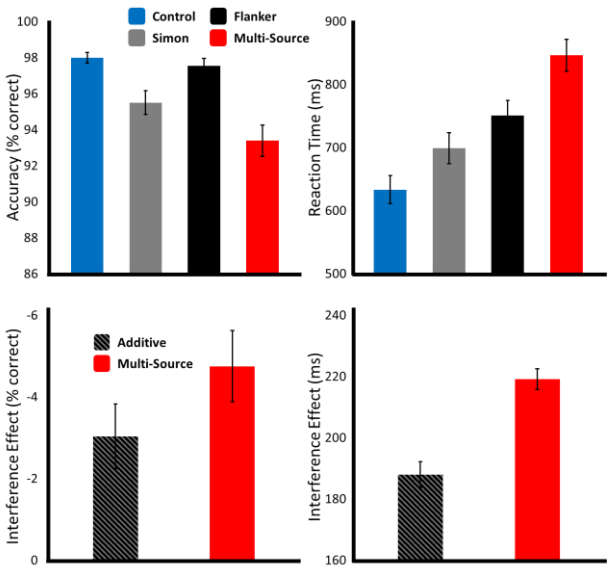

Figure 17. Divergent and superadditive effects of cognitive interference subtypes on behavior.

Results from the behavioral analyses, with reaction time and accuracy data for the main effect of interference condition (top), and for the superadditivity analyses (bottom). Bar graphs represent the mean per condition for accuracy (left; % correct) and reaction time (right; ms), with error bars representing the standard error of the mean (SEM).

comparisons for RT were generally similar to the accuracy results. Participants were significantly slower to respond on the Simon ($t(22) = 10.32$, $p < .001$), Flanker ($t(22) = 15.53$, $p < .001$), and Multi-Source ($t(22) = 19.52$, $p < .001$) trials relative to the Control trials. Further, participants were significantly slower in the Multi-Source condition than both the Simon ($t(22) = 15.61$, $p < .001$) and Flanker ($t(22) = 10.50$, $p < .001$) conditions. Interestingly, and in contrast to the accuracy results, participants performed significantly worse on Flanker than Simon trials ($t(22) = 4.34$, $p < .001$).

Upon visual inspection of these data, it became apparent that a superadditive effect of Multi-Source interference on task performance was likely. Indeed, paired-samples t-tests between the effect of Multi-Source interference and the additive model (Simon interference + Flanker interference) were significant for both accuracy ($t(22) = -2.25$, $p = .035$) and RT ($t(22) = 2.13$, $p = .044$), such that the concurrent presentation of the two interference sources significantly worsened behavior, as compared to their additive effects when presented in isolation (Figure 17).

Motor-related Neural Oscillations are Modulated by Cognitive Interference Irrespective of Subtype

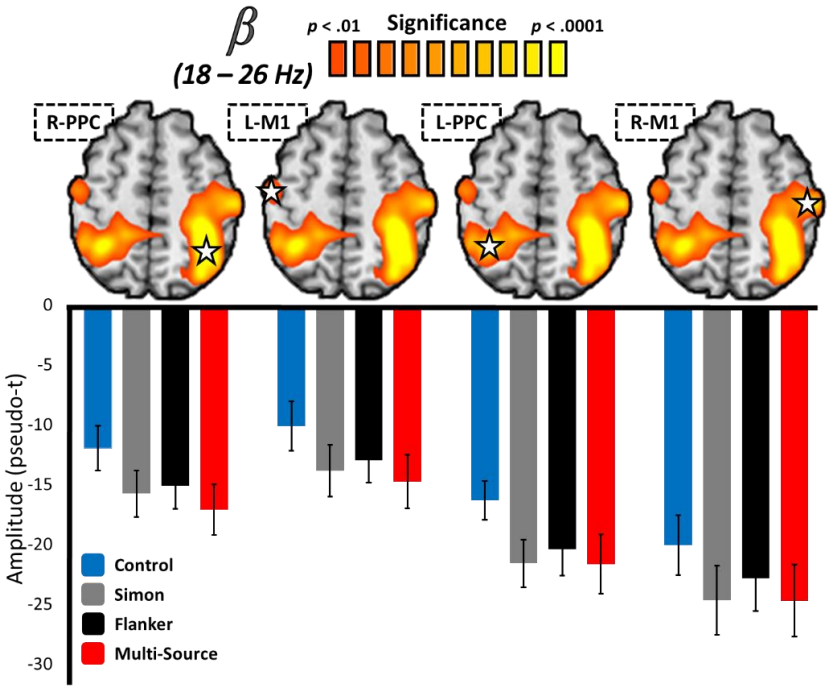

Figure 18. Divergent effects of cognitive interference subtypes on the beta ERD.

Functional images (above) reflect the significant results of a whole-brain repeated-measures ANOVA testing for a main effect of interference condition on the beta ERD response, with the color scale bar at the top denoting voxel-wise significance. Below each image are the average response amplitude values (in pseudo-t) per interference condition for the peak voxel (star) in the cluster, with error bars denoting the SEM. In virtually all cases, beta ERD responses were significantly stronger in the interference conditions than the control condition, but did not differ amongst interference conditions.

To investigate potentially-divergent effects of cognitive interference subtypes on motor-related oscillatory neural dynamics, we computed whole-brain repeated measures ANOVAs for the beta ERD and MRGS participant-level response maps separately. For the beta ERD, a robust main effect of condition was observed across four well-established motor-network regions, including peaks in bilateral M1 and bilateral posterior parietal cortex (PPC; Figure 18). Post-hoc testing revealed that beta activity in all four of these regions generally exhibited the same direction of effect. With the exception of the Simon condition in the left M1 peak, where the effect was trending, beta suppression in response to the interference conditions was significantly higher than in the control condition (all p's

< .05), but did not significantly differ between interference conditions (all p's > .05). For the MRGS, no significant ANOVA effects were found within the canonical motor network. We next computed Bayesian post-hoc analysis on the beta ERD interference data to examine whether there was greater evidence *for* or *against* the null hypothesis of no significant difference by interference condition (i.e., H_0: Simon = Flanker = Multi-Source). In every case, this analysis suggested greater evidence for the null hypothesis than the alternative hypothesis (i.e., a difference in beta ERD amplitude between interference conditions), although the strength of this evidence only reached what would typically be considered as mild to moderate. It should be noted that beta ERD ANOVA effects were also observed in the right cerebellum, right dorsolateral prefrontal, and left supramarginal cortices, and in the right superior parietal cortex for the MRGS analysis. However, the overall response amplitude in these regions was negligible, and thus we do not focus our interpretation on these effects.

The MRGS Indexes Interference Superadditivity in Premotor Cortex

Next, we examined the source of the superadditive effects of Multi-Source interference previously observed on behavior by computing whole-brain superadditivity statistical comparisons for the beta ERD and MRGS responses. Briefly, superadditivity suggests that the interference effects of the Simon and Flanker subtypes are greater when they are presented concurrently, as compared to when they are presented individually, and indicates shared neural resources between cognitive processes. To test where these shared neural resources reside, we computed whole-brain maps of the additive model (i.e., whole-brain Simon interference + whole-brain Flanker interference) and tested these against whole-brain maps of the Multi-Source interference effect. Only the MRGS response exhibited a superadditive effect of cognitive interference, and this effect was spatially constrained to the premotor cortex contralateral to movement (Figure 19).

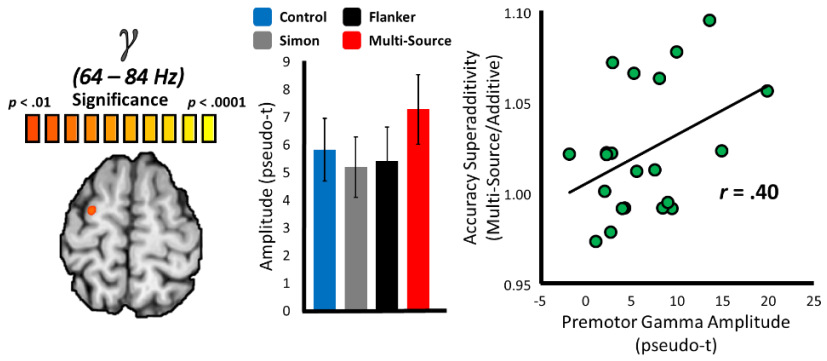

Figure 19. Superadditive effects of cognitive interference subtypes on the MRGS.

The functional image to the far left displays the results of a whole-brain statistical test for superadditivity in the motor-related gamma synchronization (MRGS), with the color scale bar at the top representing voxel-wise significance. The bar graph (middle) represents the average response amplitude values (in pseudo-t) for the peak superadditive voxel per interference condition, with error bars denoting SEM. The scatterplot to the right represents the relationship between response amplitude values extracted from the peak voxel of the whole-brain statistical superadditivity image to the left (x-axis; pseudo-t), and the superadditive effect of cognitive interference on task accuracy (y-axis; Multi-Source/Additive). A line of best-fit has been overlaid on the plot, along with the correlation coefficient for the relationship.

Supporting the association between movement-related gamma oscillations in this region and the superadditive effect on behavior, MRGS amplitude values extracted from the peak voxel of this cluster significantly covaried with the superadditive effect on accuracy (r = .40; p = .036, one-tailed). In other words, participants who exhibited a greater superadditive effect of concurrent interference presentation on behavior also exhibited a greater MRGS response in the premotor cortex. No significant superadditive effects were observed on the beta ERD.

Discussion:

Using MEG and a novel adaptation of an established cognitive interference task, we probed the potential for divergent and superadditive effects of two subtypes of cognitive interference on the oscillatory neural dynamics supporting a simple movement (i.e., a button press). Our primary findings were twofold: (1) a robust, but not subtype-specific nor compounding effect of cognitive interference on the beta ERD and (2) a more subtle

superadditive effect of simultaneously presented cognitive interference subtypes on the MRGS in premotor cortex. Below we discuss the significance and implications of these findings, as they relate to the established literature regarding oscillatory neural dynamics in the human motor system.

Our finding of a main effect of interference conditions on the beta ERD in M1 is not particularly surprising, as this has been the focus of, and consensus among, two previous studies on the topic (*156, 170*). What is perhaps surprising though, is both the spatial profile and nature of this effect. Firstly, our finding of an increased beta ERD with increased interference was located not only within bilateral M1 cortices (as has been found previously), but also across bilateral PPC. No previous studies investigating the effects of cognitive interference on motor oscillations have reported such an effect in the PPC, however, this is likely attributable to the fact that neither of the previous studies in this area performed whole-brain statistical measures at the level of the cortex (*156, 170*). This finding is especially pertinent, as the PPC has been implicated in the integration of motor plans and visual information from the environment (*132-134*), and the beta ERD in this region has specifically been found to be modulated by the complexity of the to-be-executed motor plan in a task utilizing visual sequence stimuli (*136*). Tentatively, this finding and others indicate that beta oscillations in the PPC may serve a role in integrating "bottom-up" and "top-down" signals, in the sense that these responses appear to be important for integrating top-down motor control with goal-directed processing of bottom-up visual information. A previous study by Feurra et al. (*172*) also supports the concept of a functional distinction between primary motor and posterior parietal cortices. In this study, the authors used non-invasive beta-frequency electrical stimulation over the primary motor and posterior parietal cortices, and show that only stimulation of M1, but not of PPC, altered the amplitude of TMS-induced motor evoked potentials. Secondly, the post-hoc Bayesian analysis of these data indicated that, although the beta ERD did generally

increase (i.e., exhibit a greater decrease from baseline) as a function of cognitive interference, there was no difference in the amplitude of the beta ERD as a function of interference subtype. Further, the amplitude of this response also did not significantly vary as to whether these subtypes were presented in isolation or in tandem. This suggests that the beta ERD in these distributed motor regions does not index the additive effects of cognitive interference, but rather a more general conflict between incoming bottom-up visual information and the eventual execution of the appropriate top-down motor response.

These data also exhibited an interesting, albeit surprising, pattern of behavioral results that indicated a superadditive effect of cognitive interference on task performance. To investigate the potential for a spectrally-specific oscillatory neural index of this phenomenon in the motor system, we computed whole-brain superadditivity statistical maps for both the beta ERD and MRGS. Intriguingly, we found that the MRGS, but not the beta ERD, exhibited a significant superadditivity effect in premotor cortex contralateral to movement. The amplitude of the gamma ERS response at this location was also significantly related to the superadditive effect on accuracy, providing further support for the relevance of this response to motor interference resolution. The premotor cortices have been robustly linked to the planning and execution of complex motor actions (*131, 132*); a conceptualization which aligns well with our findings of a compounding effect of cognitive interference in this region. In addition, gamma-frequency activity in frontal cortices is well supported as being essential for "top-down" control of goal-directed actions (*173-175*). Thus, this finding expands upon this literature by showing that frontal gamma signals are also essential for similar top-down control in the context of the attentional resolution of cognitive conflict in the motor system.

A number of previous tasks have found significant relationships between beta-frequency motor oscillations and behavior (*137, 138, 176, 177*), however, we found no such relationship here. Despite this null finding, we can reasonably infer from the direction

of our behavioral and beta ERD findings that the well-known pattern of greater beta desynchronizations being related to reduced performance is preserved in this study. In contrast, and as mentioned previously, the amplitude of the premotor gamma frequency response was significantly correlated with accuracy on the task. This relationship was such that, as the gamma amplitude increased, the superadditive effect on accuracy also increased. The direction of this relationship further supports our conceptualization of the gamma premotor oscillations as a top-down control signal, and lends credence to the link between this response and the superadditive effect on behavior.

Although our findings are novel and of major interest, the limitations of this work should also be considered. First, although we modulated the degree of cognitive interference at numerous levels, the motor action being integrated with these interference effects was exceedingly simple (i.e., a button press). Because of this, we were unable to examine the potential for interactive and dissociative effects of varying difficulties of motor complexity with stimulus-stimulus versus stimulus-response interference, which might be particularly interesting in light of our findings of a non-subtype-specific effect of interference on the beta ERD in PPC. Secondly, while our initial frequentist statistical approach showed robust evidence for rejection of the null hypothesis in many cases, our post-hoc Bayesian approach only indicated mild-to-moderate evidence for its acceptance in others. Interestingly, this evidence qualitatively appeared stronger in PPC than in M1 areas, but studies with larger sample sizes might further clarify this finding. Thirdly, as described in the methods, our task design did not allow careful investigation of the impact of cognitive interference on the post movement beta rebound (PMBR) response, and future studies should explore this avenue. Finally, the interactions between the brain regions identified in this study were not investigated, and thus more in-depth functional connectivity studies of this topic would be enlightening.

Despite these limitations, these findings provide compelling new evidence for a nuanced resolution of cognitive interference across a distributed and spectrally-specific series of motor regions. This is important for a number of reasons. For example, we establish that, although beta dynamics in the human motor system are affected by cognitive conflict, this influence does not differ as a function of interference subtype. This indicates that, while some portion of previously reported interference effects on behavior are likely due to conflict in the motor system, this cannot account for these effects entirely. More generally, these findings provide further evidence that neural activity at the level of the motor system is a key component in the attentional processing of cognitive conflict in the human brain. In addition, and aligning with our previous investigation (*169*), we find that gamma-frequency activity is specifically impacted by the superposition of distinct subtypes of cognitive interference. This provides a potential target to examine the impacts of competing stimulus inputs in cognitively taxing environments. By delineating the spectral specificity of these interference effects on motor function (i.e., general interference on beta oscillations and superadditive effects on gamma oscillations), we also provide more precise targets for future studies that might use non-invasive stimulation of motor cortices, with the goal of modulating goal-directed performance in health and disease.

CONCLUSIONS

These studies support the notion that attention systems interact with sensory and motor systems in the human brain, and that these interactions are extremely dynamic and frequency-dependent. In unison, these findings also give credence to the conceptualization of neural oscillations as a mechanism by which attention systems exert modulatory control on sensorimotor systems at the endogenous frequencies of each respective system: alpha frequencies in occipital cortex; theta, alpha, and beta frequencies in primary somatosensory cortex; and beta and gamma frequencies across an extended motor network. This should provide optimism for emerging non-invasive and invasive therapeutic strategies aimed at targeting spectrally specific neural activity in a spatially specific manner, as these techniques might be useful in ameliorating or even preventing attentional issues in neurologically afflicted patient groups. Of course, a great deal of research is first necessary, investigating the specific aberrations in these patterns of attention-sensorimotor interactions in such patient groups.

In the occipital cortices, we found that artificially enhanced alpha oscillations act to gate the functional flow of stimulus information into “later” visual cortices during selective attention, and that this gating effect is implemented through interference with fronto-parietal attention networks also oscillating in the alpha band. Together, these findings have established a dynamic bidirectional interplay between visual and fronto-parietal networks that is spectrally limited to the alpha band. Importantly, a number of patient populations with neurological disorders have been found to exhibit aberrant alpha-frequency activity in visual regions or during the performance of visual tasks, including HIV-associated neurocognitive disorders (*45, 178-180*), Alzheimer’s disease (*181-183*), and Parkinson’s disease (*6, 184, 185*). Since these same patient populations often present with attentional difficulties as well, future investigations of the role of oscillatory attention-

vision interactions in these patient groups may provide useful information regarding the pathophysiology of these impairments, as well as new targets for frequency-targeted therapeutic interventions.

In the somatosensory system, we found that attention differentially affects the functional gating of stimulus information in the theta, alpha, and beta bands. Specifically, these findings indicated a role for theta oscillations in initial stimulus recognition, and for alpha and beta oscillations in the attentional monitoring and interpretation of stimulus features (e.g., timing). Although previous research has suggested the importance of alpha/beta oscillations in somatosensory attention, these results extend this literature to a well-known metric of inhibition in sensory systems. Beta-frequency oscillations were also impacted robustly by the resolution of cognitive interference within the motor system, which provides further support for the general utility of beta-frequency neural activity in attentional regulation of very tightly coupled somato-motor systems. Future studies might directly probe the interplay between somatosensory and motor systems under differing attentional demands to provide additional support for this concept. Patients with Parkinson's disease have already been found to exhibit deficient functional connectivity between frontal and somato-motor cortices (*186-188*), and often present with attentional deficits that contribute to their risk of debilitating falls (*189*). Thus, similar studies of dynamic interactions between attention and somato-motor systems in this patient group would provide essential new information as well.

En masse, these studies lend credence to the theory that rhythmic patterns of neural oscillatory activity are, at least partially, responsible for the temporal organization and communication of information in the human brain. Further, the dynamic manipulation of these rhythmic patterns of neural activity by varying attentional demands indicates that they are essential to the enhancement of contextually defined "signal", and, in turn, the suppression of environmental "noise", that is required for effective cognitive function.

Perhaps more importantly, these findings also suggest that attentional modulation commonly occurs in the frequency-bands of oscillatory activity that are essential for the sensorimotor system under study. The most robust attention effects that we report across these studies align perfectly with the frequencies most essential to the respective sensorimotor system (i.e., alpha for somatosensory and visual, beta for motor), and so it seems likely that the these “preferred” frequencies are also the frequencies at which these sensory systems are most susceptible to modulation, either from endogenous sources such as top-down modulation from attention systems, or from exogenous sources of interference, such as frequency-targeted visual entrainment. As is apparent from the study described in Chapter 1, this susceptibility of sensorimotor circuits to specific input frequencies could even be exploited to influence cognitive abilities in mentally demanding environments. Further, this work holds promise for invasive and non-invasive methods of stimulating these sensorimotor systems with the goal of rectifying the relevant attentional deficiencies in patient populations. By targeting these stimulation protocols to the endogenous frequency of the sensorimotor system in question, it might be possible to correct these attentional impairments with minimal impact on other neural systems.

REFERENCES

*1. O. Jensen, A. Mazaheri, Shaping functional architecture by oscillatory alpha activity: gating by inhibition. Front Hum Neurosci **4**, 186 (2010).*

*2. T. A. Rihs, C. M. Michel, G. Thut, Mechanisms of selective inhibition in visual spatial attention are indexed by alpha-band EEG synchronization. Eur J Neurosci **25**, 603-610 (2007).*

*3. H. van Dijk, J. M. Schoffelen, R. Oostenveld, O. Jensen, Prestimulus oscillatory activity in the alpha band predicts visual discrimination ability. J Neurosci **28**, 1816-1823 (2008).*

*4. M. Bonnefond, O. Jensen, Alpha oscillations serve to protect working memory maintenance against anticipated distracters. Curr Biol **22**, 1969-1974 (2012).*

*5. E. Heinrichs-Graham, T. W. Wilson, Spatiotemporal oscillatory dynamics during the encoding and maintenance phases of a visual working memory task. Cortex **69**, 121-130 (2015).*

6. A. I. Wiesman et al., Quiet connections: Reduced fronto-temporal connectivity in nondemented Parkinson's Disease during working memory encoding. Hum Brain Mapp, (2016).

*7. A. L. Proskovec, E. Heinrichs-Graham, T. W. Wilson, Aging modulates the oscillatory dynamics underlying successful working memory encoding and maintenance. Hum Brain Mapp **37**, 2348-2361 (2016).*

*8. T. W. Wilson et al., Aberrant Neuronal Dynamics during Working Memory Operations in the Aging HIV-Infected Brain. Sci Rep **7**, 41568 (2017).*

*9. A. I. Wiesman et al., Polarity-dependent modulation of multi-spectral neuronal activity by transcranial direct current stimulation. Cortex **108**, 222-233 (2018).*

*10. J. J. Foster, E. Awh, The role of alpha oscillations in spatial attention: limited evidence for a suppression account. Curr Opin Psychol **29**, 34-40 (2018).*

*11. K. Schwab et al., Alpha entrainment in human electroencephalogram and magnetoencephalogram recordings. Neuroreport **17**, 1829-1833 (2006).*

*12. C. Keitel, C. Quigley, P. Ruhnau, Stimulus-driven brain oscillations in the alpha range: entrainment of intrinsic rhythms or frequency-following response? J Neurosci **34**, 10137-10140 (2014).*

*13. T. A. de Graaf et al., Alpha-band rhythms in visual task performance: phase-locking by rhythmic sensory stimulation. PLoS One **8**, e60035 (2013).*

14. A. I. Wiesman, B. R. Groff, T. W. Wilson, Frontoparietal Networks Mediate the Behavioral Impact of Alpha Inhibition in Visual Cortex. Cereb Cortex, (2018).

*15. R. Gulbinaite, T. van Viegen, M. Wieling, M. X. Cohen, R. VanRullen, Individual Alpha Peak Frequency Predicts 10 Hz Flicker Effects on Selective Attention. J Neurosci **37**, 10173-10184 (2017).*

*16. E. Spaak, F. P. de Lange, O. Jensen, Local entrainment of alpha oscillations by visual stimuli causes cyclic modulation of perception. J Neurosci **34**, 3536-3544 (2014).*

*17. K. E. Mathewson et al., Making waves in the stream of consciousness: entraining oscillations in EEG alpha and fluctuations in visual awareness with rhythmic visual stimulation. J Cogn Neurosci **24**, 2321-2333 (2012).*

*18. A. M. Norcia, L. G. Appelbaum, J. M. Ales, B. R. Cottereau, B. Rossion, The steady-state visual evoked potential in vision research: A review. J Vis **15**, 4 (2015).*

*19. D. J. Calderone, P. Lakatos, P. D. Butler, F. X. Castellanos, Entrainment of neural oscillations as a modifiable substrate of attention. Trends Cogn Sci **18**, 300-309 (2014).*

*20. D. H. Brainard, The Psychophysics Toolbox. Spatial Vision **10**, 433-436 (1997).*

*21. S. Taulu, J. Simola, Spatiotemporal signal space separation method for rejecting nearby interference in MEG measurements. Phys Med Biol **51**, 1759-1768 (2006).*

*22. M. A. Uusitalo, R. J. Ilmoniemi, Signal-space projection method for separating MEG or EEG into components. Med Biol Eng Comput **35**, 135-140 (1997).*

*23. C. K. Kovach, P. E. Gander, The demodulated band transform. J Neurosci Methods **261**, 135-154 (2016).*

*24. M. D. Ernst, Permutation methods: a basis for exact inference. Statistical Science **19**, 676-685 (2004).*

*25. E. Maris, R. Oostenveld, Nonparametric statistical testing of EEG- and MEG-data. J Neurosci Methods **164**, 177-190 (2007).*

*26. J. Gross et al., Dynamic imaging of coherent sources: Studying neural interactions in the human brain. Proc Natl Acad Sci U S A **98**, 694-699 (2001).*

*27. T. J. McDermott, A. I. Wiesman, A. L. Proskovec, E. Heinrichs-Graham, T. W. Wilson, Spatiotemporal oscillatory dynamics of visual selective attention during a flanker task. Neuroimage **156**, 277-285 (2017).*

*28. S. T. Morgan, J. C. Hansen, S. A. Hillyard, Selective attention to stimulus location modulates the steady-state visual evoked potential. Proc Natl Acad Sci U S A **93**, 4770-4774 (1996).*

29. J. Team. (2018).

*30. D. Tingley, T. Yamamoto, K. Hirose, L. Keele, K. Imai, mediation: R Package for Causal Mediation Analysis. . Journal of Statistical Software **59**, 1-38 (2014).*

31. R. C. Team. (R Foundation for Statistical Computing, Vienna, Austria, 2017).

*32. G. Thut, P. G. Schyns, J. Gross, Entrainment of perceptually relevant brain oscillations by non-invasive rhythmic stimulation of the human brain. Front Psychol **2**, 170 (2011).*

*33. B. A. Eriksen, C. W. Eriksen, Effects of noise letters upon the identification of a target letter in a nonsearch task. Perception & Psychophysics **16**, 143-149 (1974).*

*34. E. Heinrichs-Graham, T. W. Wilson, Presence of strong harmonics during visual entrainment: a magnetoencephalography study. Biol Psychol **91**, 59-64 (2012).*

*35. T. Womelsdorf, P. Fries, The role of neuronal synchronization in selective attention. Curr Opin Neurobiol **17**, 154-160 (2007).*

*36. T. Demiralp, E. Başar, Theta rhythmicities following expected visual and auditory targets. Int J Psychophysiol **13**, 147-160 (1992).*

*37. A. I. Wiesman, E. Heinrichs-Graham, A. L. Proskovec, T. J. McDermott, T. W. Wilson, Oscillations during observations: Dynamic oscillatory networks serving visuospatial attention. Hum Brain Mapp **38**, 5128-5140 (2017).*

*38. C. Tallon-Baudry, O. Bertrand, M. A. Henaff, J. Isnard, C. Fischer, Attention modulates gamma-band oscillations differently in the human lateral occipital cortex and fusiform gyrus. Cereb Cortex **15**, 654-662 (2005).*

*39. A. Posada, E. Hugues, N. Franck, P. Vianin, J. Kilner, Augmentation of induced visual gamma activity by increased task complexity. Eur J Neurosci **18**, 2351-2356 (2003).*

*40. T. R. Marshall, J. O'Shea, O. Jensen, T. O. Bergmann, Frontal eye fields control attentional modulation of alpha and gamma oscillations in contralateral occipitoparietal cortex. J Neurosci **35**, 1638-1647 (2015).*

*41. N. A. Busch, J. Dubois, R. VanRullen, The phase of ongoing EEG oscillations predicts visual perception. J Neurosci **29**, 7869-7876 (2009).*

*42. O. Jensen, B. Gips, T. O. Bergmann, M. Bonnefond, Temporal coding organized by coupled alpha and gamma oscillations prioritize visual processing. Trends Neurosci **37**, 357-369 (2014).*

*43. S. D. Muthukumaraswamy, K. D. Singh, Visual gamma oscillations: the effects of stimulus type, visual field coverage and stimulus motion on MEG and EEG recordings. Neuroimage **69**, 223-230 (2013).*

*44. J. R. Vidal, M. Chaumon, J. K. O'Regan, C. Tallon-Baudry, Visual grouping and the focusing of attention induce gamma-band oscillations at different frequencies in human magnetoencephalogram signals. J Cogn Neurosci **18**, 1850-1862 (2006).*

45. A. I. Wiesman et al., Aberrant occipital dynamics differentiate HIV-infected patients with and without cognitive impairment. Brain, (2018).

*46. A. Bompas, P. Sumner, S. D. Muthumumaraswamy, K. D. Singh, I. D. Gilchrist, The contribution of pre-stimulus neural oscillatory activity to spontaneous response time variability. Neuroimage **107**, 34-45 (2015).*

*47. A. I. Wiesman, E. Heinrichs-Graham, A. L. Proskovec, T. J. McDermott, T. W. Wilson, Oscillations during Observations: Dynamic Oscillatory Networks Serving Visuospatial Attention. Hum Brain Map **38**, 5128-5140 (2017).*

48. A. L. Proskovec, E. Heinrichs-Graham, A. I. Wiesman, T. J. McDermott, T. W. Wilson, Oscillatory dynamics in the dorsal and ventral attention networks during the reorienting of attention. Hum Brain Mapp, (2018).

*49. B. F. Handel, T. Haarmeier, O. Jensen, Alpha oscillations correlate with the successful inhibition of unattended stimuli. J Cogn Neurosci **23**, 2494-2502 (2011).*

*50. W. Klimesch, α-band oscillations, attention, and controlled access to stored information. Trends Cogn Sci **16**, 606-617 (2012).*

*51. J. J. Foxe, A. C. Snyder, The Role of Alpha-Band Brain Oscillations as a Sensory Suppression Mechanism during Selective Attention. Front Psychol **2**, 154 (2011).*

*52. S. P. Kelly, E. C. Lalor, R. B. Reilly, J. J. Foxe, Increases in alpha oscillatory power reflect an active retinotopic mechanism for distracter suppression during sustained visuospatial attention. J Neurophysiol **95**, 3844-3851 (2006).*

*53. P. Capotosto, C. Babiloni, G. L. Romani, M. Corbetta, Frontoparietal cortex controls spatial attention through modulation of anticipatory alpha rhythms. J Neurosci **29**, 5863-5872 (2009).*

*54. V. Romei, J. Gross, G. Thut, On the role of prestimulus alpha rhythms over occipito-parietal areas in visual input regulation: correlation or causation? J Neurosci **30**, 8692-8697 (2010).*

*55. P. Sauseng, J. F. Feldheim, R. Freunberger, F. C. Hummel, Right Prefrontal TMS Disrupts Interregional Anticipatory EEG Alpha Activity during Shifting of Visuospatial Attention. Front Psychol **2**, 241 (2011).*

*56. J. D. Herring, G. Thut, O. Jensen, T. O. Bergmann, Attention Modulates TMS-Locked Alpha Oscillations in the Visual Cortex. J Neurosci **35**, 14435-14447 (2015).*

*57. P. Ruhnau et al., Eyes wide shut: Transcranial alternating current stimulation drives alpha rhythm in a state dependent manner. Sci Rep **6**, 27138 (2016).*

*58. T. Zaehle, S. Rach, C. S. Herrmann, Transcranial alternating current stimulation enhances individual alpha activity in human EEG. PLoS One **5**, e13766 (2010).*

*59. T. W. Wilson, T. J. McDermott, M. S. Mills, N. M. Coolidge, E. Heinrichs-Graham, tDCS Modulates Visual Gamma Oscillations and Basal Alpha Activity in Occipital Cortices: Evidence from MEG. Cereb Cortex **28**, 1597-1609 (2018).*

*60. E. Heinrichs-Graham, T. J. McDermott, M. S. Mills, N. M. Coolidge, T. W. Wilson, Transcranial direct-current stimulation modulates offline visual oscillatory activity: A magnetoencephalography study. Cortex **88**, 19-31 (2017).*

*61. C. Lithari, C. Sánchez-García, P. Ruhnau, N. Weisz, Large-scale network-level processes during entrainment. Brain Res **1635**, 143-152 (2016).*

*62. G. Rohenkohl, A. C. Nobre, α oscillations related to anticipatory attention follow temporal expectations. J Neurosci **31**, 14076-14084 (2011).*

*63. A. I. Wiesman et al., Aberrant Occipital Dynamics Differentiate HIV-infected Patients With and Without Cognitive Impairment. Brain **In press**, (2018).*

*64. O. Jensen, J. Gelfand, J. Kounios, J. E. Lisman, Oscillations in the alpha band (9-12 Hz) increase with memory load during retention in a short-term memory task. Cereb Cortex **12**, 877-882 (2002).*

65. P. L. Nunez, B. A. Cutillo, Eds., Neocortical dynamics and human EEG rhythms, (Oxford University Press, USA, 1995).

*66. J. Ding, G. Sperling, R. Srinivasan, Attentional modulation of SSVEP power depends on the network tagged by the flicker frequency. Cereb Cortex **16**, 1016-1029 (2006).*

*67. C. S. Herrmann, Human EEG responses to 1-100 Hz flicker: resonance phenomena in visual cortex and their potential correlation to cognitive phenomena. Exp Brain Res **137**, 346-353 (2001).*

*68. Y. J. Kim, M. Grabowecky, K. A. Paller, K. Muthu, S. Suzuki, Attention induces synchronization-based response gain in steady-state visual evoked potentials. Nat Neurosci **10**, 117-125 (2007).*

*69. M. I. Posner, Orienting of attention. Q J Exp Psychol **32**, 3-25 (1980).*

*70. W. Klimesch, EEG alpha and theta oscillations reflect cognitive and memory performance: a review and analysis. Brain Res Brain Res Rev **29**, 169-195 (1999).*

*71. R. I. Goldman, J. M. Stern, J. Engel, M. S. Cohen, Simultaneous EEG and fMRI of the alpha rhythm. Neuroreport **13**, 2487-2492 (2002).*

*72. S. K. Andersen, M. M. Müller, Behavioral performance follows the time course of neural facilitation and suppression during cued shifts of feature-selective attention. Proc Natl Acad Sci U S A **107**, 13878-13882 (2010).*

*73. S. K. Andersen, M. M. Müller, J. Martinovic, Bottom-up biases in feature-selective attention. J Neurosci **32**, 16953-16958 (2012).*

*74. M. M. Müller et al., Feature-selective attention enhances color signals in early visual areas of the human brain. Proc Natl Acad Sci U S A **103**, 14250-14254 (2006).*

*75. B. J. Weiland, N. N. Boutros, J. M. Moran, N. Tepley, S. M. Bowyer, Evidence for a frontal cortex role in both auditory and somatosensory habituation: a MEG study. Neuroimage **42**, 827-835 (2008).*

*76. P. L. Davies, W. P. Chang, W. J. Gavin, Maturation of sensory gating performance in children with and without sensory processing disorders. Int J Psychophysiol **72**, 187-197 (2009).*

*77. L. E. Adler et al., Neurophysiological evidence for a defect in neuronal mechanisms involved in sensory gating in schizophrenia. Biol Psychiatry **17**, 639-654 (1982).*

*78. R. K. Spooner et al., Aberrant oscillatory dynamics during somatosensory processing in HIV-infected adults. Neuroimage Clin **20**, 85-91 (2018).*

79. M. J. Kurz, A. I. Wiesman, N. M. Coolidge, T. W. Wilson, Children with Cerebral Palsy Hyper-Gate Somatosensory Stimulations of the Foot. Cereb Cortex, 1-8 (2017).

80. A. I. Wiesman et al., Oscillatory dynamics and functional connectivity during gating of primary somatosensory responses. J Physiol, (2016).

*81. R. K. Spooner, A. I. Wiesman, A. L. Proskovec, E. Heinrichs-Graham, T. W. Wilson, Rhythmic Spontaneous Activity Mediates the Age-Related Decline in Somatosensory Function. Cereb Cortex **29**, 680-688 (2019).*

*82. C. H. Cheng, P. Y. Chan, S. Baillet, Y. Y. Lin, Age-Related Reduced Somatosensory Gating Is Associated with Altered Alpha Frequency Desynchronization. Neural Plast **2015**, 302878 (2015).*

*83. R. J. Thoma et al., Impaired secondary somatosensory gating in patients with schizophrenia. Psychiatry Res **151**, 189-199 (2007).*

*84. F. J. Hsiao, C. H. Cheng, W. T. Chen, Y. Y. Lin, Neural correlates of somatosensory paired-pulse suppression: a MEG study using distributed source modeling and dynamic spectral power analysis. Neuroimage **72**, 133-142 (2013).*

*85. T. Grunwald et al., Neuronal substrates of sensory gating within the human brain. Biol Psychiatry **53**, 511-519 (2003).*

*86. M. Lijffijt et al., P50, N100, and P200 sensory gating: relationships with behavioral inhibition, attention, and working memory. Psychophysiology **46**, 1059-1068 (2009).*

*87. L. P. Karper et al., Preliminary evidence of an association between sensorimotor gating and distractibility in psychosis. J Neuropsychiatry Clin Neurosci **8**, 60-66 (1996).*

*88. L. A. Jones, P. J. Hills, K. M. Dick, S. P. Jones, P. Bright, Cognitive mechanisms associated with auditory sensory gating. Brain Cogn **102**, 33-45 (2016).*

*89. L. Wan, B. H. Friedman, N. N. Boutros, H. J. Crawford, P50 sensory gating and attentional performance. Int J Psychophysiol **67**, 91-100 (2008).*

90. S. J. Golubic et al., Attention modulates topology and dynamics of auditory sensory gating. Hum Brain Mapp, (2019).

*91. T. Rosburg, P. Trautner, C. E. Elger, M. Kurthen, Attention effects on sensory gating--intracranial and scalp recordings. Neuroimage **48**, 554-563 (2009).*

*92. K. H. Kho et al., P50 gating is not affected by selective attention. Journal of Psychophysiology **17**, 23 (2003).*

93. K. Gjini, S. Burroughs, N. N. Boutros, Relevance of Attention in Auditory Sensory Gating Paradigms in Schizophrenia. Journal of psychophysiology, (2011).

*94. S. Haegens, L. Luther, O. Jensen, Somatosensory anticipatory alpha activity increases to suppress distracting input. J Cogn Neurosci **24**, 677-685 (2012).*

*95. S. Haegens, B. F. Händel, O. Jensen, Top-down controlled alpha band activity in somatosensory areas determines behavioral performance in a discrimination task. J Neurosci **31**, 5197-5204 (2011).*

*96. S. R. Jones et al., Cued spatial attention drives functionally relevant modulation of the mu rhythm in primary somatosensory cortex. J Neurosci **30**, 13760-13765 (2010).*

*97. T. Bardouille, T. W. Picton, B. Ross, Attention modulates beta oscillations during prolonged tactile stimulation. Eur J Neurosci **31**, 761-769 (2010).*

*98. F. van Ede, S. Szebényi, E. Maris, Attentional modulations of somatosensory alpha, beta and gamma oscillations dissociate between anticipation and stimulus processing. Neuroimage **97**, 134-141 (2014).*

*99. F. van Ede, O. Jensen, E. Maris, Tactile expectation modulates pre-stimulus beta-band oscillations in human sensorimotor cortex. Neuroimage **51**, 867-876 (2010).*

*100. Y. Hlushchuk, R. Hari, Transient suppression of ipsilateral primary somatosensory cortex during tactile finger stimulation. J Neurosci **26**, 5819-5824 (2006).*

*101. R. Hari, N. Forss, Magnetoencephalography in the study of human somatosensory cortical processing. Philos Trans R Soc Lond B Biol Sci **354**, 1145-1154 (1999).*

*102. A. Schnitzler, R. Salmelin, S. Salenius, V. Jousmaki, R. Hari, Tactile information from the human hand reaches the ipsilateral primary somatosensory cortex. Neurosci Lett **200**, 25-28 (1995).*

*103. J. Huttunen, E. Pekkonen, R. Kivisaari, T. Autti, S. Kahkonen, Modulation of somatosensory evoked fields from SI and SII by acute GABA A-agonism and paired-pulse stimulation. Neuroimage **40**, 427-434 (2008).*

*104. A. Kanno, N. Nakasato, K. Hatanaka, T. Yoshimoto, Ipsilateral area 3b responses to median nerve somatosensory stimulation. Neuroimage **18**, 169-177 (2003).*

*105. L. M. Andersen, D. Lundqvist, Somatosensory responses to nothing: an MEG study of expectations during omission of tactile stimulations. NeuroImage **184**, 78-89 (2019).*

*106. C. Dockstader, D. Cheyne, R. Tannock, Cortical dynamics of selective attention to somatosensory events. Neuroimage **49**, 1777-1785 (2010).*

*107. S. Whitmarsh, H. Barendregt, J. M. Schoffelen, O. Jensen, Metacognitive awareness of covert somatosensory attention corresponds to contralateral alpha power. Neuroimage **85 Pt 2**, 803-809 (2014).*

*108. L. E. Adler, L. J. Hoffer, J. Griffith, M. C. Waldo, R. Freedman, Normalization by nicotine of deficient auditory sensory gating in the relatives of schizophrenics. Biol Psychiatry **32**, 607-616 (1992).*

*109. L. E. Adler et al., Schizophrenia, sensory gating, and nicotinic receptors. Schizophr Bull **24**, 189-202 (1998).*

*110. H. C. Cromwell, R. P. Mears, L. Wan, N. N. Boutros, Sensory gating: a translational effort from basic to clinical science. Clin EEG Neurosci **39**, 69-72 (2008).*

*111. C. H. Cheng, Y. Y. Lin, Aging-related decline in somatosensory inhibition of the human cerebral cortex. Exp Brain Res **226**, 145-152 (2013).*

*112. C. H. Cheng, S. Baillet, Y. Y. Lin, Region-specific reduction of auditory sensory gating in older adults. Brain Cogn **101**, 64-72 (2015).*

*113. C. Thomas et al., P50 gating deficit in Alzheimer dementia correlates to frontal neuropsychological function. Neurobiol Aging **31**, 416-424 (2010).*

*114. B. A. Ally, G. E. Jones, J. A. Cole, A. E. Budson, Sensory gating in patients with Alzheimer's disease and their biological children. Am J Alzheimers Dis Other Demen **21**, 439-447 (2006).*

*115. M. Lijffijt et al., Diminished P50, N100 and P200 auditory sensory gating in bipolar I disorder. Psychiatry Res **167**, 191-201 (2009).*

*116. I. Zakharova, J. C. Kohlmeyer, M. E. Kornhuber, Facilitation dynamics of late somatosensory evoked potentials after sural nerve stimulation. Clin Neurophysiol **127**, 2545-2550 (2016).*

*117. N. Bak, B. Y. Glenthoj, E. Rostrup, H. B. Larsson, B. Oranje, Source localization of sensory gating: a combined EEG and fMRI study in healthy volunteers. Neuroimage **54**, 2711-2718 (2011).*

*118. D. J. Arpin, J. E. Gehringer, T. W. Wilson, M. J. Kurz, A reduced somatosensory gating response in individuals with multiple sclerosis is related to walking impairment. J Neurophysiol **118**, 2052-2058 (2017).*

*119. K. Hoechstetter et al., BESA source coherence: a new method to study cortical oscillatory coupling. Brain Topogr **16**, 233-238 (2004).*

*120. N. Papp, P. Ktonas, Critical evaluation of complex demodulation techniques for the quantification of bioelectrical activity. Biomed Sci Instrum **13**, 135-145 (1977).*

*121. R. D. Pascual-Marqui, Standardized low-resolution brain electromagnetic tomography (sLORETA): technical details. Methods Find Exp Clin Pharmacol **24**, 5-12 (2002).*

*122. J. M. Schoffelen, J. Gross, Source connectivity analysis with MEG and EEG. Hum Brain Mapp **30**, 1857-1865 (2009).*

123. JASP-Team. (2018).

*124. W. R. Staines, S. J. Graham, S. E. Black, W. E. McIlroy, Task-relevant modulation of contralateral and ipsilateral primary somatosensory cortex and the role of a prefrontal-cortical sensory gating system. Neuroimage **15**, 190-199 (2002).*

*125. S. Yamaguchi, R. T. Knight, Gating of somatosensory input by human prefrontal cortex. Brain Res **521**, 281-288 (1990).*

*126. T. W. Wilson et al., Multimodal neuroimaging evidence of alterations in cortical structure and function in HIV-infected older adults. Hum Brain Mapp **36**, 897-910 (2015).*

*127. C. Janssens, E. De Loof, C. N. Boehler, G. Pourtois, T. Verguts, Occipital alpha power reveals fast attentional inhibition of incongruent distractors. Psychophysiology **55**, (2018).*

*128. W. Klimesch, P. Sauseng, S. Hanslmayr, EEG alpha oscillations: the inhibition-timing hypothesis. Brain Res Rev **53**, 63-88 (2007).*

129. A. I. Wiesman, T. W. Wilson, Alpha Frequency Entrainment Reduces the Effect of Visual Distractors. Journal of cognitive neuroscience, 1-12 (2019).

*130. K. Torquati et al., "Gating" effects of simultaneous peripheral electrical stimulations on human secondary somatosensory cortex: a whole-head MEG study. Neuroimage **20**, 1704-1713 (2003).*

*131. G. Rizzolatti, L. Fogassi, V. Gallese, Motor and cognitive functions of the ventral premotor cortex. Curr Opin Neurobiol **12**, 149-154 (2002).*

*132. T. Hanakawa, M. A. Dimyan, M. Hallett, Motor planning, imagery, and execution in the distributed motor network: a time-course study with functional MRI. Cereb Cortex **18**, 2775-2788 (2008).*

*133. V. B. Mountcastle, J. C. Lynch, A. Georgopoulos, H. Sakata, C. Acuna, Posterior parietal association cortex of the monkey: command functions for operations within extrapersonal space. J Neurophysiol **38**, 871-908 (1975).*

*134. M. Desmurget et al., Role of the posterior parietal cortex in updating reaching movements to a visual target. Nat Neurosci **2**, 563-567 (1999).*

*135. D. Cheyne, L. Bakhtazad, W. Gaetz, Spatiotemporal mapping of cortical activity accompanying voluntary movements using an event-related beamforming approach. Hum Brain Mapp **27**, 213-229 (2006).*

*136. E. Heinrichs-Graham, T. W. Wilson, Coding complexity in the human motor circuit. Hum Brain Mapp **36**, 5155-5167 (2015).*

*137. E. Heinrichs-Graham, T. W. Wilson, Is an absolute level of cortical beta suppression required for proper movement? Magnetoencephalographic evidence from healthy aging. Neuroimage **134**, 514-521 (2016).*

*138. E. Heinrichs-Graham et al., The lifespan trajectory of neural oscillatory activity in the motor system. Dev Cogn Neurosci **30**, 159-168 (2018).*

*139. T. W. Wilson et al., Functional brain abnormalities during finger-tapping in HIV-infected older adults: a magnetoencephalography study. J Neuroimmune Pharmacol **8**, 965-974 (2013).*

*140. T. W. Wilson, E. Heinrichs-Graham, K. M. Becker, Circadian modulation of motor-related beta oscillatory responses. Neuroimage **102 Pt 2**, 531-539 (2014).*

*141. W. Gaetz, M. Macdonald, D. Cheyne, O. C. Snead, Neuromagnetic imaging of movement-related cortical oscillations in children and adults: age predicts post-movement beta rebound. Neuroimage **51**, 792-807 (2010).*

*142. A. K. Engel, P. Fries, Beta-band oscillations--signalling the status quo? Curr Opin Neurobiol **20**, 156-165 (2010).*

*143. M. T. Jurkiewicz, W. C. Gaetz, A. C. Bostan, D. Cheyne, Post-movement beta rebound is generated in motor cortex: evidence from neuromagnetic recordings. Neuroimage **32**, 1281-1289 (2006).*

*144. G. Pfurtscheller, F. H. Lopes da Silva, Event-related EEG/MEG synchronization and desynchronization: basic principles. Clin Neurophysiol **110**, 1842-1857 (1999).*

*145. E. Heinrichs-Graham, D. J. Arpin, T. W. Wilson, Cue-related Temporal Factors Modulate Movement-related Beta Oscillatory Activity in the Human Motor Circuit. J Cogn Neurosci **28**, 1039-1051 (2016).*

*146. M. J. Kurz, K. M. Becker, E. Heinrichs-Graham, T. W. Wilson, Neurophysiological abnormalities in the sensorimotor cortices during the motor planning and movement execution stages of children with cerebral palsy. Dev Med Child Neurol **56**, 1072-1077 (2014).*

*147. T. W. Wilson et al., Abnormal gamma and beta MEG activity during finger movements in early-onset psychosis. Dev Neuropsychol **36**, 596-613 (2011).*

*148. T. W. Wilson et al., An extended motor network generates beta and gamma oscillatory perturbations during development. Brain Cogn **73**, 75-84 (2010).*

*149. A. Brovelli et al., Beta oscillations in a large-scale sensorimotor cortical network: directional influences revealed by Granger causality. Proc Natl Acad Sci U S A **101**, 9849-9854 (2004).*

*150. L. M. Doyle, K. Yarrow, P. Brown, Lateralization of event-related beta desynchronization in the EEG during pre-cued reaction time tasks. Clin Neurophysiol **116**, 1879-1888 (2005).*

*151. J. Kaiser, N. Birbaumer, W. Lutzenberger, Event-related beta desynchronization indicates timing of response selection in a delayed-response paradigm in humans. Neurosci Lett **312**, 149-152 (2001).*

*152. C. Tzagarakis, N. F. Ince, A. C. Leuthold, G. Pellizzer, Beta-band activity during motor planning reflects response uncertainty. J Neurosci **30**, 11270-11277 (2010).*

*153. T. Grent-'t-Jong, R. Oostenveld, O. Jensen, W. P. Medendorp, P. Praamstra, Competitive interactions in sensorimotor cortex: oscillations express separation between alternative movement targets. J Neurophysiol **112**, 224-232 (2014).*

*154. P. Praamstra, D. Kourtis, K. Nazarpour, Simultaneous preparation of multiple potential movements: opposing effects of spatial proximity mediated by premotor and parietal cortex. J Neurophysiol **102**, 2084-2095 (2009).*

*155. S. D. Muthukumaraswamy, Functional properties of human primary motor cortex gamma oscillations. J Neurophysiol **104**, 2873-2885 (2010).*

*156. E. Heinrichs-Graham, J. M. Hoburg, T. W. Wilson, The peak frequency of motor-related gamma oscillations is modulated by response competition. Neuroimage **165**, 27-34 (2018).*

*157. W. Gaetz, J. C. Edgar, D. J. Wang, T. P. Roberts, Relating MEG measured motor cortical oscillations to resting γ-aminobutyric acid (GABA) concentration. Neuroimage **55**, 616-621 (2011).*

*158. W. Gaetz, C. Liu, H. Zhu, L. Bloy, T. P. Roberts, Evidence for a motor gamma-band network governing response interference. Neuroimage **74**, 245-253 (2013).*

*159. S. D. Muthukumaraswamy, Temporal dynamics of primary motor cortex γ oscillation amplitude and piper corticomuscular coherence changes during motor control. Exp Brain Res **212**, 623-633 (2011).*

*160. M. P. Trevarrow et al., The developmental trajectory of sensorimotor cortical oscillations. Neuroimage **184**, 455-461 (2019).*

*161. G. Bush, L. M. Shin, The Multi-Source Interference Task: an fMRI task that reliably activates the cingulo-frontal-parietal cognitive/attention network. Nat Protoc **1**, 308-313 (2006).*

*162. S. Frühholz, B. Godde, M. Finke, M. Herrmann, Spatio-temporal brain dynamics in a combined stimulus-stimulus and stimulus-response conflict task. Neuroimage **54**, 622-634 (2011).*

*163. A. J. González-Villar, M. T. Carrillo-de-la-Peña, Brain electrical activity signatures during performance of the Multisource Interference Task. Psychophysiology **54**, 874-881 (2017).*

*164. S. Hanslmayr et al., The electrophysiological dynamics of interference during the Stroop task. J Cogn Neurosci **20**, 215-225 (2008).*

*165. X. Liu, M. T. Banich, B. L. Jacobson, J. L. Tanabe, Common and distinct neural substrates of attentional control in an integrated Simon and spatial Stroop task as assessed by event-related fMRI. Neuroimage **22**, 1097-1106 (2004).*

*166. B. S. Peterson et al., An event-related functional MRI study comparing interference effects in the Simon and Stroop tasks. Brain Res Cogn Brain Res **13**, 427-440 (2002).*

*167. D. C. Zhu, R. T. Zacks, J. M. Slade, Brain activation during interference resolution in young and older adults: an fMRI study. Neuroimage **50**, 810-817 (2010).*

*168. V. van Veen, C. S. Carter, The anterior cingulate as a conflict monitor: fMRI and ERP studies. Physiol Behav **77**, 477-482 (2002).*

169. A. I. Wiesman, T. W. Wilson, Posterior Alpha and Gamma Oscillations Index Divergent and Superadditive Effects of Cognitive Interference. Cerebral Cortex, (2019).

*170. T. Grent-'t-Jong, R. Oostenveld, O. Jensen, W. P. Medendorp, P. Praamstra, Oscillatory dynamics of response competition in human sensorimotor cortex. Neuroimage **83**, 27-34 (2013).*

*171. G. Bush, L. M. Shin, J. Holmes, B. R. Rosen, B. A. Vogt, The Multi-Source Interference Task: validation study with fMRI in individual subjects. Mol Psychiatry **8**, 60-70 (2003).*

*172. M. Feurra et al., Frequency-dependent tuning of the human motor system induced by transcranial oscillatory potentials. Journal of Neuroscience **31**, 12165-12170 (2011).*

*173. K. Benchenane, P. H. Tiesinga, F. P. Battaglia, Oscillations in the prefrontal cortex: a gateway to memory and attention. Curr Opin Neurobiol **21**, 475-485 (2011).*

*174. S. M. Doesburg, A. B. Roggeveen, K. Kitajo, L. M. Ward, Large-scale gamma-band phase synchronization and selective attention. Cereb Cortex **18**, 386-396 (2008).*

*175. O. Jensen, J. Kaiser, J. P. Lachaux, Human gamma-frequency oscillations associated with attention and memory. Trends Neurosci **30**, 317-324 (2007).*

*176. A. Pogosyan, L. D. Gaynor, A. Eusebio, P. Brown, Boosting cortical activity at beta-band frequencies slows movement in humans. Current biology **19**, 1637-1641 (2009).*

*177. A. A. Kühn et al., Event-related beta desynchronization in human subthalamic nucleus correlates with motor performance. Brain **127**, 735-746 (2004).*

*178. B. J. Lew et al., Neural dynamics of selective attention deficits in HIV-associated neurocognitive disorder. Neurology **91**, e1860-e1869 (2018).*

*179. T. W. Wilson et al., Abnormal MEG oscillatory activity during visual processing in the prefrontal cortices and frontal eye-fields of the aging HIV brain. PLoS One **8**, e66241 (2013).*

*180. B. R. Groff et al., Age-related visual dynamics in HIV-infected adults with cognitive impairment. Neurology-Neuroimmunology Neuroinflammation **7**, (2020).*

*181. D. Osipova, J. Ahveninen, O. Jensen, A. Ylikoski, E. Pekkonen, Altered generation of spontaneous oscillations in Alzheimer's disease. Neuroimage **27**, 835-841 (2005).*

*182. T. Montez et al., Altered temporal correlations in parietal alpha and prefrontal theta oscillations in early-stage Alzheimer disease. Proceedings of the National Academy of Sciences **106**, 1614-1619 (2009).*

*183. L. Koelewijn et al., Alzheimer's disease disrupts alpha and beta-band resting-state oscillatory network connectivity. Clinical Neurophysiology **128**, 2347-2357 (2017).*

*184. C. Schmiedt, A. Meistrowitz, G. Schwendemann, M. Herrmann, C. Basar-Eroglu, Theta and alpha oscillations reflect differences in memory strategy and visual discrimination performance in patients with Parkinson's disease. Neuroscience letters **388**, 138-143 (2005).*

*185. A. Oswal, P. Brown, V. Litvak, Synchronized neural oscillations and the pathophysiology of Parkinson's disease. Current opinion in neurology **26**, 662-670 (2013).*

*186. J. Rowe et al., Attention to action in Parkinson's disease: impaired effective connectivity among frontal cortical regions. Brain **125**, 276-289 (2002).*

*187. V. Litvak et al., Resting oscillatory cortico-subthalamic connectivity in patients with Parkinson's disease. Brain **134**, 359-374 (2011).*

*188. A. Suppa et al., Dopamine influences primary motor cortex plasticity and dorsal premotor-to-motor connectivity in Parkinson's disease. Cerebral Cortex **20**, 2224-2233 (2010).*

*189. L. M. Allcock et al., Impaired attention predicts falling in Parkinson's disease. Parkinsonism Relat Disord **15**, 110-115 (2009).*